WIND TUNNEL INVESTIGATION OF A SUPERSONIC TAILLESS AIRPLANE AT LOW SUBSONIC SPEED

Thesis

by

Arnold A. Jensen

Warren G. Koerner

In Partial Fulfillment of the Requirements

For the Degree of

Aeronautical Engineer

California Institute of Technology

Pasadena, California

1948

ACKNOWLEDGMENT

The authors wish to express their gratitude to Mr. Henry Nagamatsu for his continued advice and assistance in the experimental work and the preparation of this thesis.

ABSTRACT

An investigation was made in the Cal Tech-Merrill low speed wind tunnel at Pasadena City College to determine the lift and moment characteristics of a sweptback wing and a comparable delta wing, both with a 65° sweptback leading edge and a double wedge symmetrical airfoil section. Both wings were tested with and without a fuselage. Leading edge flaps and slats, trailing edge plain flaps, split flaps, Fowler type flaps, and fillets were tried to determine their effects on these characteristics. The complete airplane was designed with the idea that it should be a tailless airplane.

The results showed unfavorable longitudinal static stability characteristics which could be improved, but which could never be completely overcome at the stall when the wings were tested with the fuselage. A horizontal tail surface was necessary for longitudinal static stability at the stall but proved ineffective at the lower angles of attack.

The maximum lift coefficients for both wings of about 1.3 were higher than for a two dimensional double wedge airfoil section of approximately 0.8. The angles of attack at which these were reached were about twice as high as for the two dimensional section.

Tuft surveys showed the formation of two strong vortices from the leading edge of both wings first appearing at an angle of attack of approximately 10°. These vortices separated from the upper surface of the wing before reaching the trailing edge.

Comparison of results for the two wings indicated that the discontinuity of the trailing edge at the root of the sweptback wing was detrimental to the maximum lift.

There was an optimum deflection of the trailing edge split flap as a high lift device.

On the delta wing alone the plain flaps were very effective in increasing the maximum lift while the split flaps were ineffective.

Ailerons on the sweptback wing were effective at all angles of attack through the stall.

TABLE OF CONTENTS

I. INTRODUCTION

At the present time there is considerable interest in and work being done on the problem of designing wings for flight at supersonic speeds which possess the proper characteristics at subsonic speeds.

It is well known that a supersonic wing must have a thin section which preferably has a sharp leading edge. Also, if the wing is to be used on a tailless design, it must have considerable sweepback for control. Because of the thin section, structural considerations require that the wing have a fairly low aspect ratio.

The above requirements introduce certain problems concerning the aerodynamic characteristics of the wing. The sweepback of the wing and the thin pointed airfoil section can both be expected to produce a low maximum lift coefficient. Sweepback can be expected to produce tip stalling, and the combination of sweepback and low aspect ratio will give poor longitudinal stability and high angles of attack for the high lift necessary for landing.

Thus this investigation was undertaken to obtain systematic results for various high lift devices to be used principally at low subsonic speed.

II. EQUIPMENT AND MODELS

The wind tunnel tests of this investigation were run in the low speed 2-foot by 4-foot Cal Tech-Merrill wind tunnel at the Pasadena City College. This tunnel operates at a maximum dynamic pressure of 13.5 pounds per square foot (approximately 80 m.p.h.). Force measurements were made on the three component balance usually used in this tunnel. The model was supported upright on two struts to the wing trunnions and a strut to the tail. In the tests of the wing alone the rear support strut of the balance system was attached to a steel sting mounted on the lower side of the wing.

Sweptback Wing Model: The first model tested, that of the sweptback wing, was one previously constructed according to a supersonic tailless airplane design by Frank Dore (reference 1). The wing had a double wedge symmetrical airfoil section with maximum thickness at the 50 per cent chord point. This maximum thickness was 8 per cent of the chord at the root section and 2 per cent at the tip. The model was made of mahogany. All measurements in per cent of chord were made considering the chord parallel to the direction of flight. This wing had a leading edge sweepback of 65°, giving the 50 per cent chord line a sweepback of 61°. The aspect ratio was 1.72, the taper ratio 0.513, the area 98.35 square inches, and the span 13 inches. This wing was mounted in the fuselage of Dore's design. (See figs. 1 and 3.)

The flaps used on this wing were of dural sheet of sufficient thickness for rigidity. They were secured in place by Scotch tape. Wooden blocks were used to maintain the deflection angles of the split flaps. The dimensions of the various flaps are given in the figures. For the aileron effectiveness tests ailerons were cut into the wings and dural angles used to hold the ailerons at the various deflections. The trailing edge fillet plates used were flat sheets of dural secured in the plane of the wing chords. Wing fuselage fillets were formed with model wax.

The horizontal tail surfaces, when used, were attached at two different heights on the vertical fin. They were made of .040 inch dural sheet and their dimensions are given in figure 17. They had an area of 18.2 square inches, an aspect ratio of 1.50, and a leading edge sweepback angle of 65°. The vertical tail surface of .064 inch dural sheet had 10 per cent of the wing area, an aspect ratio of .64, and a leading edge sweepback angle of 65°.

Delta Wing Model: The delta wing was machined from jeweler's brass. The wing was made with the same leading edge sweepback angle and area as the sweptback wing for comparison reasons. This gave an aspect ratio of 1.86 and a span of 13.54 inches. The airfoil in this case was also a double wedge section with the maximum thickness at the 50 per cent chord point, with 5 per cent thickness at the root section. Plain flaps were made as part of the wing. All further flaps were attached as with the sweptback wing. (See fig. 4.)

III. TESTS

The maximum dynamic pressure used in the tests was 13.5 pounds per square foot. The dynamic pressure was regulated by setting the voltage on the electric motor driving the tunnel fan. Thus the dynamic pressure dropped as the temperature went up and especially as the angle of attack of the model was increased. It dropped as much as 10 per cent on some tests. Also it was convenient because of the limitations of the balance in measuring moments to run parts of many tests at a dynamic pressure of 8 or 9 pounds per square foot. This was also necessary on hot days to preserve the wax fillets if they were being used. Repetition of runs over this range of dynamic pressure gave no measurable change in force and moment coefficient measurements. The Reynolds number range was approximately 325,000 to 475,000 based on the mean aerodynamic chord.

The force tests were run through a range of angle attack from -4° to as high as 40° depending on the stall. Increments of 4° were used up to 28° and then increments of 2° were used to get a better idea of the shape of the curves. The tuft tests were run from -5° up to the stall. In this case the increments were larger, since it was only desired to investigate changes in the character of the flow.

The flap deflections given in the figures were measured from the surface of the wing on the side from which they were deflected.

IV. CORRECTIONS

The purpose of the investigation was to find the characteristics of the models and the relative effects of various modifications rather than any absolute force measurements. For example, it was desired to find effects of modifications on the moment curve. Thus certain corrections were not applied in the presentation of the data.

No wind tunnel wall corrections were applied. With these highly swept wings it would not seem logical to apply the available correction formulas for straight wings. Thus the corrected angle of attack at $C_{L_{max}}$ may be a little greater than that in the data, because closed section tunnel corrections on α are additive.

The apparatus did not allow for inversion of the model or for the use of dummy struts. Thus the angle of zero lift is not corrected. It will be noted in figure 43 that the zero lift angles are not equal to zero as would be expected for symmetrical airfoils. Previous experiments in the tunnel had indicated an inclination in the flow of about -20 minutes at the wing struts. This can hardly explain the angles of zero lift of from one to two degrees.

In attempting to find an explanation, a careful check was made with a surface plate to see that the leveling surface on the model and the plane of the wing were parallel. Also in the delta wing alone tests a dummy sting was mounted on the top side of the wing making the model completely symmetric, but no change in the lift and moment coefficients was measurable.

The best explanation seems to be that there is a curvature of flow in the tunnel which could effectively change the angle of attack of these highly swept models of low aspect ratio.

Since drag was not one of the primary considerations in this investigation, the following simple procedure was used to make corrections. The drag of the support struts alone (no model) was measured and the results reduced to a coefficient based on the wing area of the model. This value turned out to be $C_{D_\tau} = .010$. This was then subtracted as a constant term from all model drag coefficients over the entire angle of attack range. No attempt was made to estimate the effect on drag of the interference between support struts and model.

All force and moment coefficients were calculated on the basis of the area of the basic wing. Additional areas of the various flaps are given in the figures.

The moment coefficients of both wings with and without fuselage were calculated about the aerodynamic center determined from the average slope of the moment curve near zero lift for the wing alone. Oddly enough the aerodynamic center was at 0.343 of the mean aerodynamic chord for both wings.

Because of the high angle of attack to which it was necessary to take the wings, the tips or trailing edge of the wings approached rather close to the floor of the tunnel owing to the sweepback. This may have had some effect on the measurements made at high angles of attack, especially in the case of the fuselage with a tail.

V. RESULTS AND DISCUSSION

The results of the force measurements are shown in figures 33 to 68. Some of the results of the tuft tests are shown in figures 25 to 42.

The Sweptback Wing: The wing alone results given in figure 45 for the sweptback wing show a $C_{L_{max}}$ of 1.21 which is considerably greater than a $C_{L_{max}}$ of about 0.75 to 0.80 to be expected of a two dimensional wing of the same section (reference 2). This is attained, however, at an angle of attack three or four times as great as that of the two dimensional section. It is interesting to note in reference 3 that for a similar wing with a high-speed airfoil section the wing $C_{L_{max}}$ decreased from that of the two dimensional airfoil section. In this case also the angle of attack of the sweptback wing at $C_{L_{max}}$ was considerably increased from the two dimensional case.

As in reference 3, at about the time the moment curve becomes unstable there is a decrease in the slope of the lift curve. This is discussed in the reference and similar boundary layer phenomena were observed in our case. There is a hook in the stable direction at the top of the moment curve.

The results of the wing with full span split flaps of chord equal to 25 per cent of the wing chord are shown in figure 46. There is an expected increase in lift. The flap deflections of 40°, 60°, and 75° all give about the same increment of lift at the lower angles of attack, but the lift increments drop off at the higher angles of attack with those

of the higher flap deflections dropping off first. In fact, $C_{L_{max}}$ with the flap deflected 75° is 0.12 less than with the wing alone. The moment curves show the expected positive moment. The moment curves for the 40°, 60°, and 75° flap deflections all have unstable hooks at the stall. Of those tried, the 20° deflection seems to be the best.

Since full span split flaps would be impractical with wing control surfaces, tests were run with the 70 per cent span flaps of the same chord as shown in figure 6. The results are given in figure 47. The partial span flaps were a little less effective at low angles but gave just as high maximum lift as the full span flaps. This is probably due to the fact that the flaps are ineffective in the spanwise flow on the outer portion of the wing which the tuft studies show at high angles of attack.

Full span nose flaps of 10 per cent chord as shown in figure 7 were tested. The results are shown in figures 48 and 49. The lift increment increases with angle of attack, and the optimum deflections of 120° and 160° give an increase in $C_{L_{max}}$ of about 0.25. This implies it is advantageous to improve the flow at the leading edge. The moment curve is, however, considerably more unstable than that of the wing alone.

Combinations of the full span nose flaps and split flaps were tested. The results in figure 50 show the combined advantage of the lift increment at low angles of attack due to the split flaps and the high $C_{L_{max}}$ due to nose flaps. There is no increase in $C_{L_{max}}$ over that of the nose flaps. The mo-

ment curves are somewhat more stable than for the nose flaps, but the unstable hook of the split flaps prevails.

The effect of adding the fuselage is shown in figure 45. There is an increase in lift at angles above 10° and an increase in $C_{L_{max}}$. This is discussed later. The addition of the fuselage gives an unstable hook to the end of the moment curve as contrasted to the stable hook for the wing alone.

Full span split flaps were then tested with the fuselage, and the results are shown in figure 51. The increase in lift due to the flaps is not as great as with the wing alone, which fact can probably be explained by the inability of the fuselage to carry the loads across it. Also in this case the split flaps gave practically no increase in $C_{L_{max}}$.

Results of testing full span nose flaps with the fuselage are shown in figure 52. The results are similar to those with the wing alone except that the moment curve shows less instability. Combinations of nose flaps and split flaps with results shown in figure 53 gave no unexpected results.

An interrupter plate was put on the upper surface of the wing as shown in figure 10 to see what effect would be obtained by trying to prevent the spanwise flow indicated by the tuft studies. The results are shown in figure 54. There is a decrease in lift above an angle of attack of 12°, which is about the angle where the spanwise flow and vortex formation become prominent. Thus it appears that attempts to prevent the spanwise flow are detrimental to lift.

A 50 per cent span leading edge slat as shown in figure 7 was tried with a view to improving the flow over the sharp leading edge. No increase in lift is observed in figure 54. In fact over most of the angle of attack range the lift was decreased. Tuft studies showed that the flow behind the slat was chordwise even up to the stall while it was spanwise without the slat. Thus again the obstruction of the spanwise flow seems to be detrimental to lift. Also the use of leading edge slats for the improvement of stability does not seem to be indicated by these results. It should be remarked here that the effects of leading edge slats, because they are used to improve the flow over a sharp edge, are very critical to geometry. Thus these results for one slat should not be considered in any way conclusive.

A 40 per cent span split (figure 55) gave some improvement in the slope of the moment curve up to about 24° angle of attack.

A 25 per cent span leading edge slat (figure 55) gave a definite improvement in the moment curve over that of the 50 per cent span slat. This leads to the supposition that a more stable moment curve can be attained by applying high lift devices to the outer portion of the wing. The results of a combination of these last two configurations is also shown in figure 55.

The results of testing 50 per cent span and 25 per cent span nose flaps are given in figure 56. A noticeable improvement in the moment curves was obtained over those of the full

span nose flaps. A small amount of this improvement is due to the fact that the partial span nose flaps were run with the wing-fuselage fillets installed. It thus seems that the moment curve or the longitudinal static stability can be improved by applying the high lift devices to the outer portion of the wing as was supposed.

Results are shown in figure 57 of the partial span trailing edge flaps (Fowler type). These flaps gave more stable moment curves than just the wing with the fuselage, but gave large moments to be balanced by a tail.

Because of the improved moment curves obtained with the partial span nose flaps of 10 per cent chord, a 25 per cent span nose flap of 20 per cent chord was tested. The results are given in figure 58. This configuration gave the straightest moment curve thus far found. The curve, however, still has the unstable hook at the stall. The 40 per cent trailing edge flap was also tried in combination with this nose flap with the result to be expected (figure 58).

Then, because of the acute angle at the root of a swept-back wing, a fillet plate at the wing-fuselage junction as shown in figure 16 was used. It was also tested with the above nose flap. The results in figure 59 show that the increase in C_L at high angles of attack was considerable, although of course this is based on the original wing area. These fillet plates caused the moment curve to slope in a stable direction except for the hook at the stall.

Up to this point the wing and fuselage combination always have an unstable hook on the moment curve at the stall. A horizontal tail surface was tested at two different heights (figures 17 and 18) and the expected stable hook near the stall shown in figure 60 was obtained for the moment curve. However, it is very noticeable that the usual stabilizing effect of a horizontal tail surface behind a straight wing is not present at lower angles. Thus the downwash behind this low aspect ratio sweptback wing is evidently such as to make the horizontal tail surface rather ineffective as a means of producing a stabilizing moment.

Ailerons were cut out of the wing as shown in figure 1. These were tested with both ailerons being deflected in the same direction, because the balance could not measure rolling moment. At the low angles of attack the effect of deflection on lift is about linear as shown in figure 61. However, at high angles of attack there is a positive deflection giving maximum effectiveness. This is the same phenomenon observed for the split flaps at high angles of attack.

The Delta Wing: The delta wing shown in figure 4 was tested alone and the results are shown in figure 62. The $C_{L_{max}}$ of 1.36 is 0.15 higher than for the sweptback wing. (See figure 43.) The moment curve is somewhat straighter than that of the sweptback wing alone. In the case of the delta wing, as in the case of the sweptback wing, the wing alone has a stable hook on the end of the moment curve while the addition of the fuselage makes the hook unstable.

With the wing alone a plain hinged flap of constant chord, namely 25 per cent of the mean aerodynamic chord (figure 4), was tested and the results are given in figure 63. They show that as far as increased lift is concerned there is an optimum deflection, probably near 20°. For the 20° flap deflection an increase in $C_{L_{max}}$ of 0.25 was obtained, and the angle of attack for $C_{L_{max}}$ was lowered from 34° for the wing alone to 28° with the flaps. The great advantage of this flap is the increase in lift at low angles of attack. For example, at $\alpha = 16°$ the lift is doubled. However, as would be expected, the pitching moments are very large and are also unstable and erratic.

A split flap of the same size as the plain flap was tested at 20° deflection and gave only about 0.6 as much increase in C_L at low angles (figure 64). The $C_{L_{max}}$ with this flap was 0.04 less than for the wing alone.

The results of adding the fuselage to the delta wing are given in figure 62. It will be noted from figure 45 and figure 62 that the wing-fuselage fillets were considerably more helpful in increasing the lift for the case of the sweptback wing than for that of the delta wing. This can probably be related to the great improvement in $C_{L_{max}}$ given by the trailing edge fillet plates already discussed. In other words, the acute angle formed by the trailing edge of the sweptback wing and the fuselage is a discontinuity detrimental to the maximum lift. This is borne out by the fact that the delta wing alone had a $C_{L_{max}}$ 0.15 greater than the sweptback wing alone.

Another way of looking at the same thing is to look first at the effect of the fuselage on the wing alone. Adding the fuselage to the sweptback wing increased $C_{L_{max}}$ about 0.07, while adding it to the delta wing decreased $C_{L_{max}}$ about 0.08. If this difference in maximum lift can be attributed to the smoothing out of the trailing edge discontinuity, then it would be expected, as found, that any further filleting at the trailing edge of the sweptback wing would be advantageous to $C_{L_{max}}$.

At this point the respective wing areas covered by the fuselage should be considered. The percentage of the delta wing covered, 42.8 per cent, is of course greater than that of the sweptback wing, 31.8 per cent. However, it is to be expected that the lift is almost completely carried across the fuselage. This is confirmed by the relative ineffectiveness of the wing-fuselage fillets in the case of the delta wing. The area decrease from the wing alone due to the covering of the front point of the wing is the same for both wings.

The plain flaps were then tested on the delta wing with fuselage. The results are given in figure 65. The comparison between the 20° and 40° deflections is similar to that when they were on the wing alone. The increment of lift is, however, not as great as with the wing alone. This is probably, as with the full span split flaps on the sweptback wing, due to the inability of the fuselage to carry the load across it.

A full span nose flap of chord equal to 10 per cent of the wing mean aerodynamic chord was tested and the results are given in figure 66. There is an increase in lift over the

wing-fuselage alone proportional to the effective angle of attack as with the sweptback wing. In this case, in contrast to the sweptback wing, the increase in $C_{L_{max}}$ is too great to be attributed entirely to the increase in wing area. The moment curves are unstable but fairly straight.

Again, as in the case of the sweptback wing, an attempt was made to obtain a stable moment curve by applying a high lift device to the outer portion of the wing. A 25 per cent span nose flap of chord equal to 20 per cent of the wing mean aerodynamic chord was used and, although there was no noticeable increase in lift, there was enough improvement in the moment curve so that it might be called "neutrally stable" as shown in figure 67. The hook at the end of the moment curve is also in the stable direction.

The same horizontal tail surface was tested with the delta wing as with the sweptback wing, and the results given in figure 68 are similar. They again show that the downwash behind the low aspect ratio wing makes the horizontal tail ineffective as a means of obtaining stability except at very high angles.

Tuft studies were made, and some of these are illustrated in figures 25 to 42. Some of the findings of these studies have been mentioned in the preceding discussion. The character of the flow at the leading edge led to studying the flow above the wing with a streamer. It was found that at angles of attack above about 10° a vortex was formed on each half of the wing along a considerable portion of the sharp leading edge.

This vortex immediately converged and passed the trailing edge of the wing as a strong single vortex above the surface of the wing. This is illustrated in figure 42. Thus the tuft pictures of the tufts on the wing surface do not give a very complete picture of the flow.

In figures 25 and 26 are shown tuft pictures of the sweptback wing alone. At -5° and 0° angles of attack the flow on the top surface is smooth and in the free stream direction. At 5° a path of spanwise flow appears. At 10° a definite path of spanwise flow is evident. It was this that led to the observation of the vortices mentioned above. At 20° the picture is about the same except that the "path" has moved inboard. At 30° the spanwise flow is developing from most of the leading edge, and considerable turbulence is observed on most of the outer portion of the wing. At 34°, which is about the angle of maximum lift, the picture is about the same. At 38° there is still a further increase in turbulence.

In figures 37 to 39 the tuft pictures for the delta wing alone show essentially the same phenomenon. The only noticeable difference seems to be that the "path" goes to the point of the delta wing where on the sweptback wing it crossed the trailing edge about two-thirds of the way from the root.

VI. CONCLUSIONS

The results of low speed tests on a low aspect ratio highly sweptback wing and a comparable delta wing indicate the following:

1. The maximum lift coefficient of both the sweptback wing and the delta wing was much higher than for the two dimensional airfoil section data. It was also attained at a much greater angle of attack due to the low aspect ratio of the wing.

2. For trailing edge split flaps as a high lift device there was an optimum deflection. That is, at high angles of attack a flap deflection greater than about 20° no longer gave an increase in lift.

3. The discontinuity of the geometry of a swept-back wing at the root was detrimental to high lift. Thus anything tending to fill this discontinuity gave an increase in maximum lift coefficient.

4. With the two wings tested with the fuselage it was not possible to attain static longitudinal stability at the stall without a horizontal tail surface. There was, however, a considerable increase in stability with partial span leading edge flaps. This agrees with reference 3.

5. The horizontal tail surface was ineffective in the downwash behind the wings tested almost until the stall angle was reached.

6. Above about 10° angle of attack, when the spanwise flow became noticeable, one vortex was shed from the leading

edge on each side of the wing which separated from the wing surface before it reached the trailing edge.

7. The plain flaps on the delta wing alone were very effective in increasing the maximum lift while the split flaps of the same size were ineffective. Also the plain flaps with a deflection of 20° were twice as effective as the split flaps in increasing lift at low angles of attack.

8. Ailerons on the sweptback wing were effective at all angles of attack through the stall. This indicates the absence of a "tip stall" on this low aspect ratio highly sweptback wing.

REFERENCES

1. Dore, Frank: The Design of Tailless Airplanes. Thesis, California Institute of Technology (1947).

2. Pollock, A. D., Jr., and Reck, F. F.: A Study of Methods to Increase the Lift of Supersonic Airfoils at Low Speeds. Thesis, California Institute of Technology (1947).

3. Lowry, J. G., and Schneiter, L. E.: Investigation at Low Speed of the Longitudinal Stability Characteristics of a 60° Swept-Back Tapered Low-Drag Wing. N.A.C.A. T.N. No. 1284 (May, 1947).

INDEX OF FIGURES

	Figure Numbers		
	Curve	Illustration	Tuft Study
Comparison of W and W_Δ	43		
Comparison of WBV and $W_\Delta BV$	44		
Model Build-Up with W	45	1,3	25,31,35
Full Span Split Flap on W	46	5	27
Partial Span (70%) Split Flap on W	47	6	
Full Span Nose Flap on W	48	7	29
Full Span Nose Flap on W (cont'd)	49		
Full Span Nose Flap and Full Span Split Flap Combinations on W	50		
Full Span Split Flap on WBV	51	8	
Full Span Nose Flap on WBV	52	8	
Full Span Nose Flap and Full Span Split Flap Combinations on WBV	53		
Partial Span (50%) Slat and Interrupter Plate on WBV	54	9,10	33
Partial Span (40%) Split Flap and Partial Span (25%) Slat on WBXV	55	11	
Partial Span (50% and 25%) Nose Flaps on WBXV	56	12,13	
Partial Span (40%) Trailing Edge Flap on WBXV	57		
Partial Span (25%) Nose Flap and Partial Span (40%) Trailing Edge Flap on WBXV	58	14,15	

	Figure Numbers		
	Curve	Illustration	Tuft Study
Trailing Edge Fillet Plate and Partial Span (25%) Nose Flap on WBXV	59	16	
Horizontal Tail and Partial Span (40%) Trailing Edge Flap on WBXV	60	17,18	
Aileron Effectiveness of WBXV	61	1	
Model Build-Up with W_Δ	62	2,4	37,40
Full Span Plain Flap on W_Δ	63	4	
Full Span Split Flap on W_Δ	64	19	
Full Span Plain Flap on $W_\Delta BV$	65	2	
Full Span Nose Flap on $W_\Delta BV$	66	21	
Partial Span (25%) Nose Flap on $W_\Delta BV$	67	22	
Horizontal Tail on $W_\Delta BV$	68	23,24	

CODE OF MODEL CONFIGURATIONS

Superscript on flap configuration refers to the angular displacement in degrees from the retracted position, measured perpendicular to the flap hinge line; hence F_1^{40} is the partial span split flap deflected 40 degrees.

W Basic sweptback wing, $\Lambda = 65^\circ$ at leading edge, aspect ratio = 1.72, taper ratio = .513, double wedge section, area = 98.35 square inches.

W_Δ Basic delta wing, $\Lambda = 65^\circ$ at leading edge, aspect ratio = 1.86, double wedge section, area = 98.35 square inches.

H_1 Horizontal sweptback tail, 18.5% wing area, mounted 1.84 inches above thrust line, $\Lambda = 65^\circ$, aspect ratio = 1.50, taper ratio = .74, area = 18.2 square inches.

H_2 Same as H_1, mounted 3.68 inches above thrust line.

V Vertical sweptback tail, 10.0% wing area, $\Lambda = 65^\circ$, aspect ratio = .64, taper ratio = .63.

B Circular fuselage with full length air duct, used with W and W_Δ.

X Wing-fuselage fillet, 1.62 inches radius at thickest section.

F Full span split flap used on W, 25% chord.

F_1 Partial span split flap used on W, 70% span, 25% chord.

F_2 Full span split flap used on WBV, 25% chord.

F_3 Partial span split flap used on WBXV, 40% span, 25% chord.

F_4 Partial span trailing edge flap used on WBXV, 40% span, 25% chord.

F_5 Full span plain flap used on W_Δ, 25% M.A.C.

F_6 Full span plain flap used on W_ΔBV, 25% M.A.C.

F_7 Full span split flap used on W_Δ, 25% M.A.C.

K Full span nose flap used on W, 10% chord.

K_1 Full span nose flap used on WBV, 10% chord.

K_2 Partial span nose flap used on WBXV, 50% span, 10% chord.

K_3 Partial span nose flap used on WBXV, 25% span, 10% chord.

K_4 Partial span nose flap used on WBXV, 25% span, 20% chord.

K_5 Full span nose flap used on $W_\Delta BV$, 10% M.A.C.

K_6 Partial span nose flap used on $W_\Delta BV$, 25% span, 20% M.A.C.

S Partial span leading edge slat, 50% span, 15% M.A.C.

S_1 Partial span leading edge slat, 25% span, 15% M.A.C.

I Interrupter plate, .5 inch high, full chord, located at 50% of span not covered by fuselage (2.42 inches in from tip).

T Trailing edge fillet plate, 1.5 inches radius in plan form.

A Aileron of wing W, 34% span, 25% chord.

COMPLETE SWEPTBACK WING
TAILLESS MODEL
(CONFIGURATION WBXV)

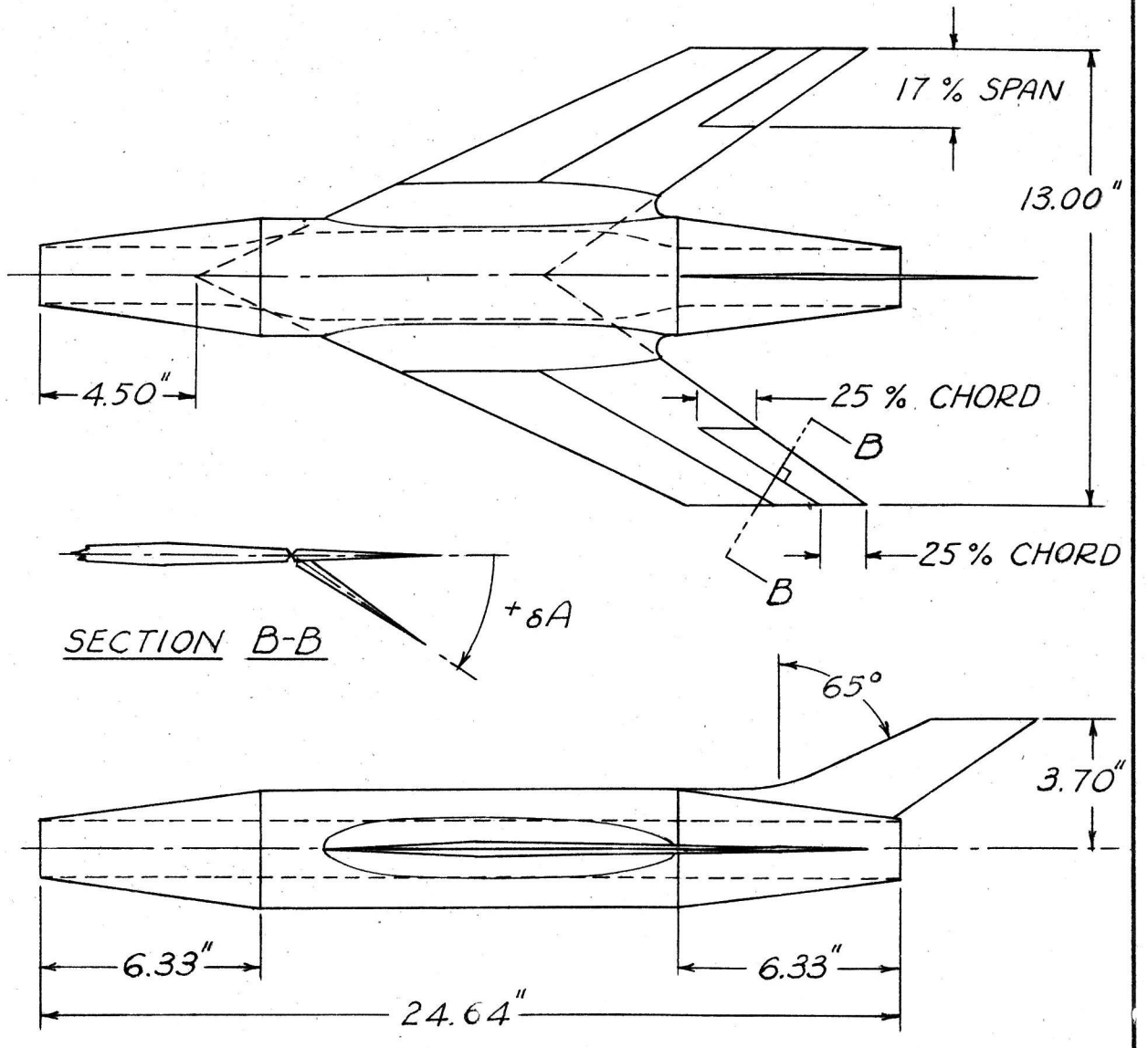

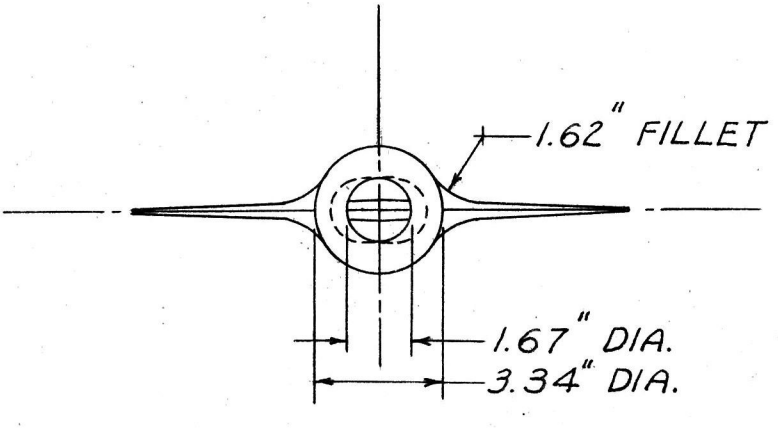

WING INCIDENCE = 0°
A AILERON AREA = 6.70% WING AREA

SCALE: $\frac{1}{5}" = 1"$

COMPLETE DELTA WING TAILLESS MODEL (CONFIGURATION $W_{\Delta}BV$)

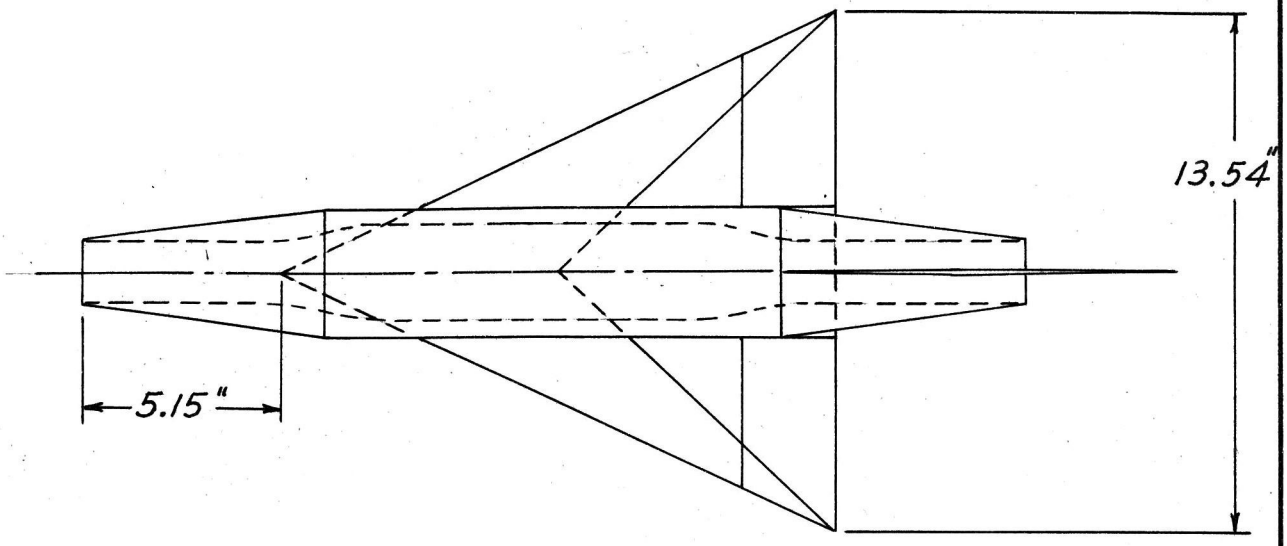

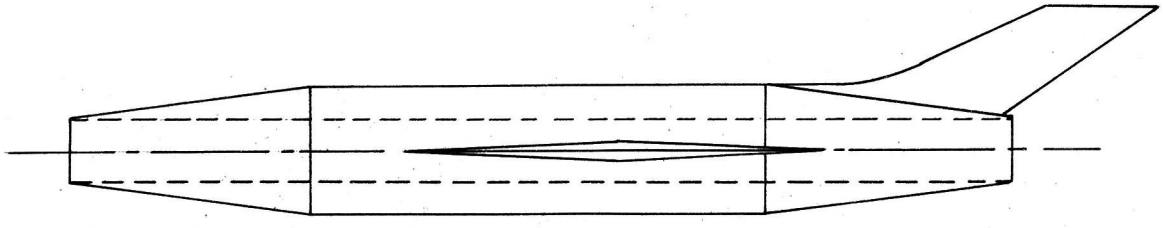

FUSELAGE DIMENSIONS IDENTICAL TO FIG. 1

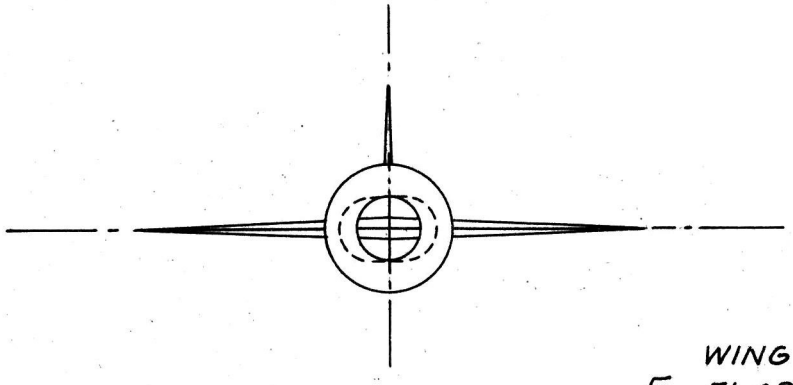

WING INCIDENCE = 0°

F_6 FLAP AREA = 21.7% WING AREA

SCALE: $\frac{1}{5}" = 1"$

DETAIL OF SWEPTBACK WING (CONFIGURATION W)

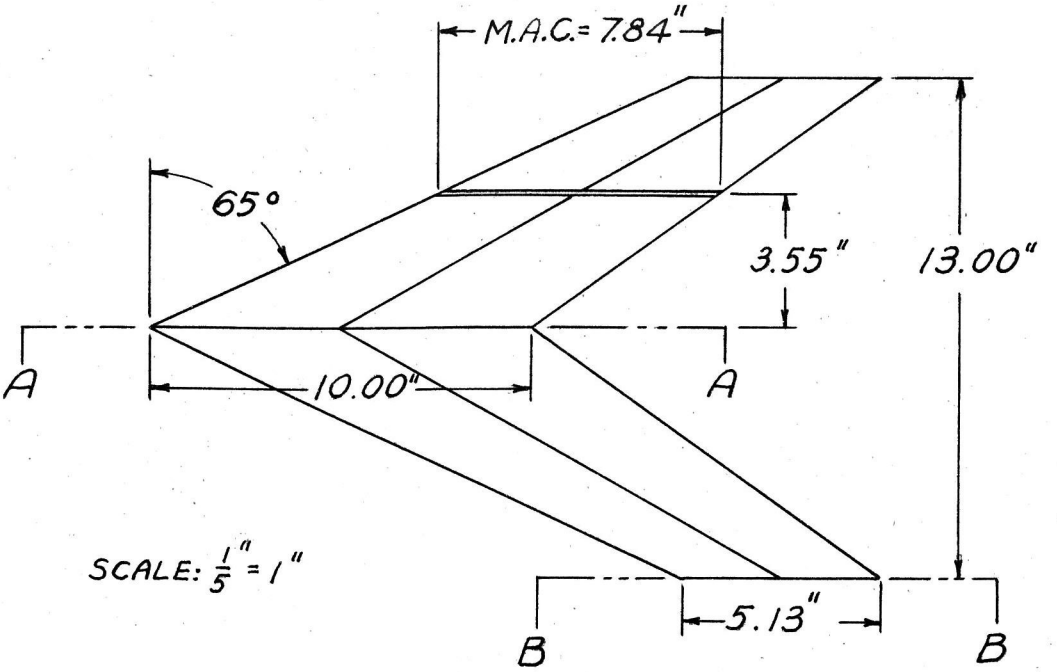

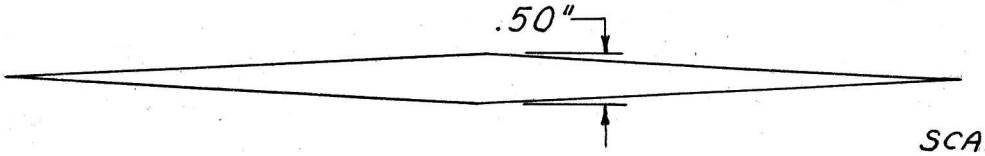

ROOT CHORD (SECTION A-A)

5 % THICKNESS SYMMETRICAL DOUBLE WEDGE SECTION;
MAXIMUM THICKNESS LOCATED AT .5 CHORD

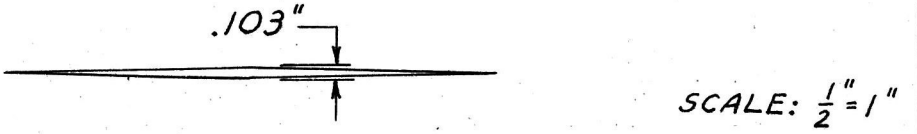

TIP CHORD (SECTION B-B)

2 % THICKNESS SYMMETRICAL DOUBLE WEDGE SECTION;
MAXIMUM THICKNESS LOCATED AT .5 CHORD

DETAIL OF DELTA WING (CONFIGURATION W_Δ)

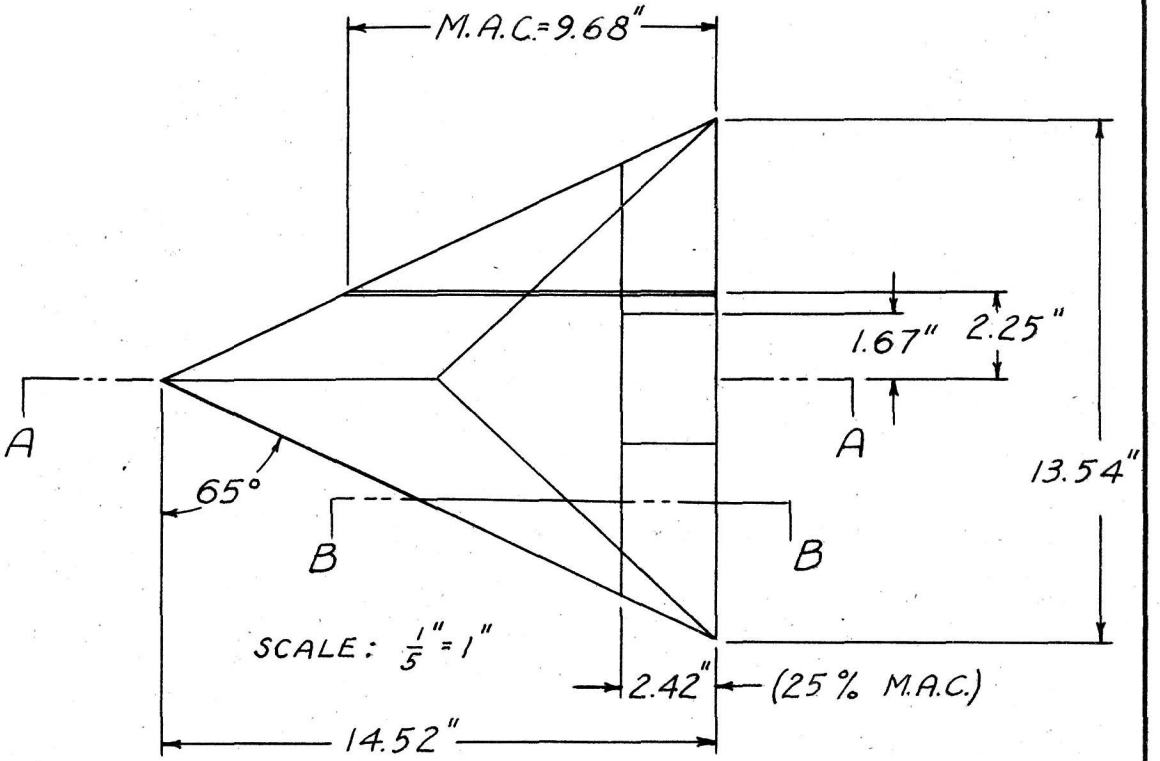

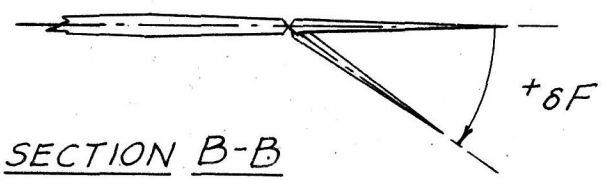

SECTION B-B

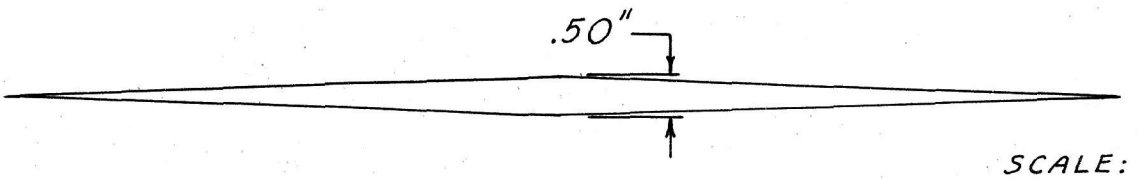

ROOT CHORD (SECTION A-A)

3.44% THICKNESS SYMMETRICAL DOUBLE WEDGE SECTION;
MAXIMUM THICKNESS LOCATED AT .5 CHORD

F_5 FLAP AREA = 30.4% WING AREA

FULL SPAN SPLIT FLAP (CONFIGURATION WF)

FIG. 5

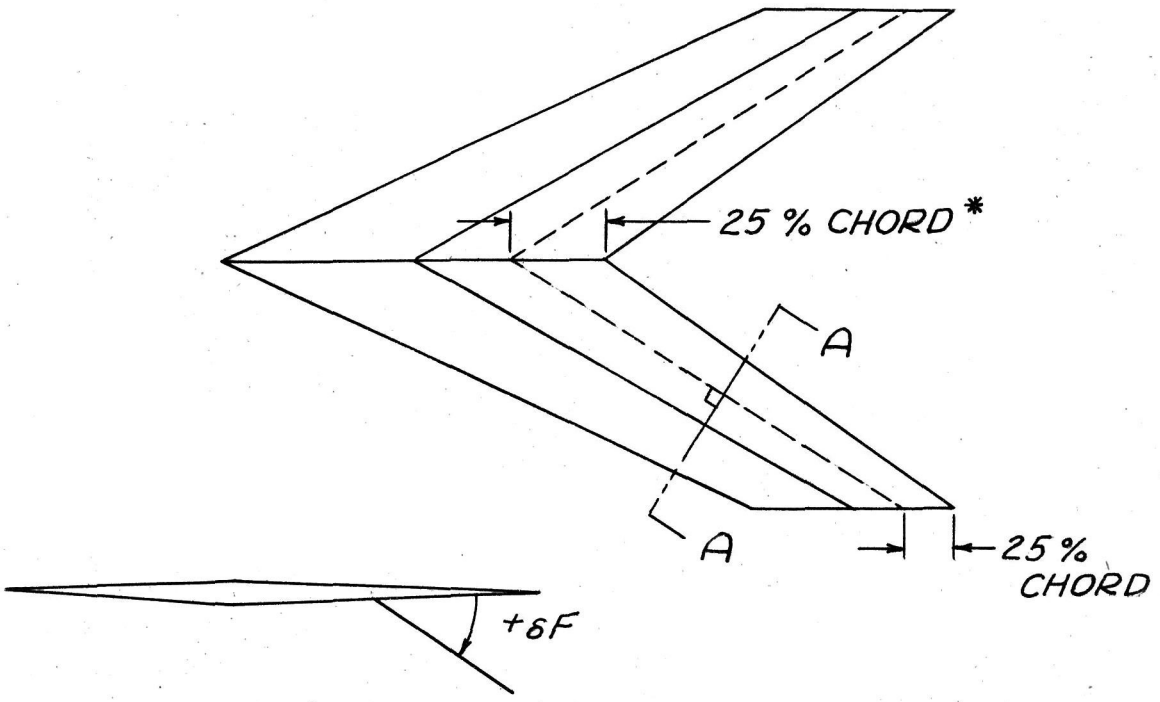

SECTION A-A

F FLAP AREA = 25.0 % WING AREA

PARTIAL SPAN (70%) SPLIT FLAP (CONFIGURATION WF,)

FIG. 6

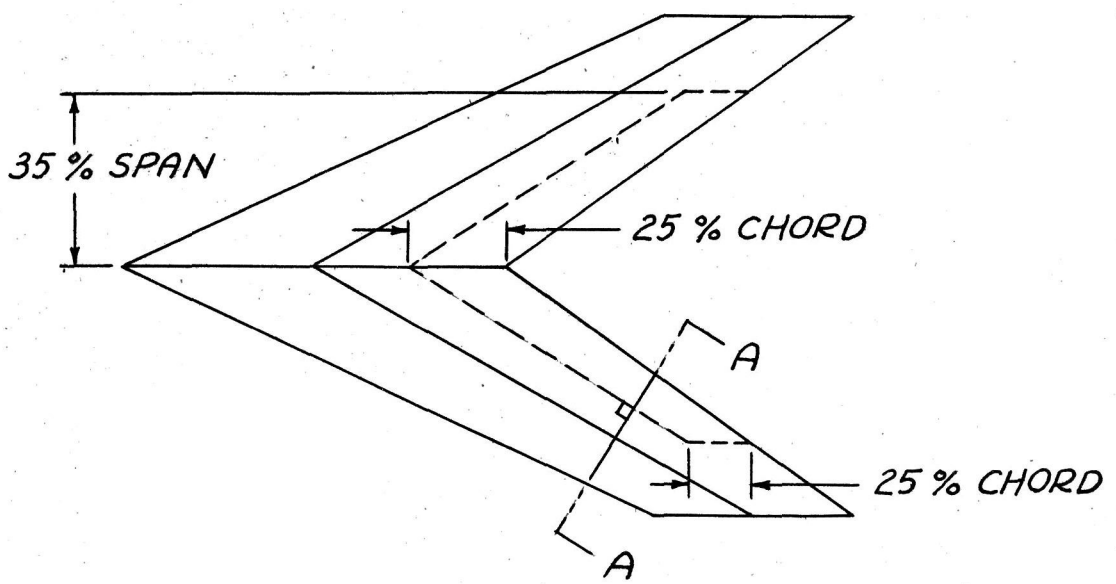

F, FLAP AREA = 19.2 % WING AREA

* DIMENSIONS GIVEN IN PERCENT CHORD REFER TO THE LOCAL CHORD (PARALLEL TO ROOT CHORD).

FULL SPAN NOSE FLAP (CONFIGURATION WK)

FIG. 7

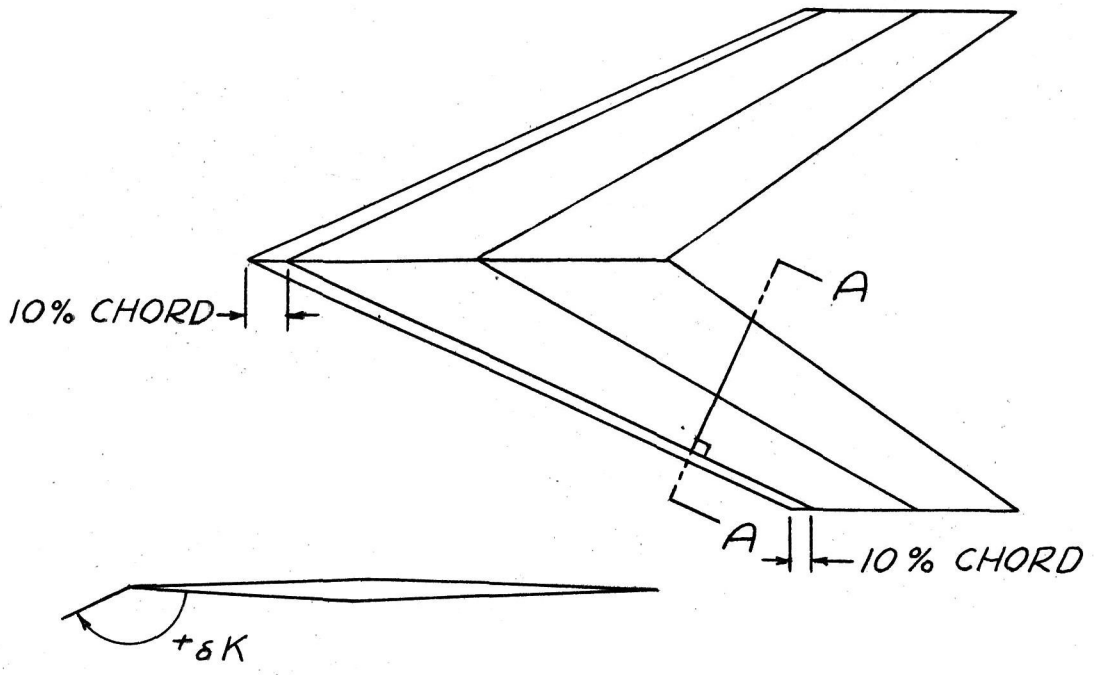

SECTION A-A

K FLAP AREA = 10.0% WING AREA

FULL SPAN NOSE FLAP & FULL SPAN SPLIT FLAP ON WBV (CONFIGURATION WBK, F_2V)

FIG. 8

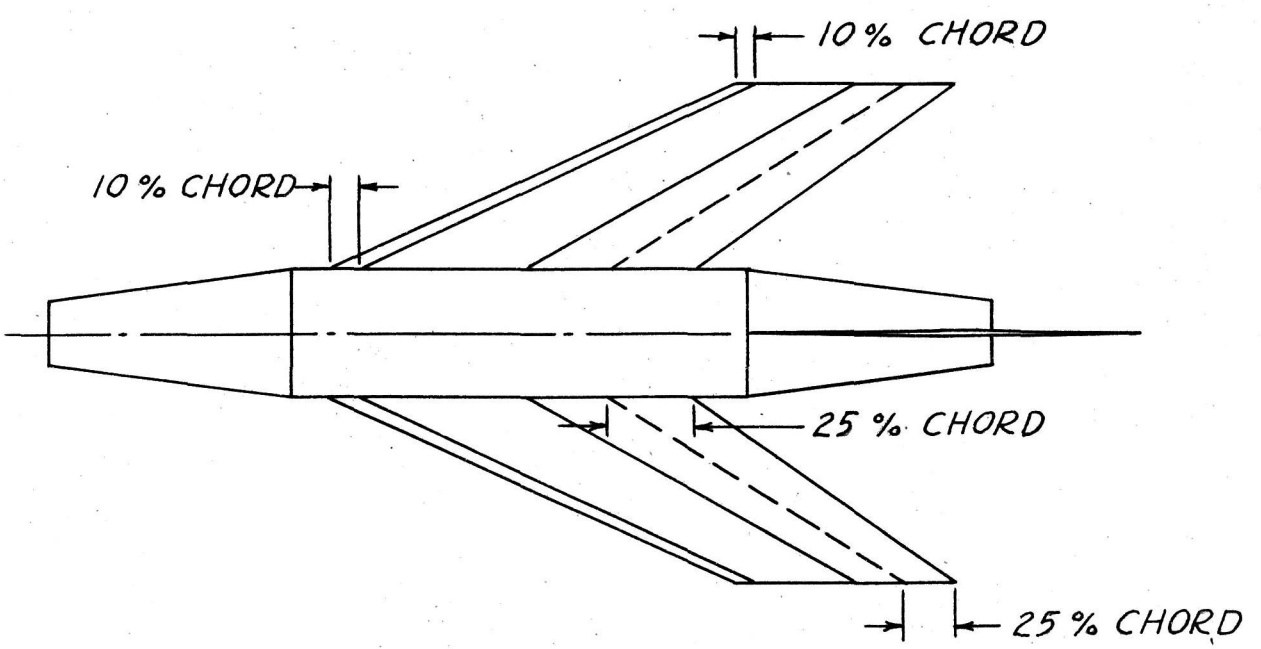

K_1 FLAP AREA = 6.91% WING AREA

F_2 FLAP AREA = 17.0% WING AREA

PARTIAL SPAN (50 %) SLAT (CONFIGURATION WBSV)

FIG. 9

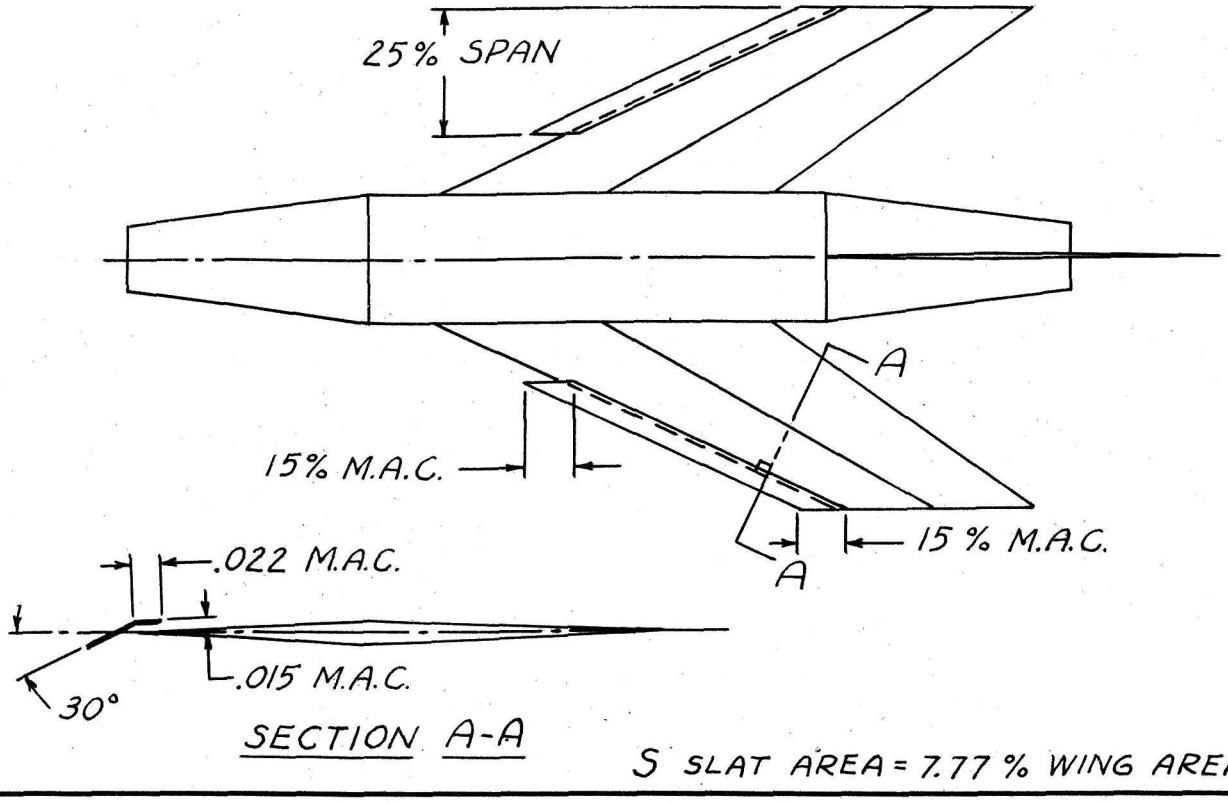

SECTION A-A

S SLAT AREA = 7.77 % WING AREA

INTERRUPTER PLATE (CONFIGURATION WBIV)

FIG. 10

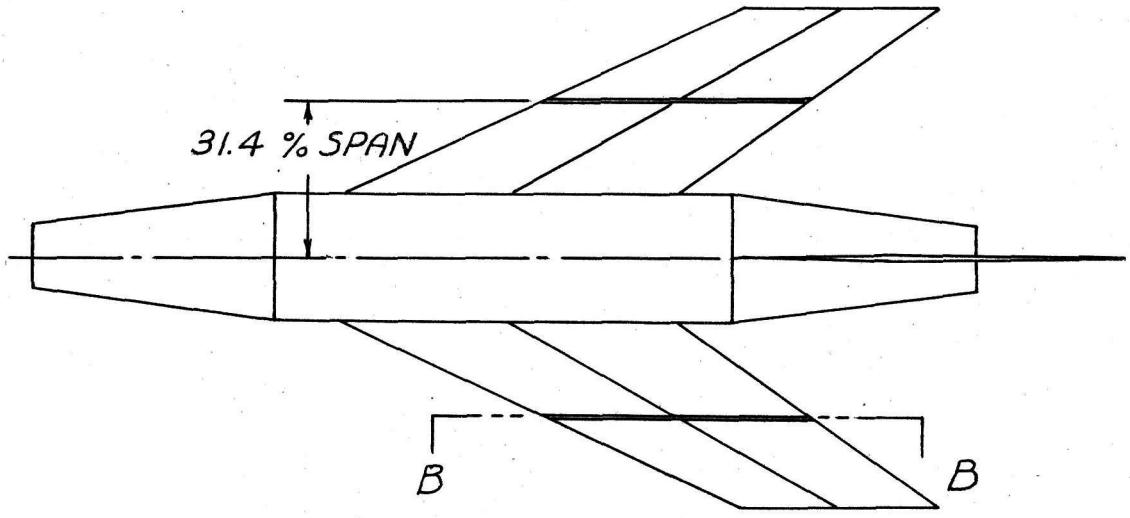

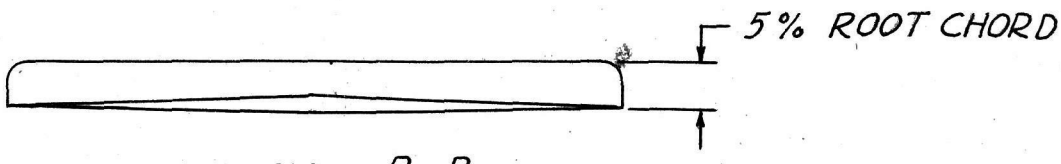

SECTION B-B

PARTIAL SPAN (40%) SPLIT FLAP & PARTIAL SPAN (25%) SLAT (CONFIGURATION WBXS$_1$F$_3$V)

FIG. 11

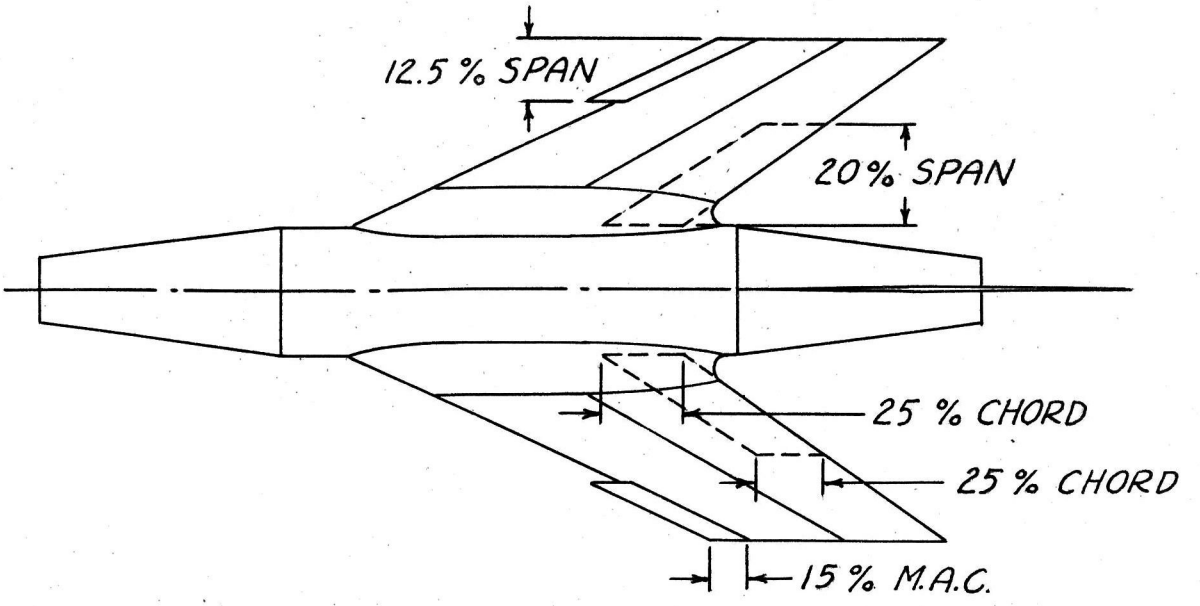

SLAT CROSS-SECTION IDENTICAL TO SECTION A-A, FIG. 9

S_1 SLAT AREA = 3.88% WING AREA

F_3 FLAP AREA = 10.03% WING AREA

PARTIAL SPAN (50%) NOSE FLAP (CONFIGURATION WBXK$_2$V)

FIG. 12

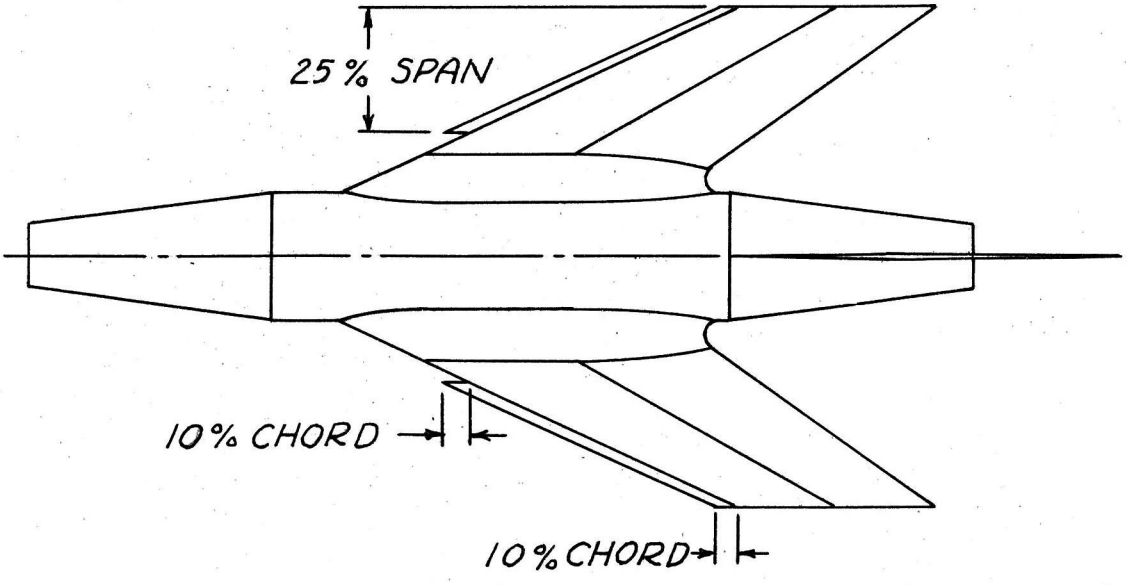

K_2 FLAP AREA = 4.2 % WING AREA

PARTIAL SPAN (25 %) NOSE FLAP, 10 % CHORD (CONFIGURATION WBXK$_3$V)

FIG. 13

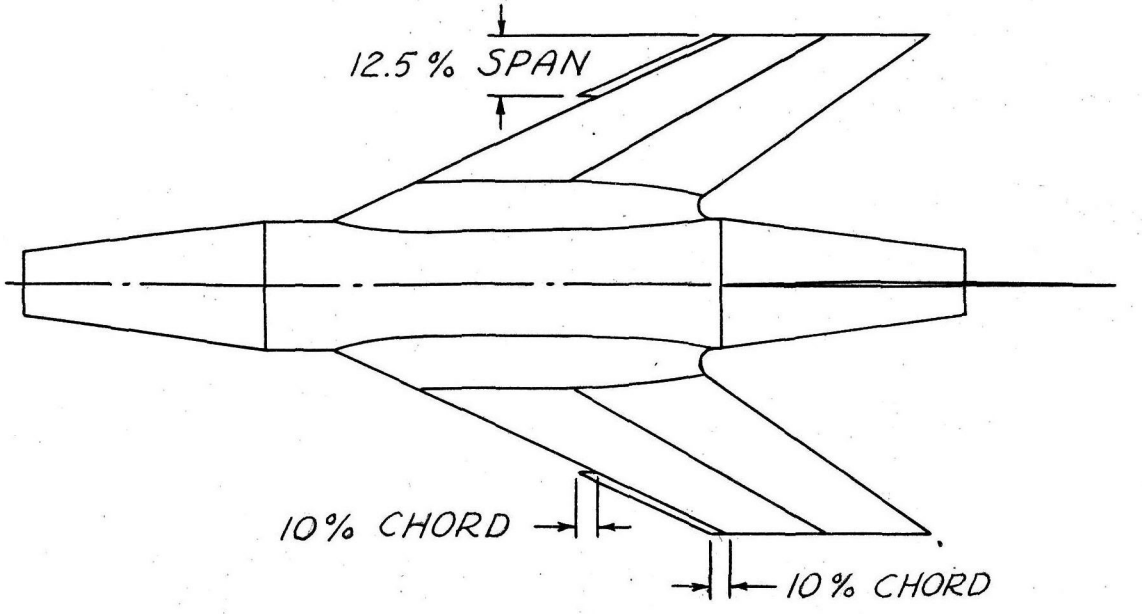

K_3 FLAP AREA = 1.90 % WING AREA

PARTIAL SPAN (25 %) NOSE FLAP, 20 % CHORD (CONFIGURATION WBXK$_4$V)

FIG. 14

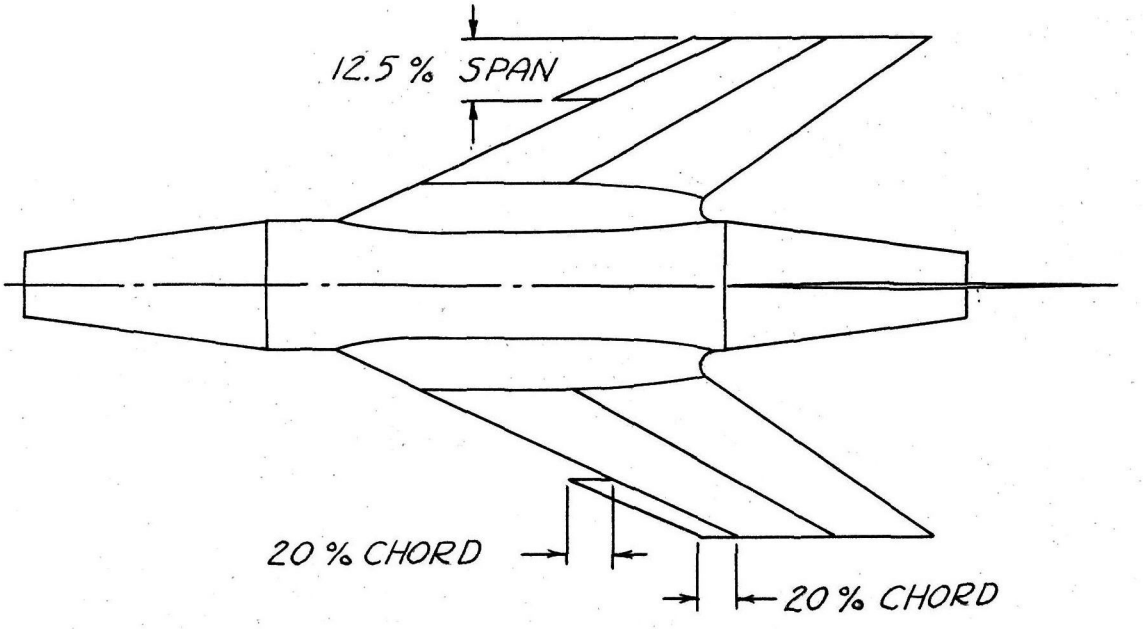

K_4 FLAP AREA = 3.80 % WING AREA

PARTIAL SPAN (40%) TRAILING EDGE FLAP (CONFIGURATION WBXF$_4$V)

FIG. 15

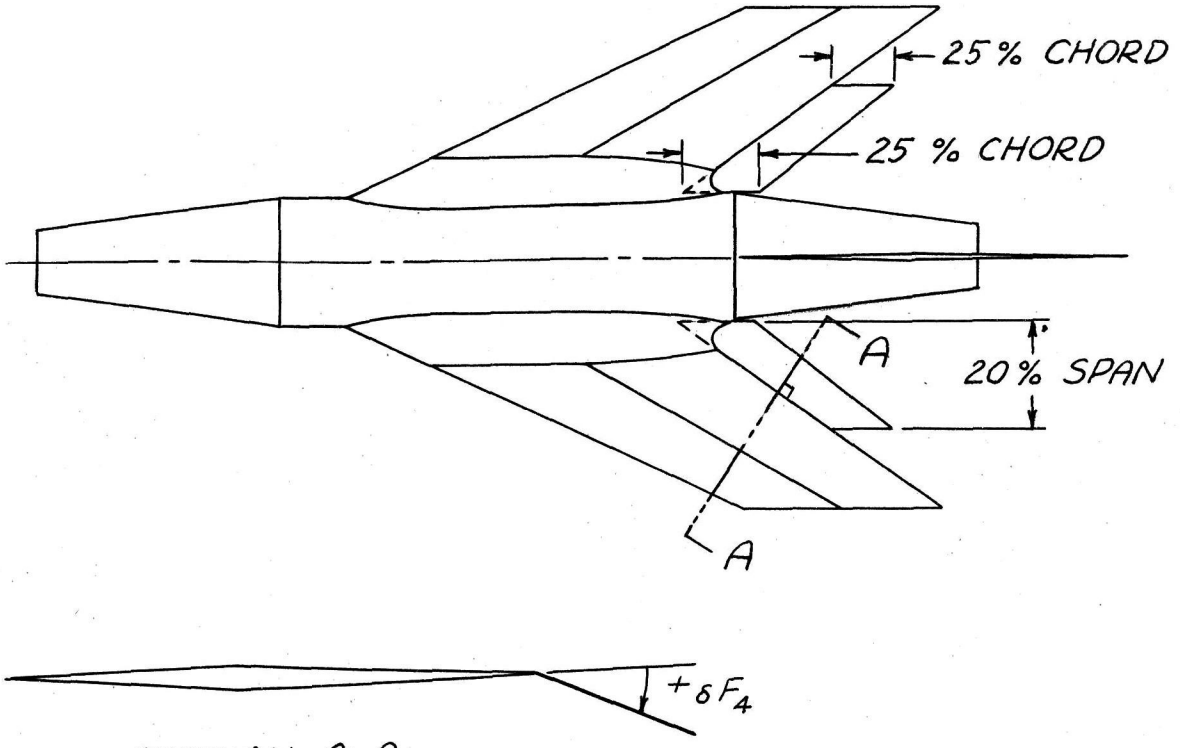

SECTION A-A

F_4 FLAP AREA = 10.03 % WING AREA

TRAILING EDGE FILLET PLATE (CONFIGURATION WBXTV)

FIG. 16

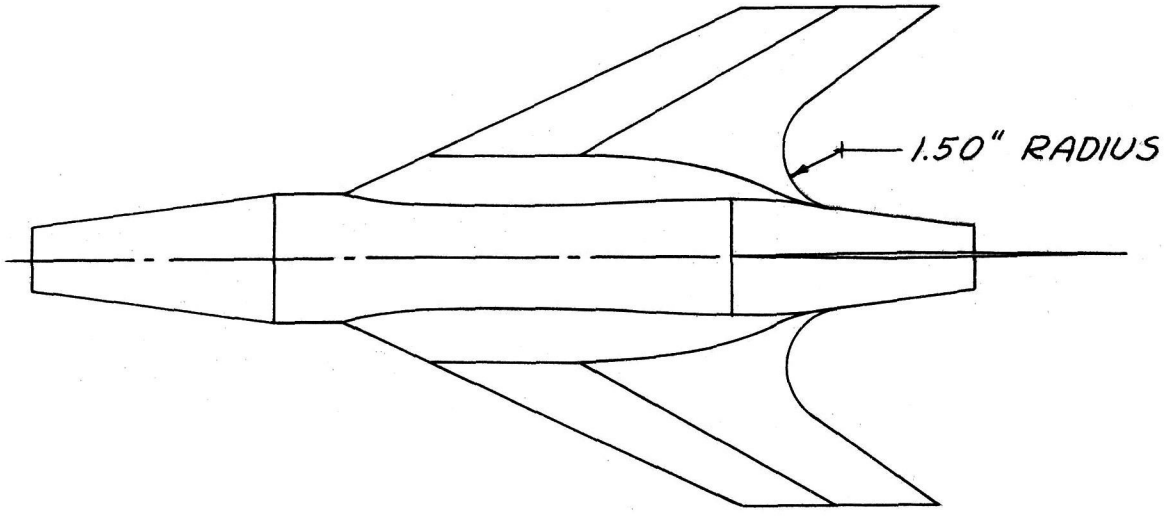

T FILLET PLATE AREA = 6.22 % WING AREA

HORIZONTAL TAIL IN LOWER POSITION
(CONFIGURATION WBXH,V)

FIG. 17

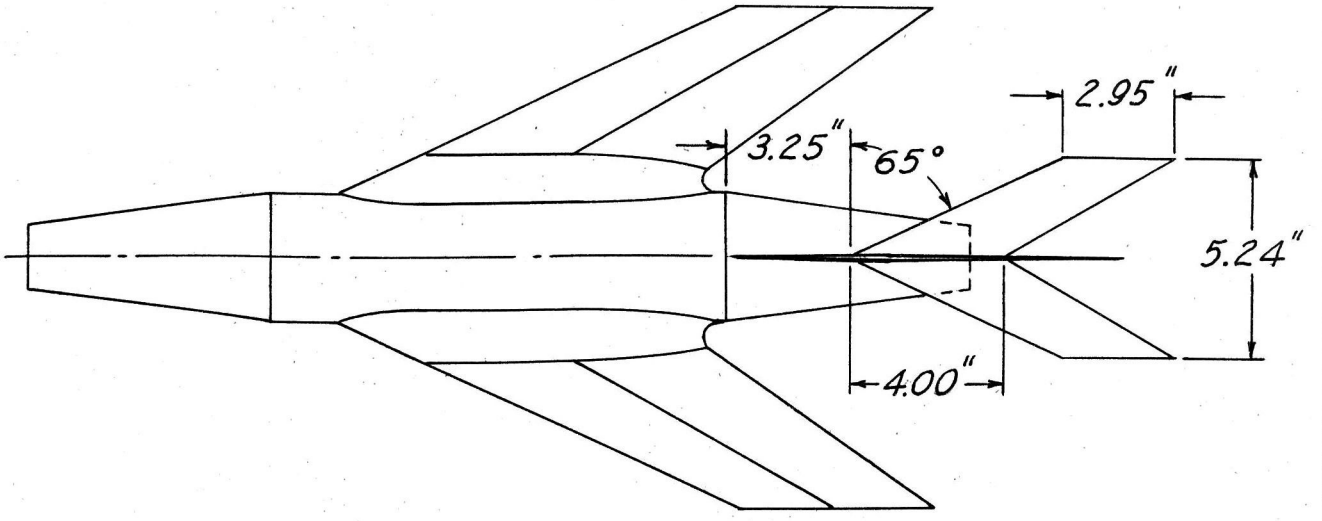

TAIL INCIDENCE = 0°

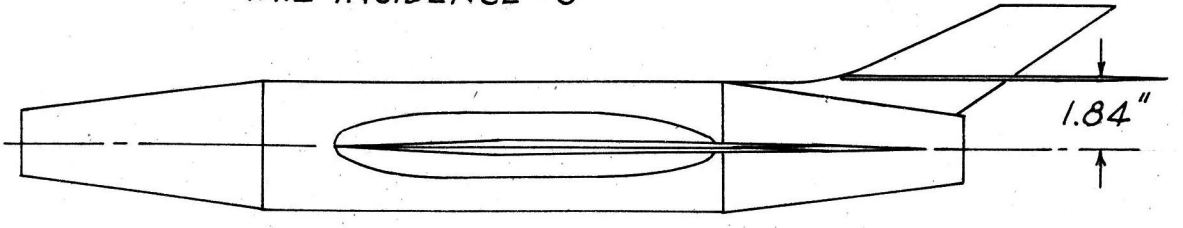

HORIZONTAL TAIL AREA = 18.5 % WING AREA

HORIZONTAL TAIL IN UPPER POSITION
(CONFIGURATION WBXH$_2$V)

FIG. 18

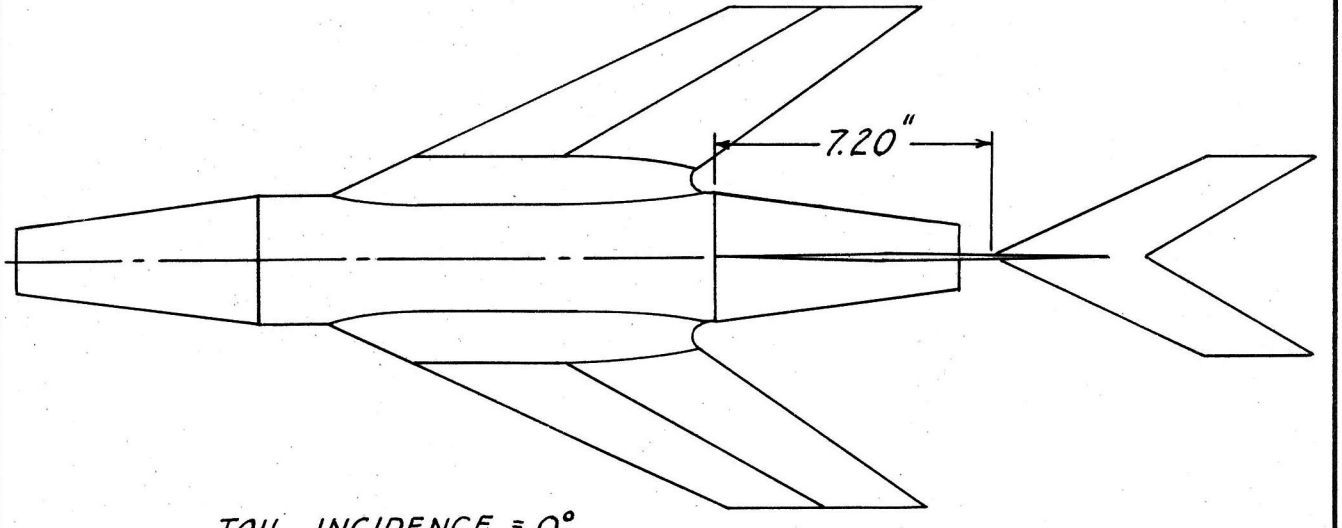

TAIL INCIDENCE = 0°

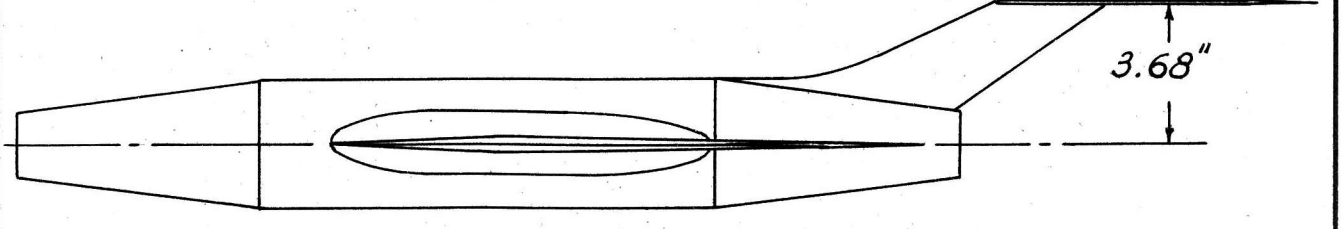

FULL SPAN SPLIT FLAP (CONFIGURATION $W_\Delta F_7$)

FIG. 19

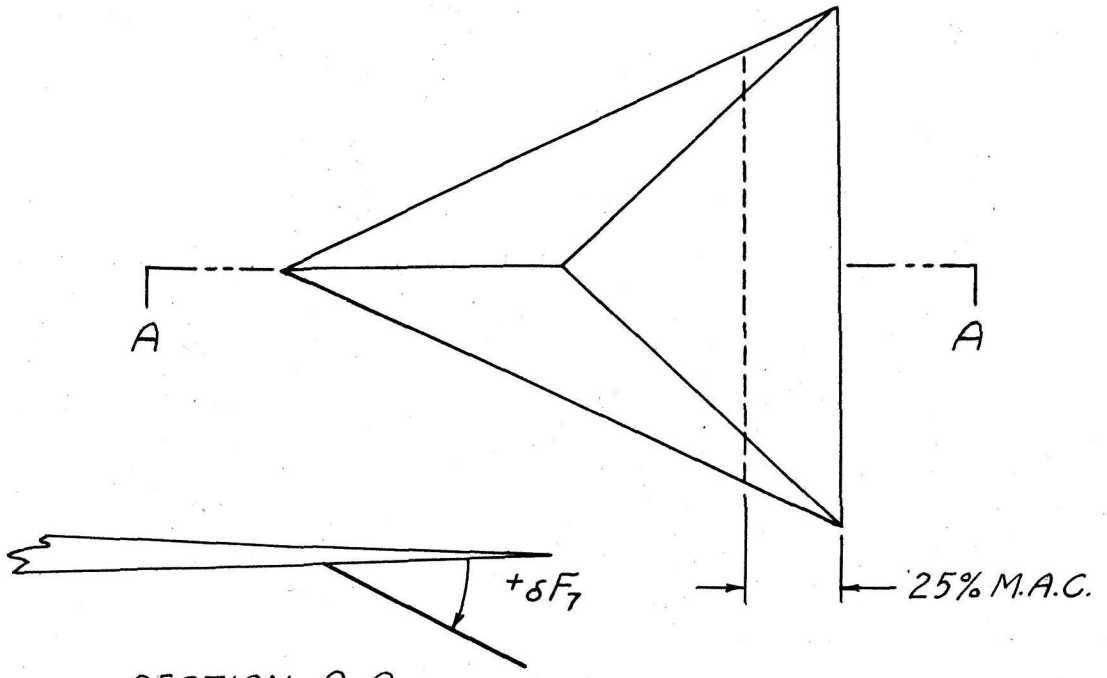

SECTION A-A

F_7 FLAP AREA = 30.4 % WING AREA

FILLET (CONFIGURATION $W_\Delta BXV$)

FIG. 20

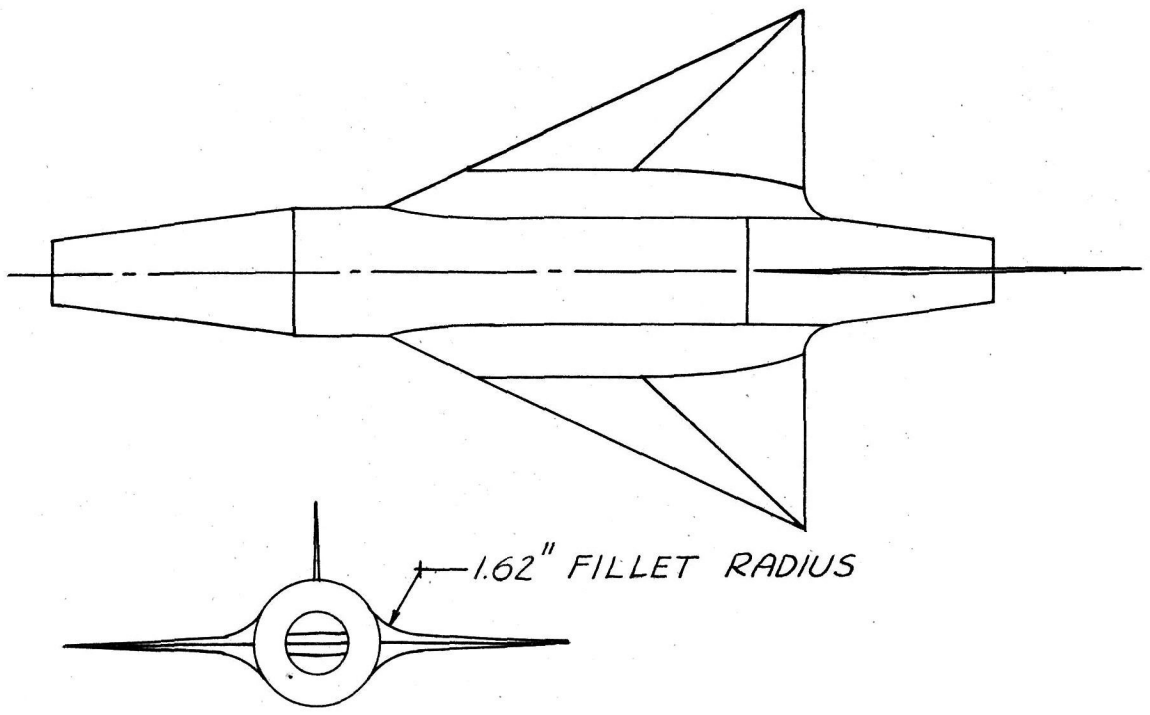

FULL SPAN NOSE FLAP (CONFIGURATION $W_\Delta BK_5V$)

FIG. 21

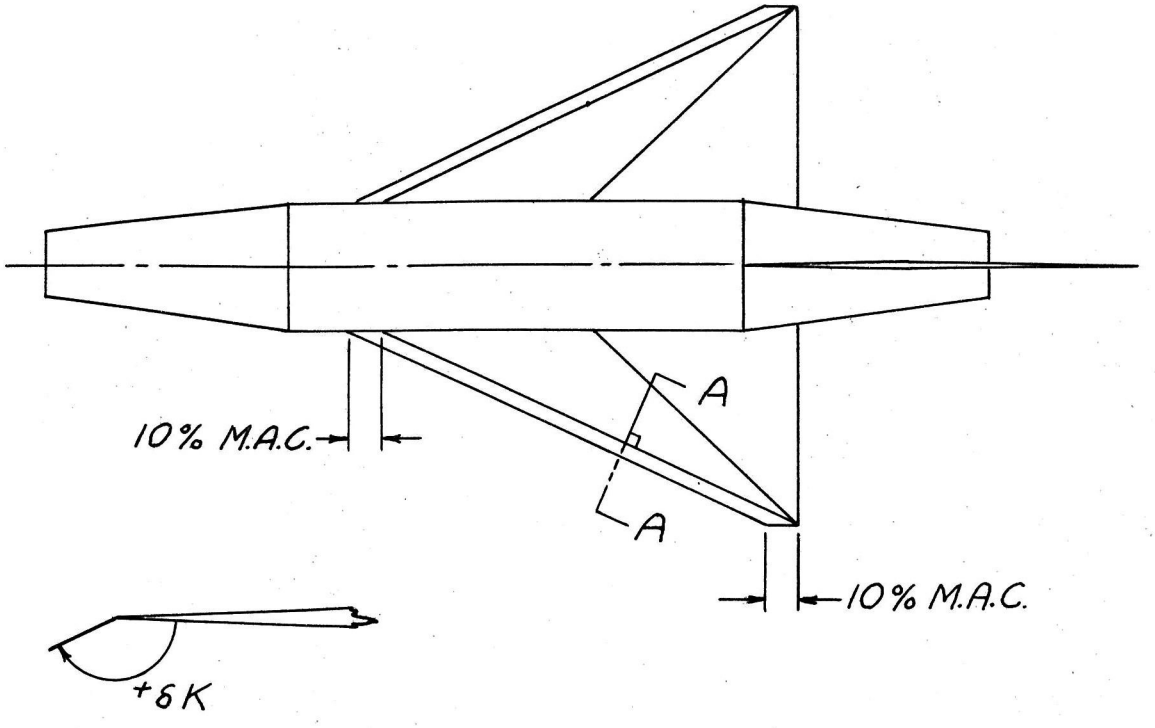

SECTION A-A

K_5 FLAP AREA = 10.04% WING AREA

PARTIAL SPAN 25% NOSE FLAP (CONFIGURATION $W_\Delta BK_6V$)

FIG. 22

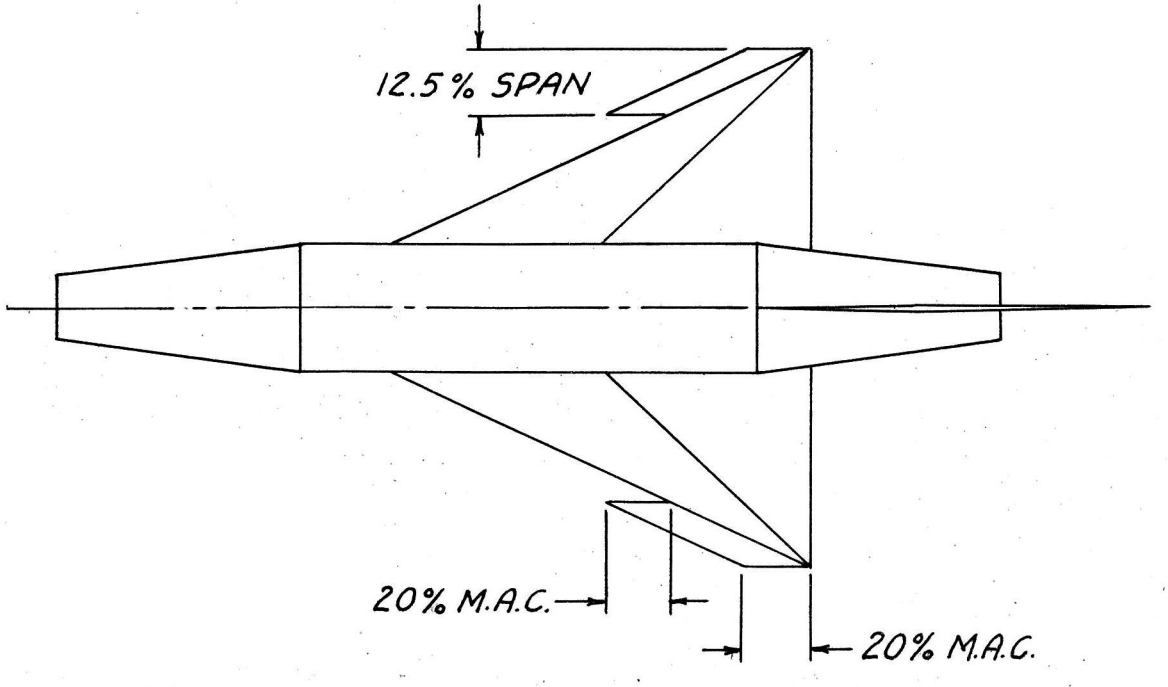

K_6 FLAP AREA = 6.66% WING AREA

HORIZONTAL TAIL IN LOWER POSITION
(CONFIGURATION $W_\Delta BH_1V$)

FIG. 23

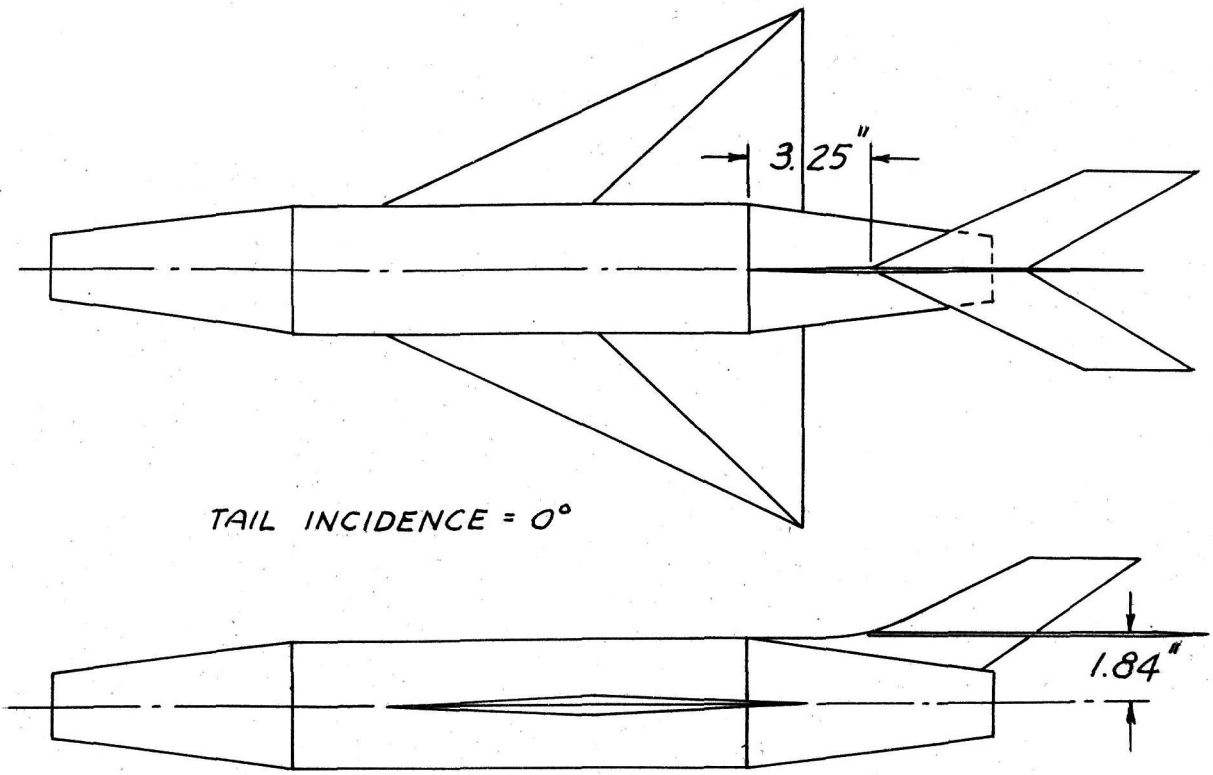

HORIZONTAL TAIL AREA = 18.5% WING AREA

HORIZONTAL TAIL IN UPPER POSITION
(CONFIGURATION $W_\Delta BH_2V$)

FIG. 24

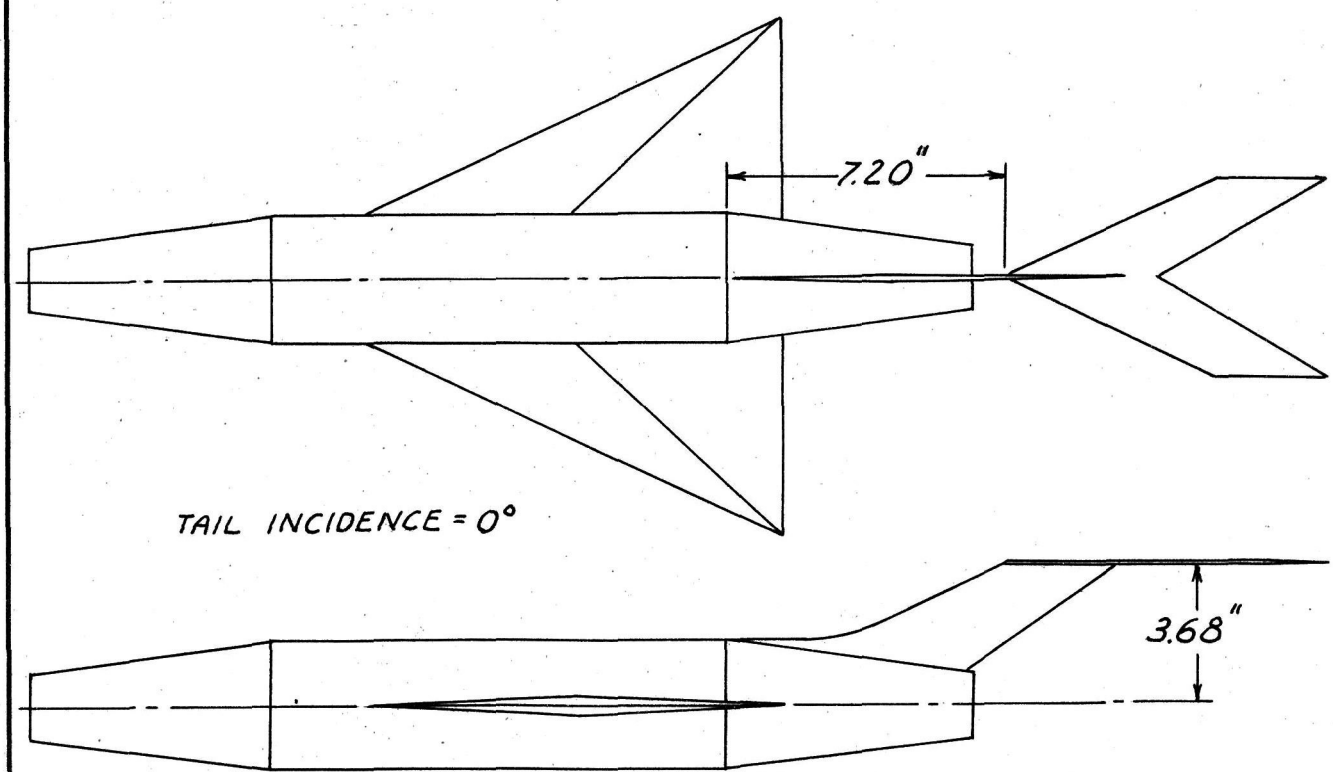

Tuft Symbol Definitions

—— Full line indicates a steady position of the tuft (smooth laminar flow).

– – Broken line indicates a tuft vibration of small amplitude and fairly constant frequency.

—< Crow-foot line indicates a violent oscillation of large amplitude (completely stalled).

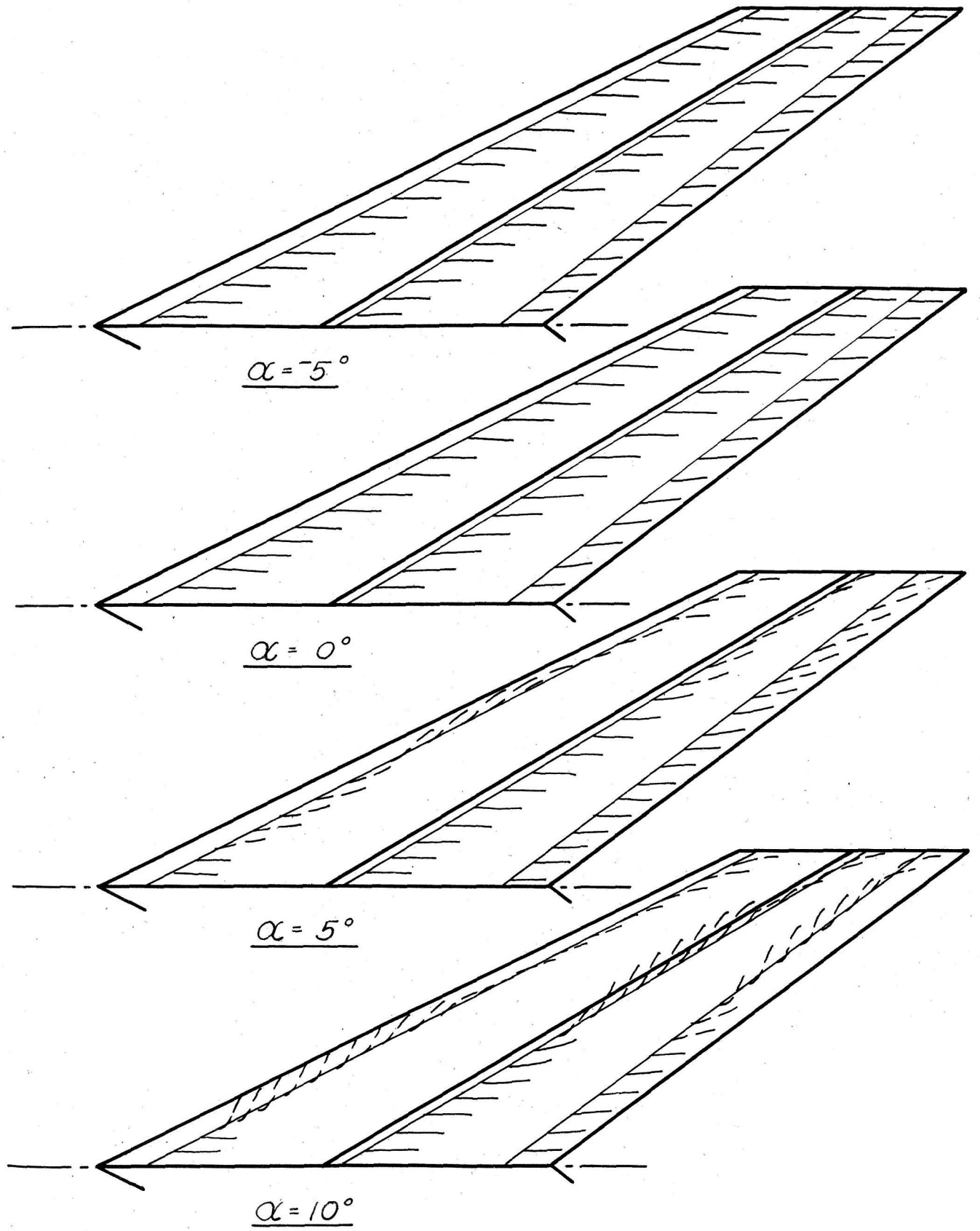
α = -5°
α = 0°
α = 5°
α = 10°

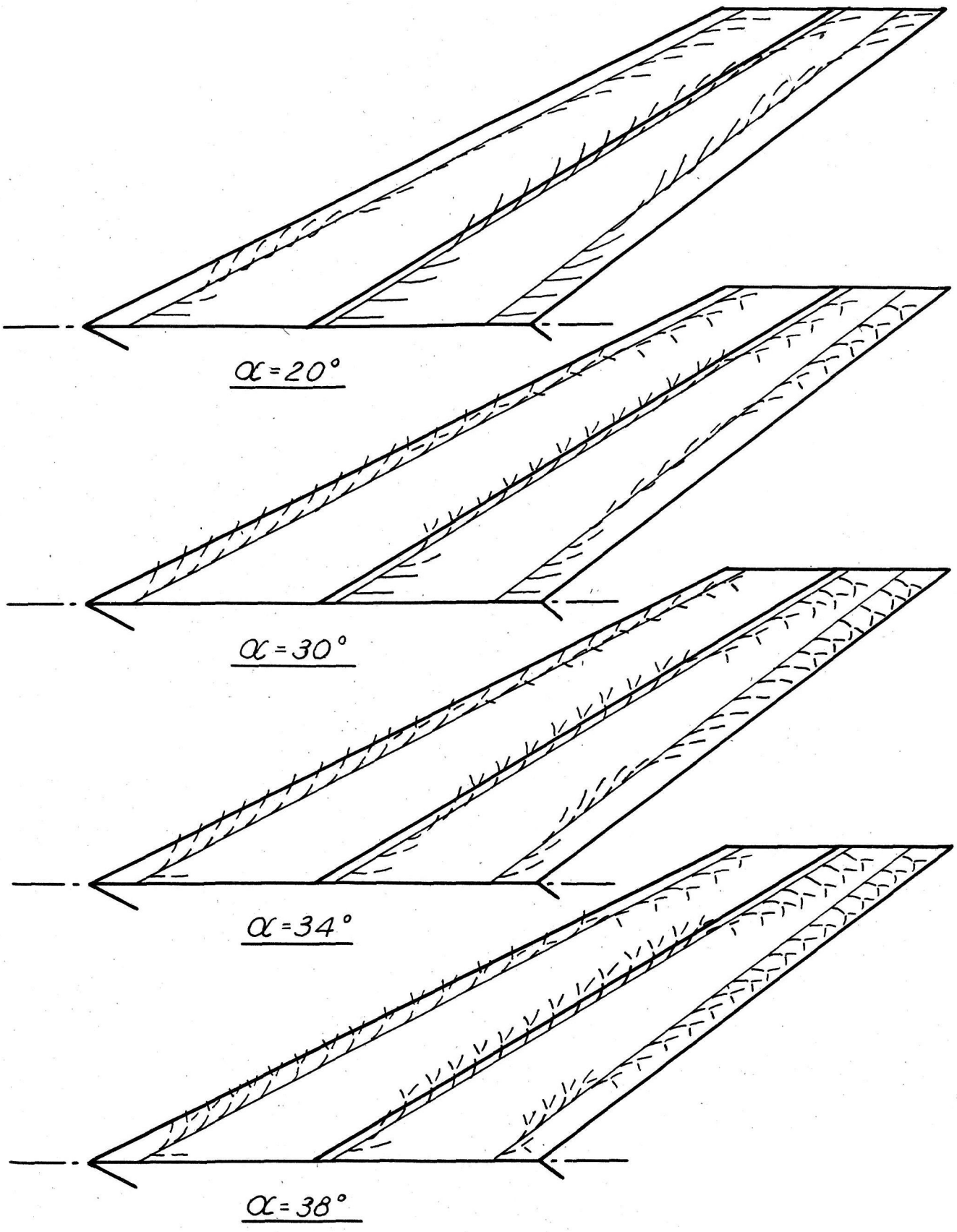
α = 20°
α = 30°
α = 34°
α = 38°

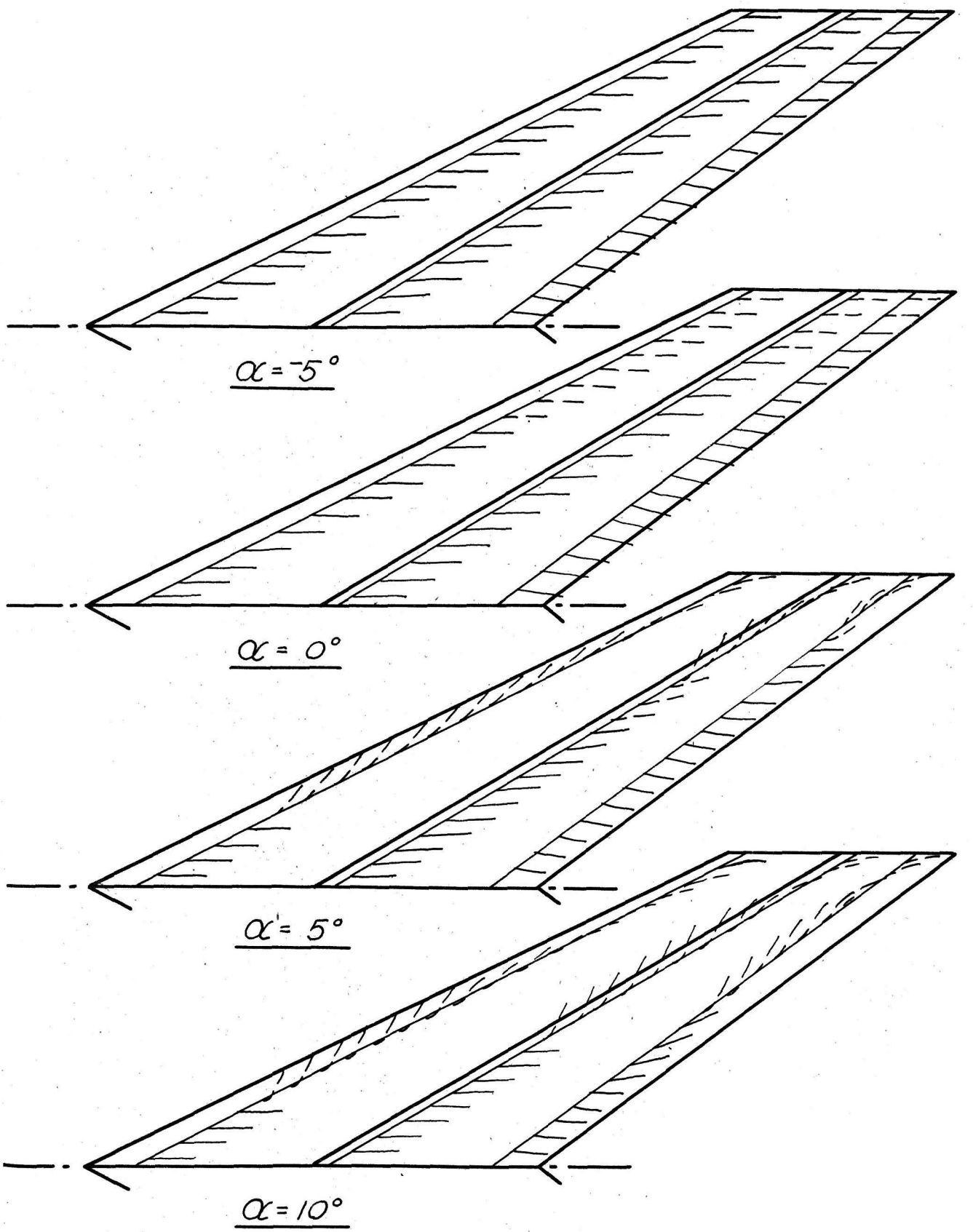
α = -5°
α = 0°
α = 5°
α = 10°

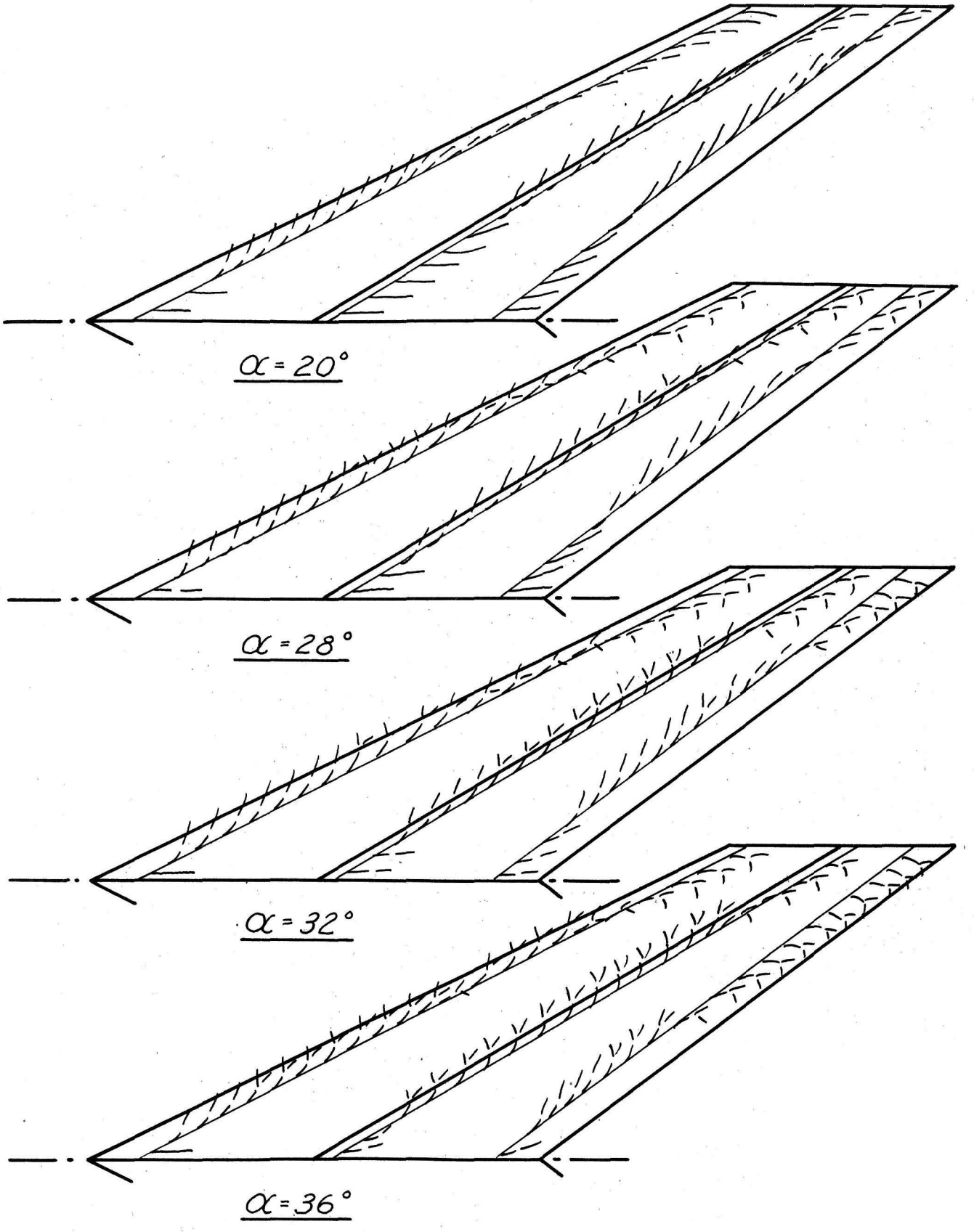
α = 20°
α = 28°
α = 32°
α = 36°

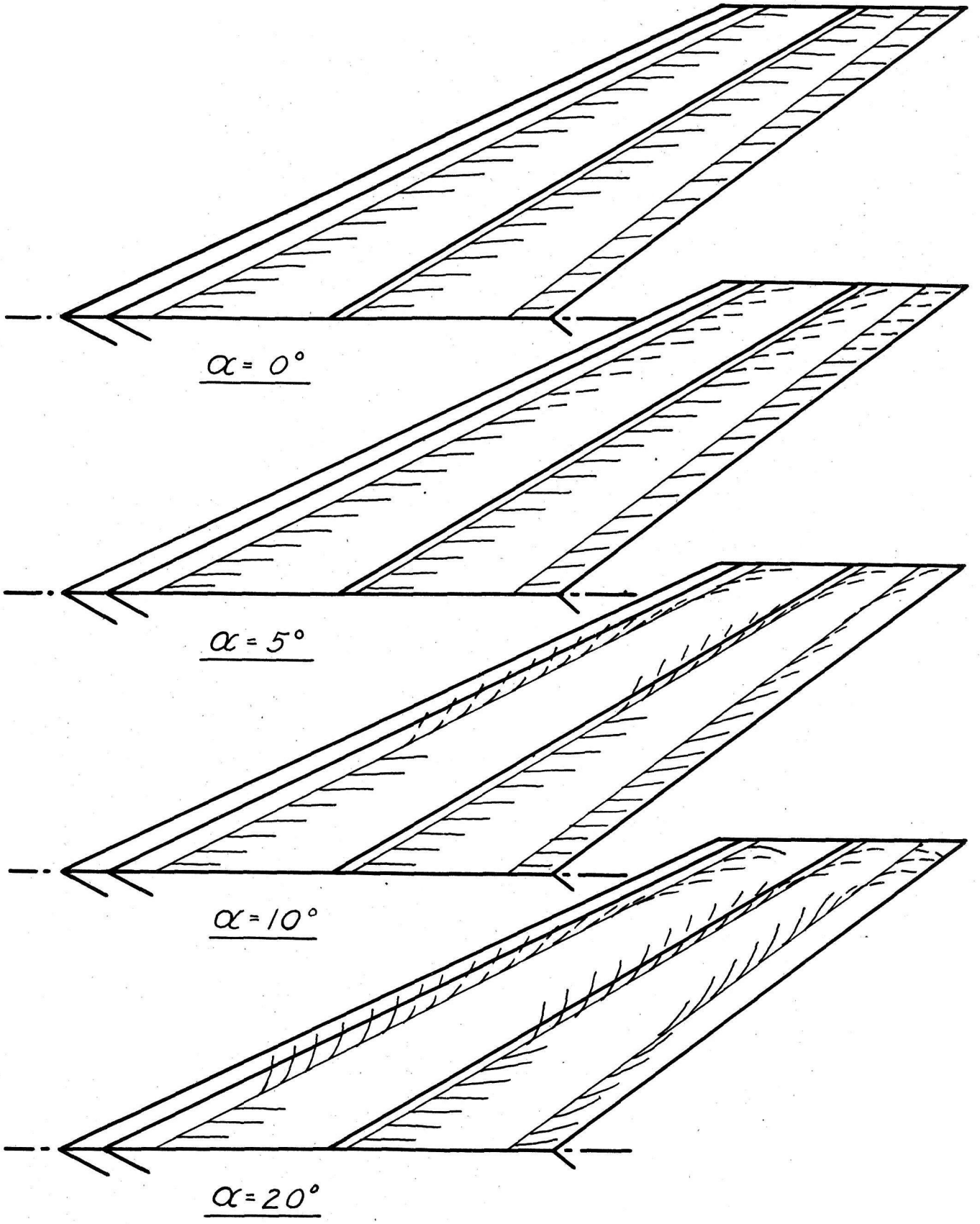
α = 0°
α = 5°
α = 10°
α = 20°

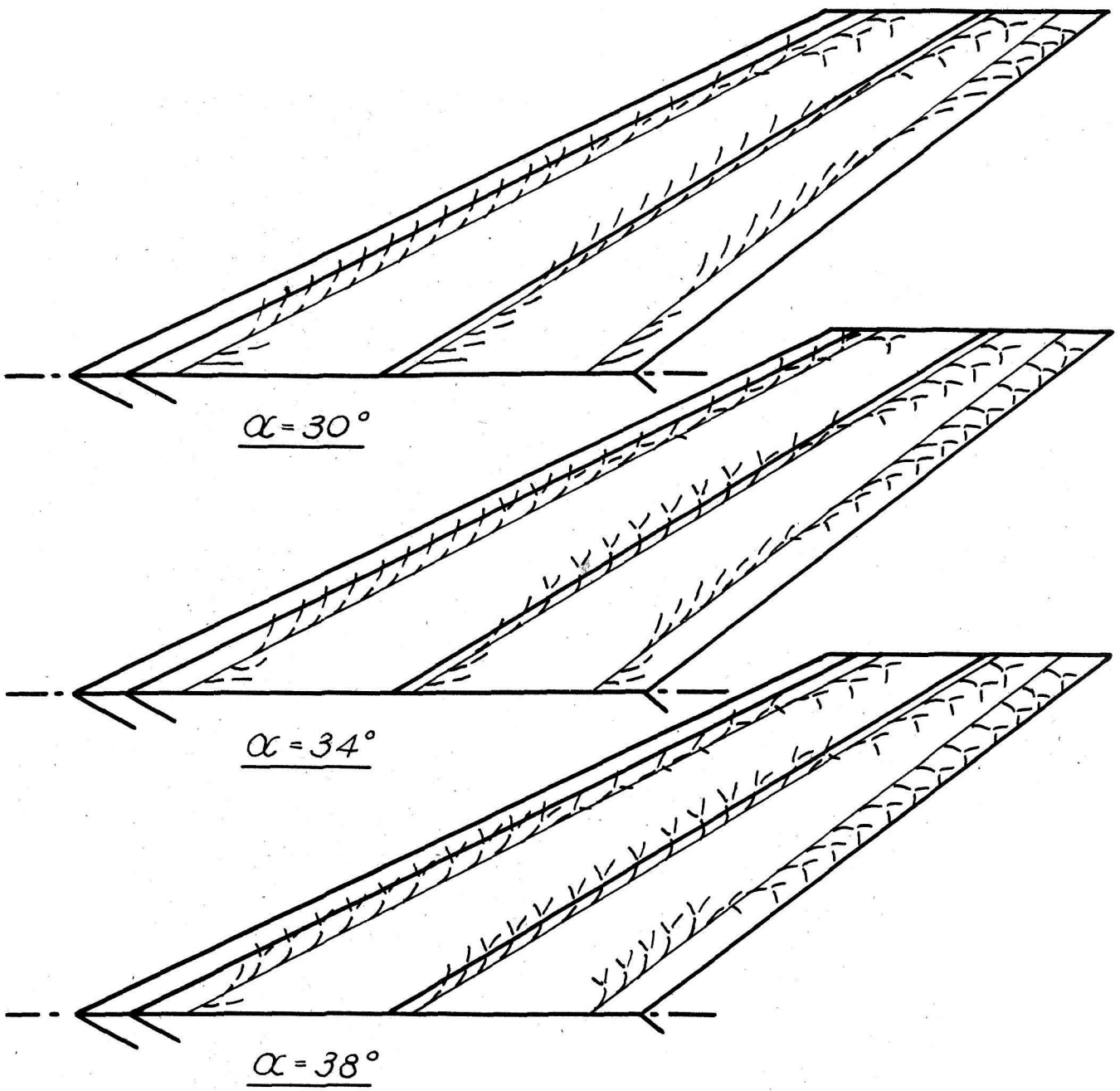
α = 30°
α = 34°
α = 38°

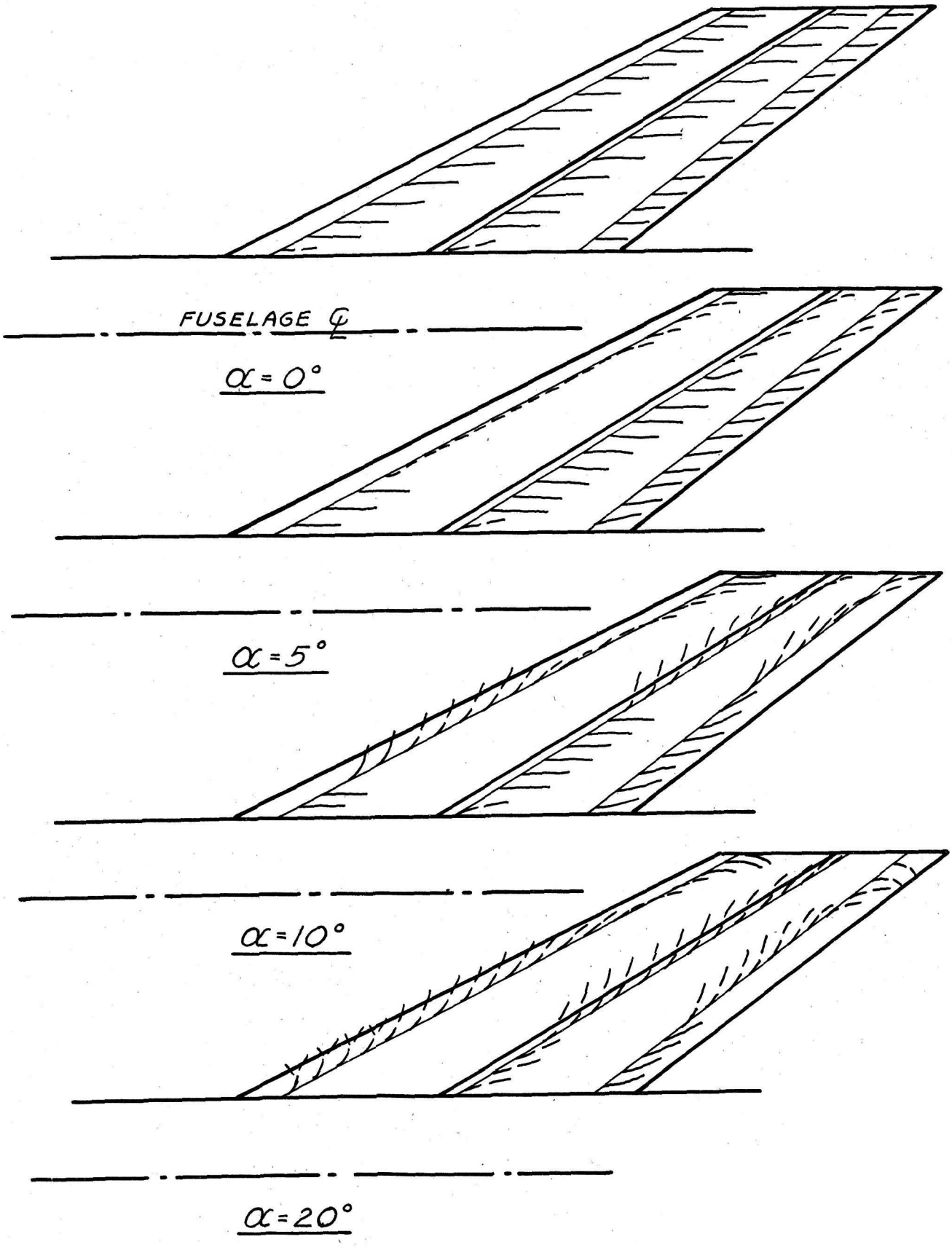
FUSELAGE ℄
α = 0°
α = 5°
α = 10°
α = 20°

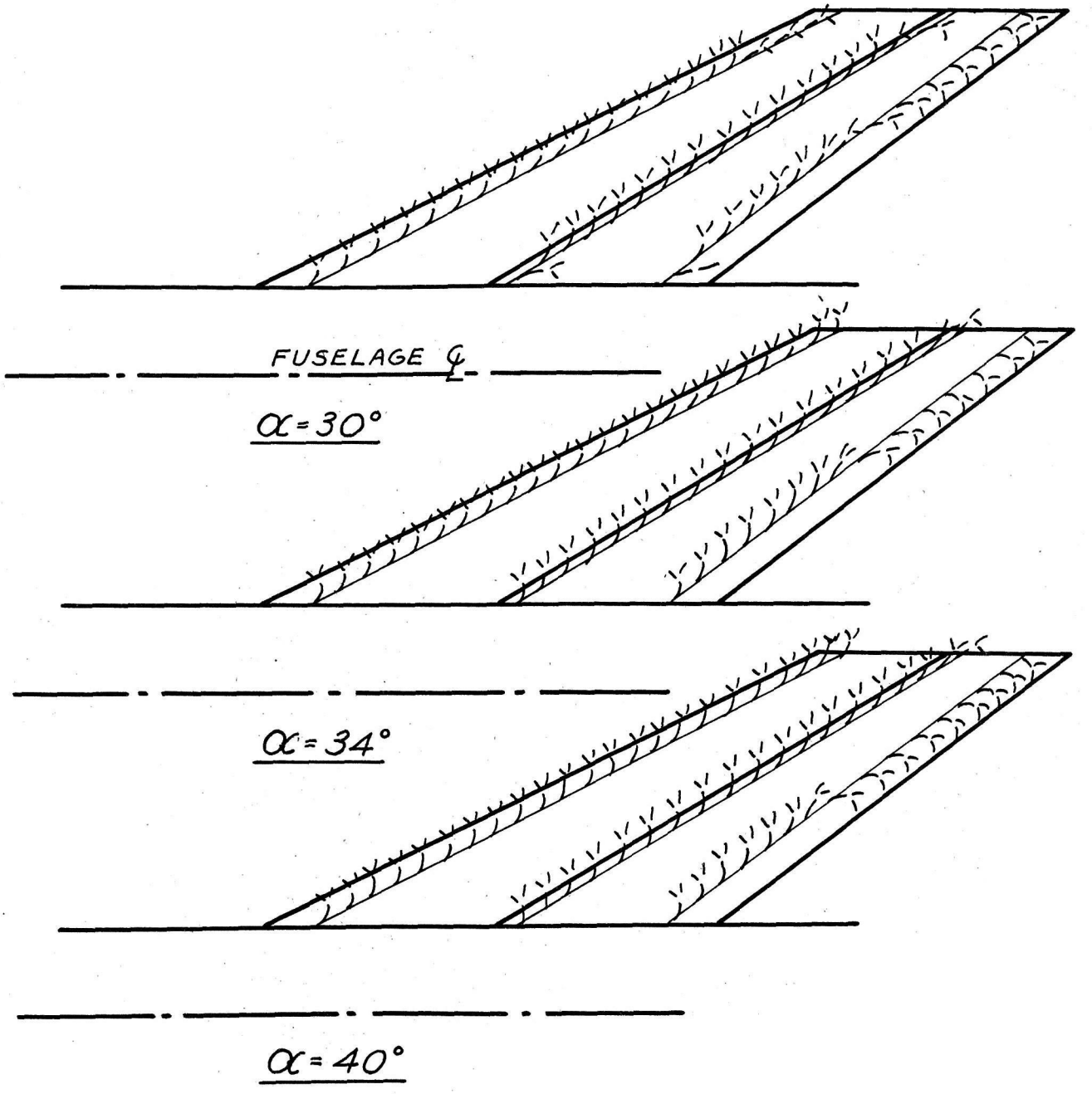
FUSELAGE ℄
α = 30°
α = 34°
α = 40°

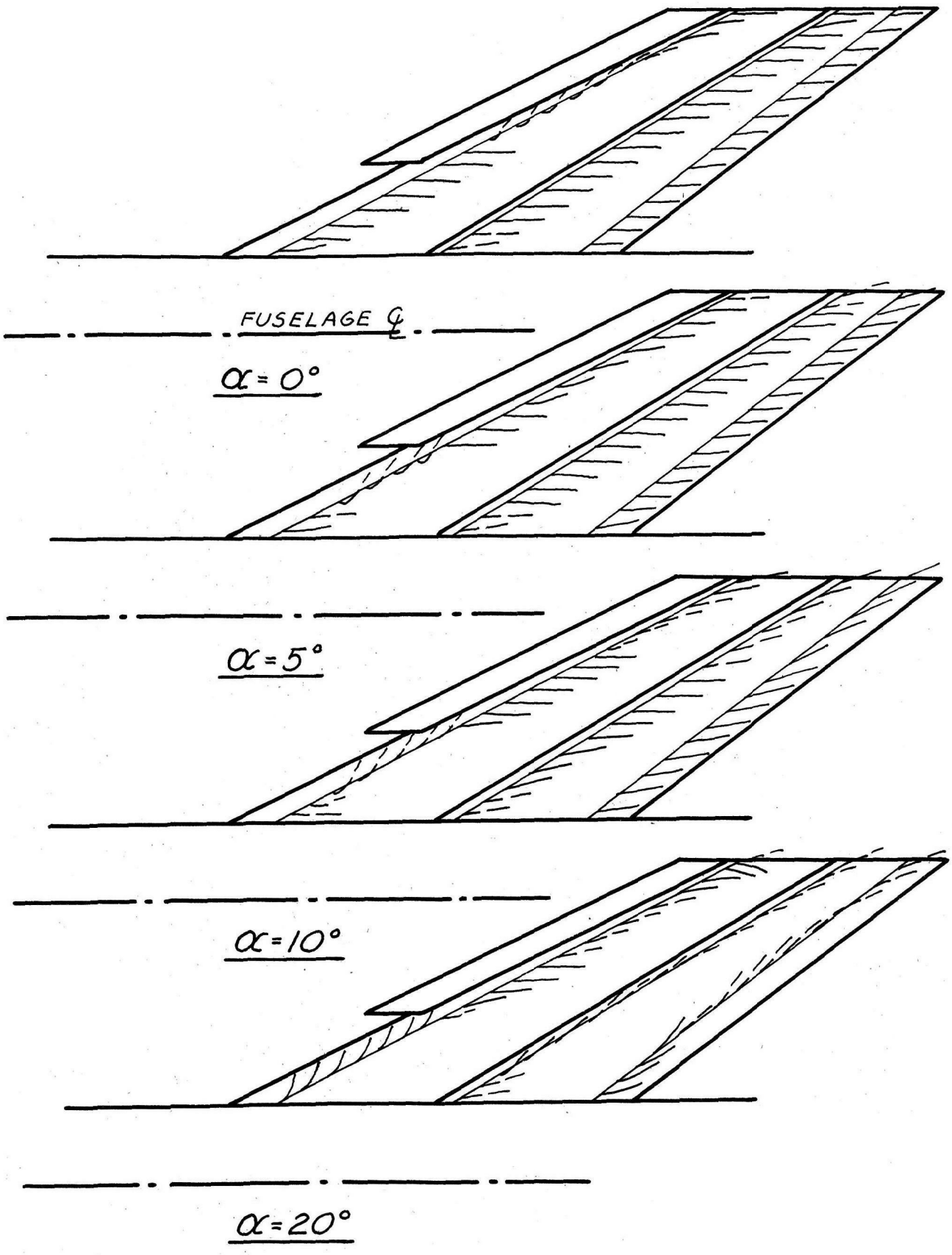
FUSELAGE ℄
α = 0°
α = 5°
α = 10°
α = 20°

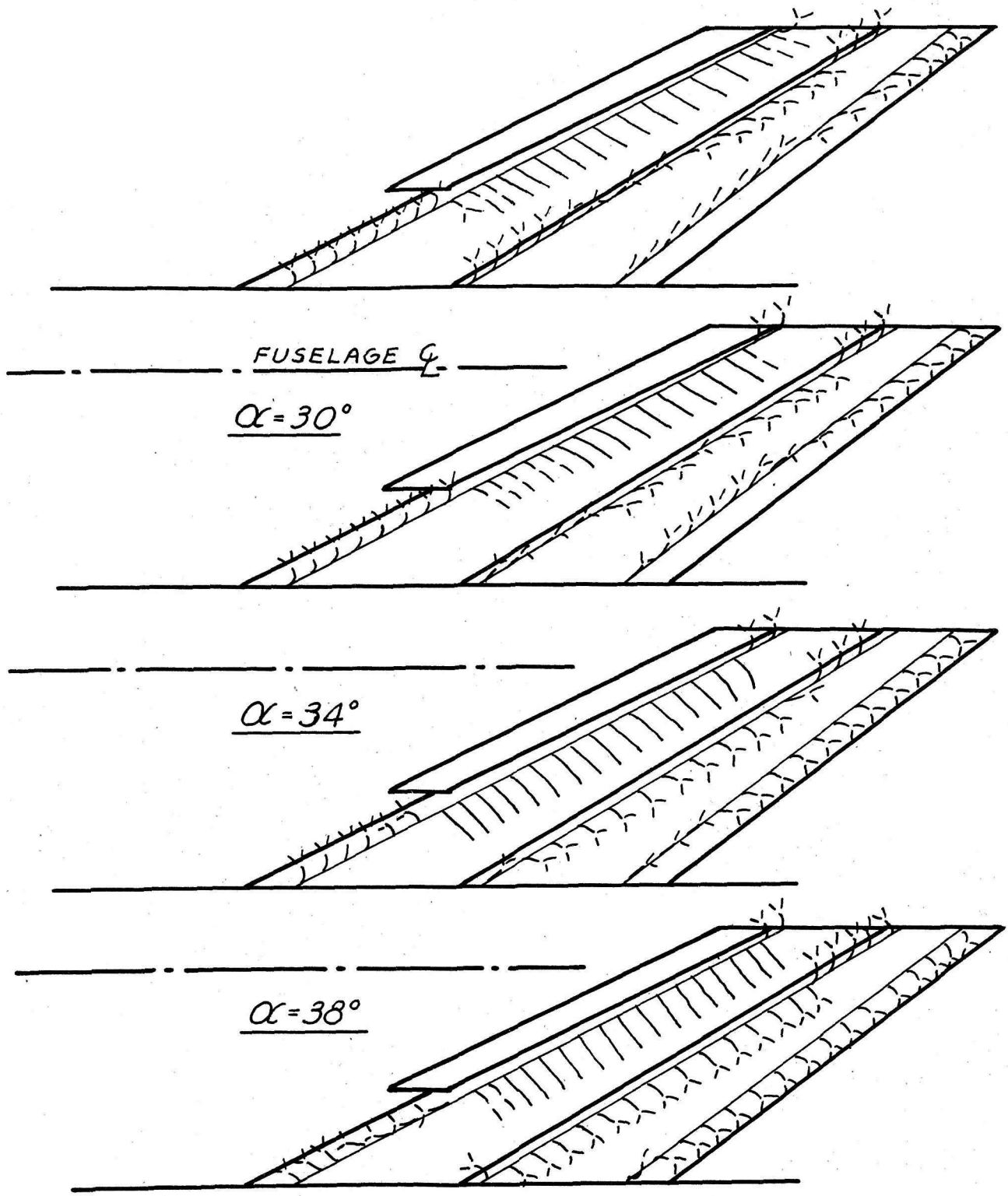
FUSELAGE ℄
α = 30°
α = 34°
α = 38°
α = 40°

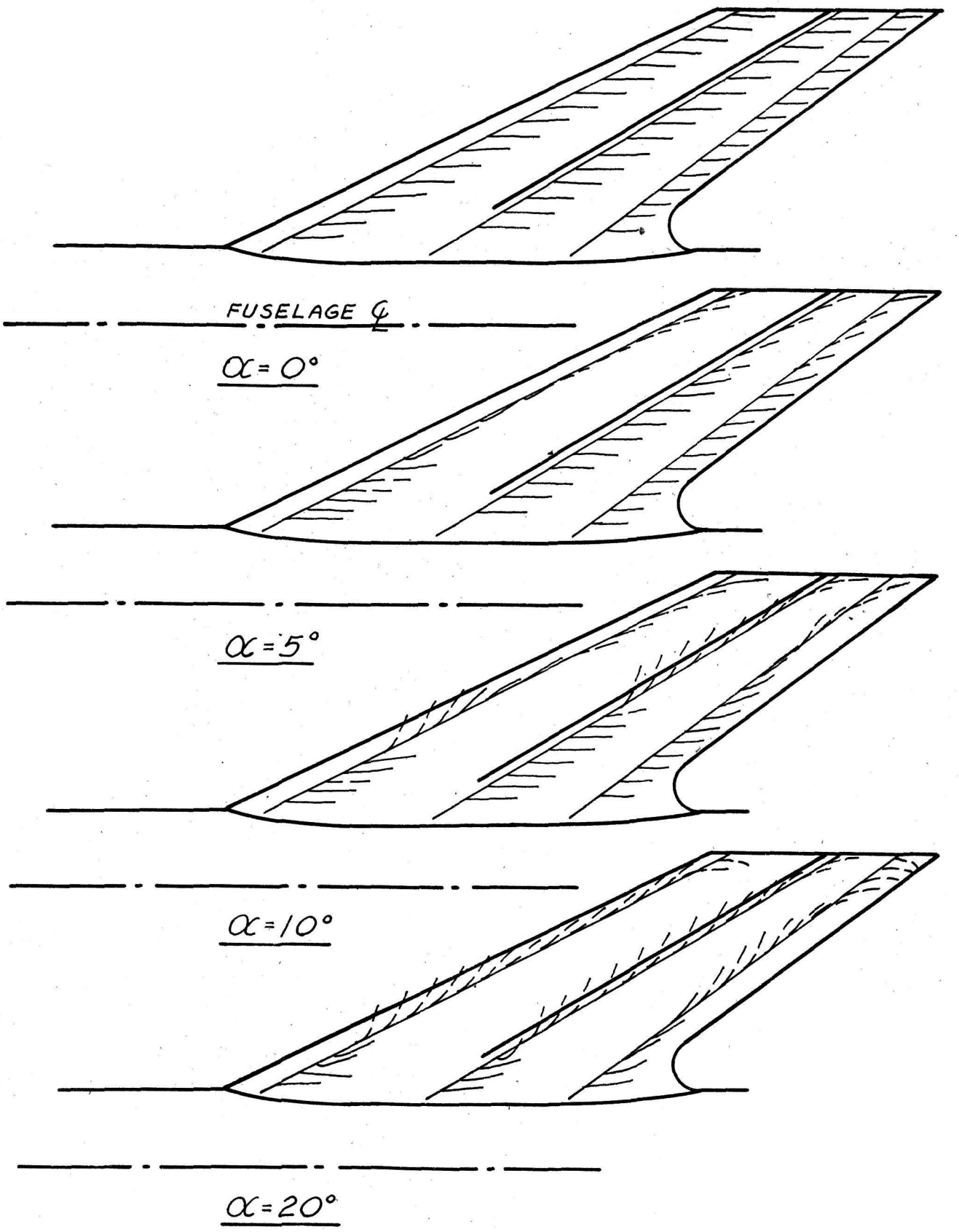
FUSELAGE ℄
α = 0°
α = 5°
α = 10°
α = 20°

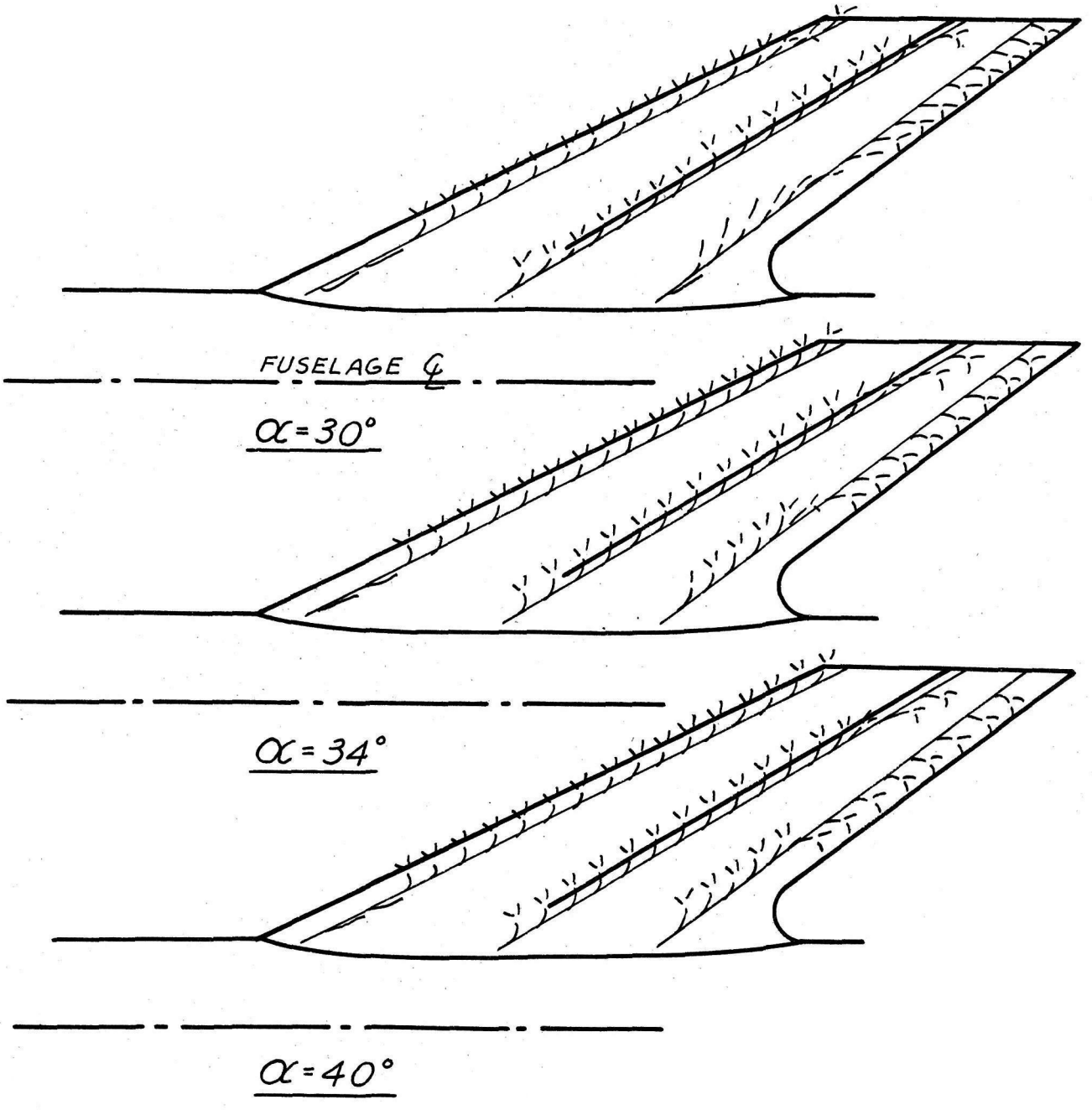
FUSELAGE ℄
α = 30°
α = 34°
α = 40°

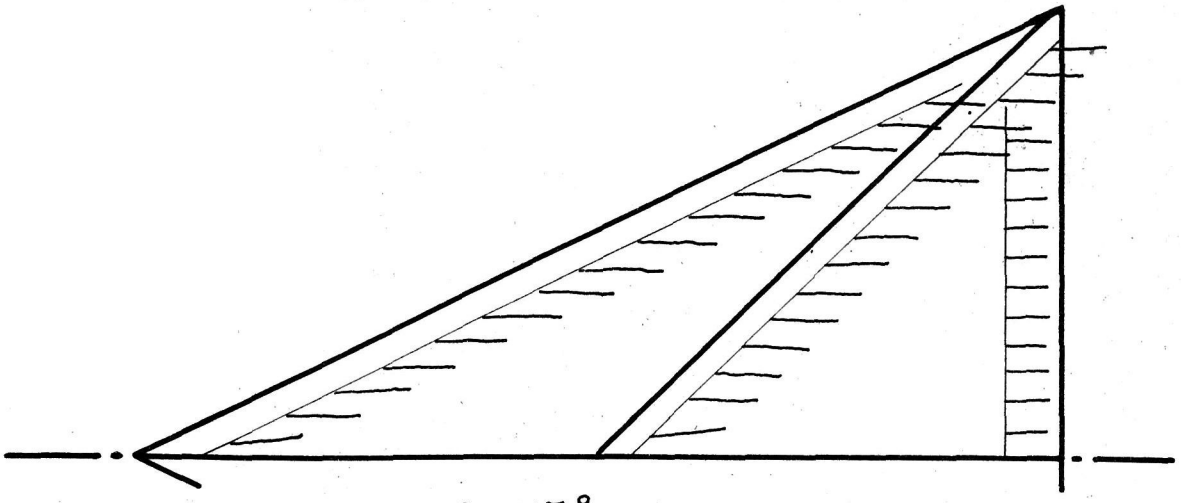

$\alpha = -5°$

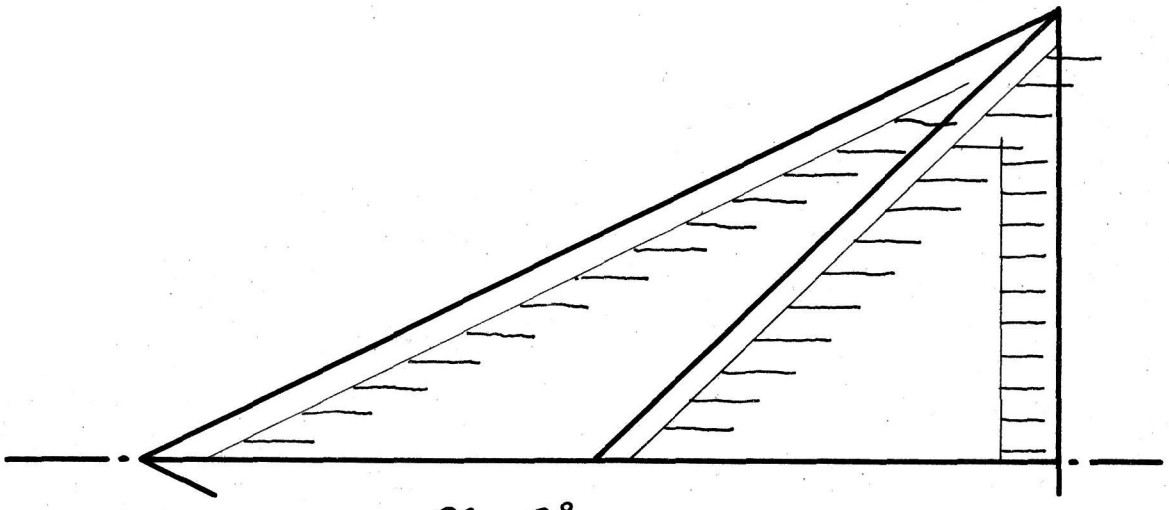

$\alpha = 0°$

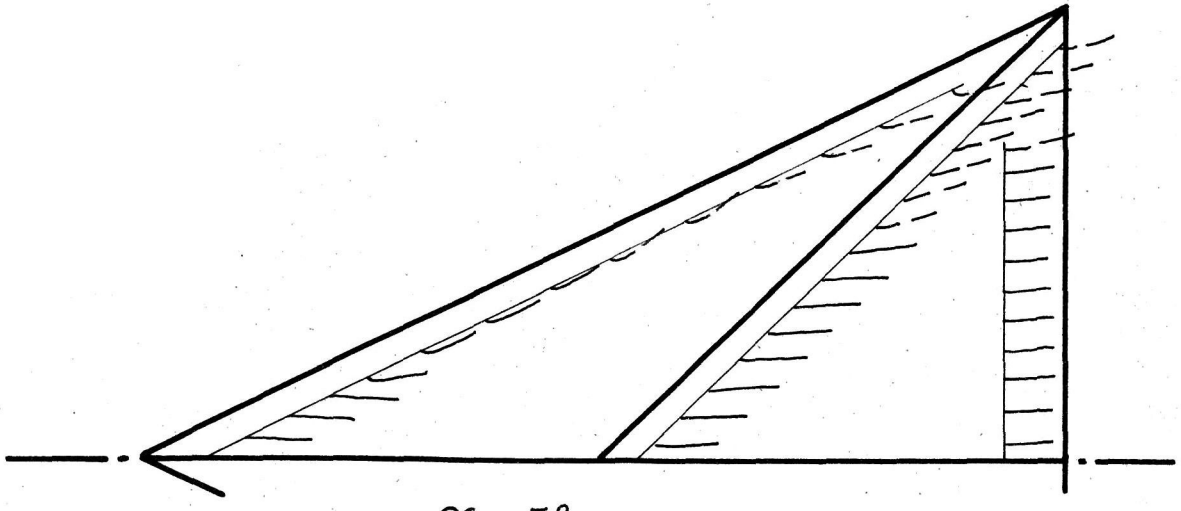

$\alpha = 5°$

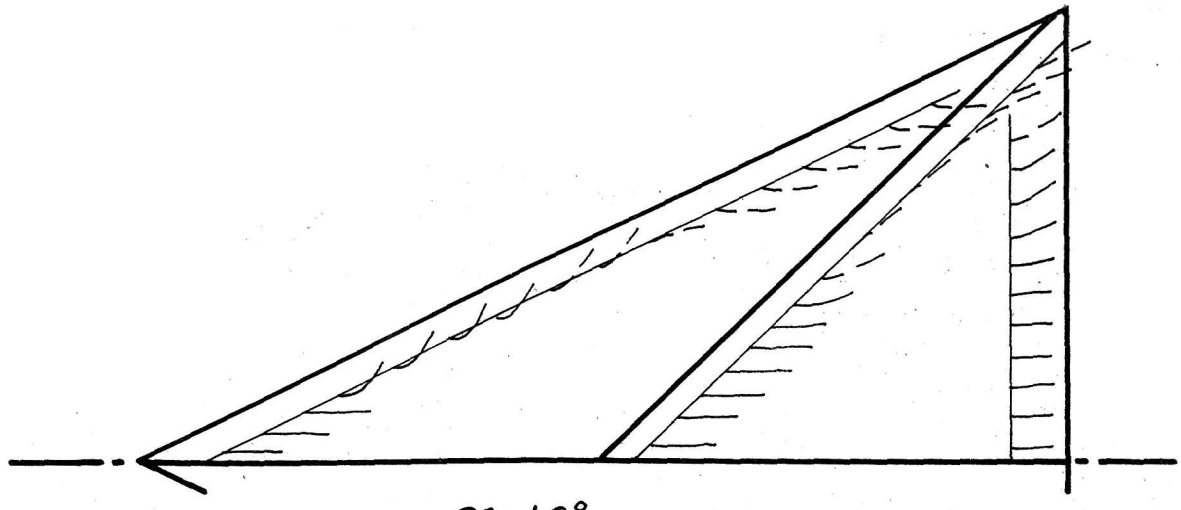

$\alpha = 10°$

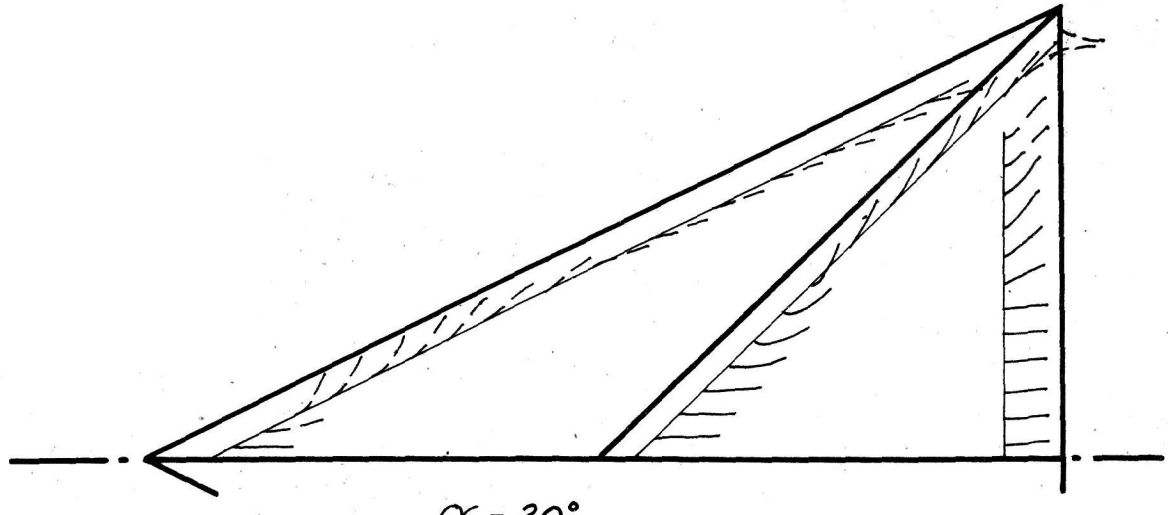

$\alpha = 20°$

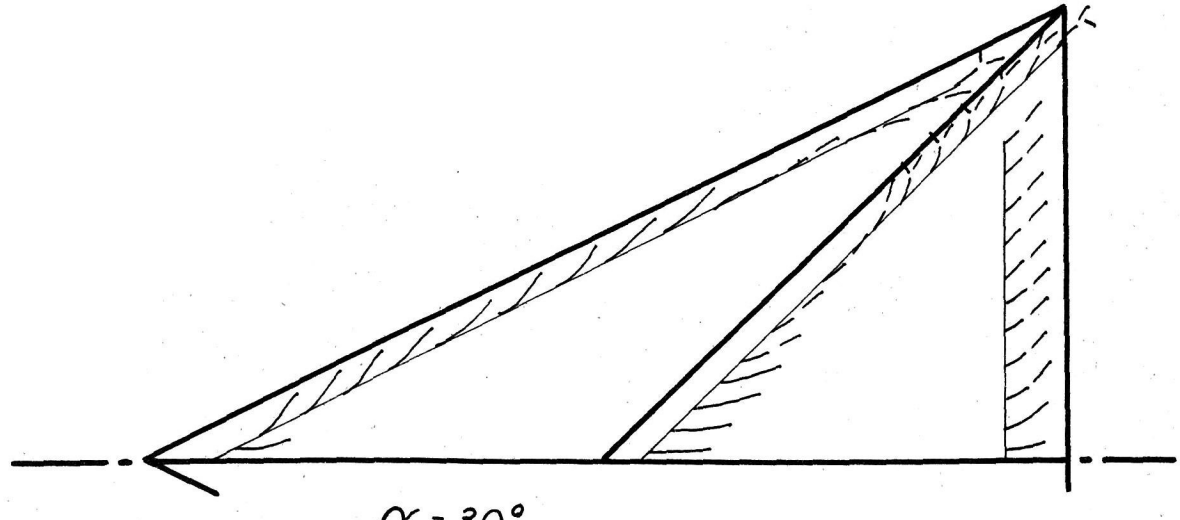

$\alpha = 30°$

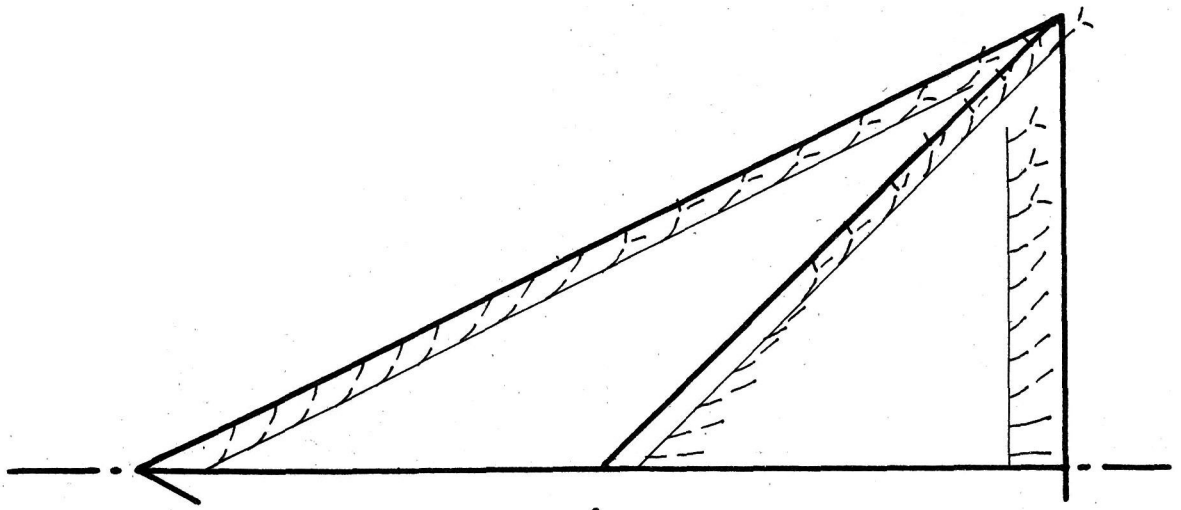

$\alpha = 34°$

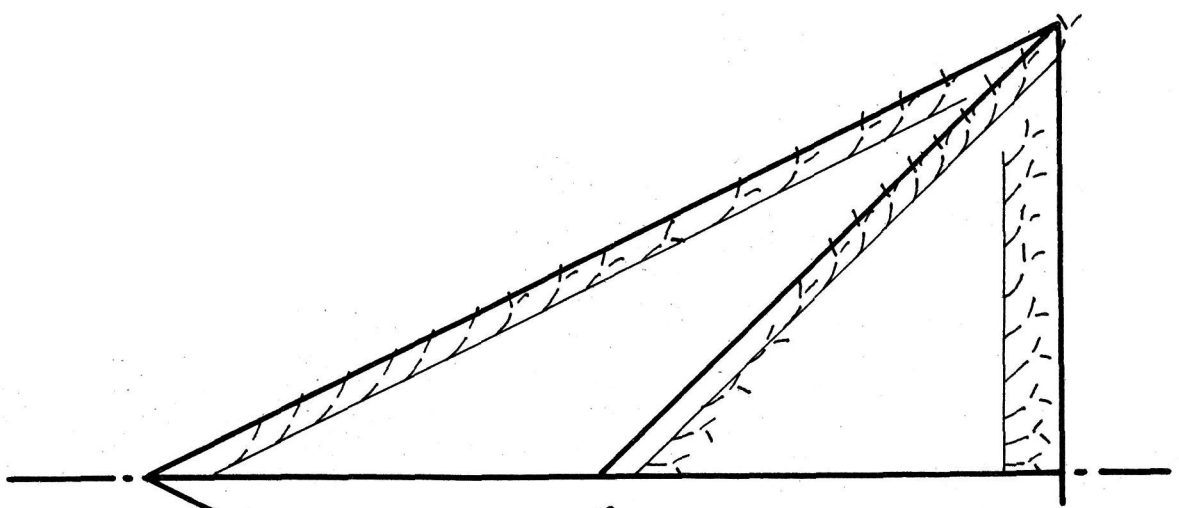

$\alpha = 37\frac{1}{2}°$

$W_\Delta BV$

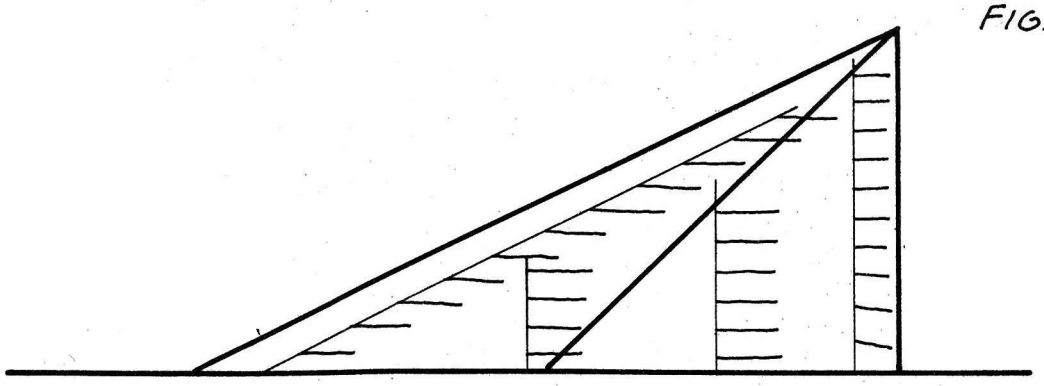

FUSELAGE $\mathcal{L}$

$\alpha = 0°$

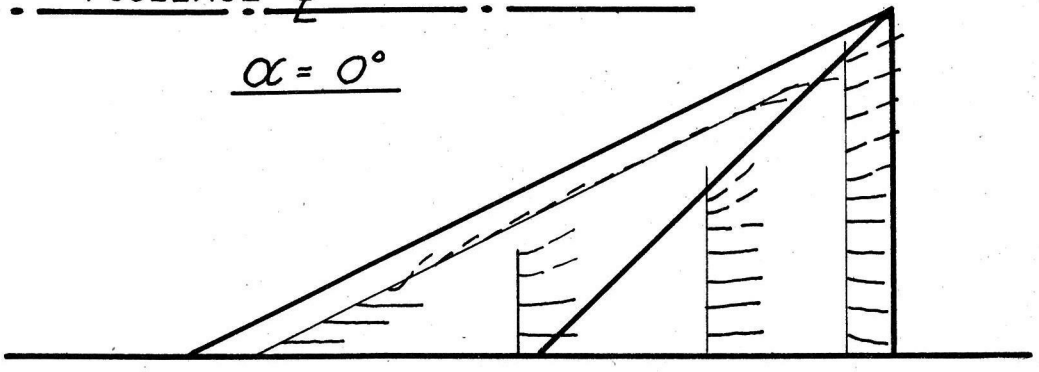

$\alpha = 5°$

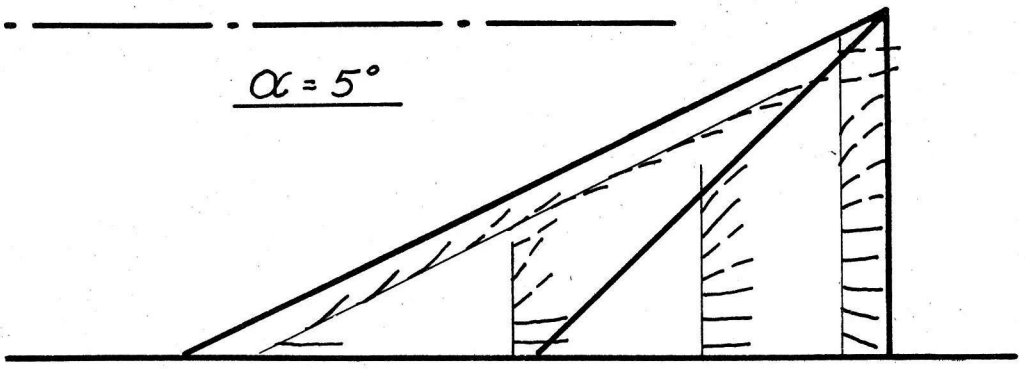

$\alpha = 10°$

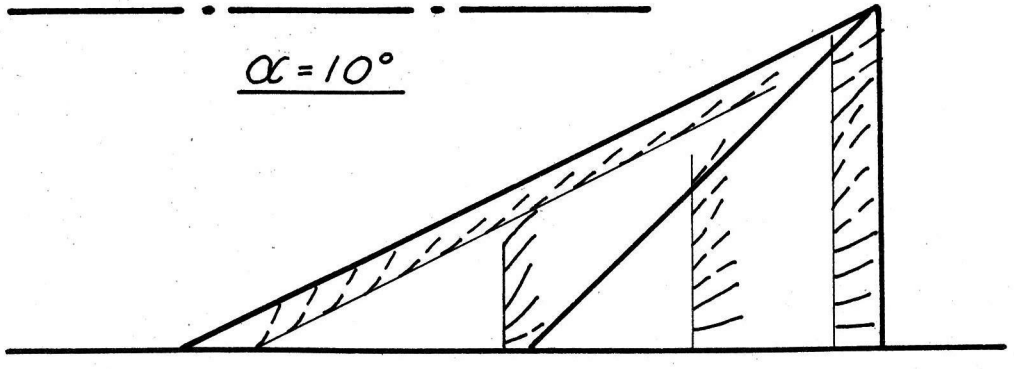

$\alpha = 20°$

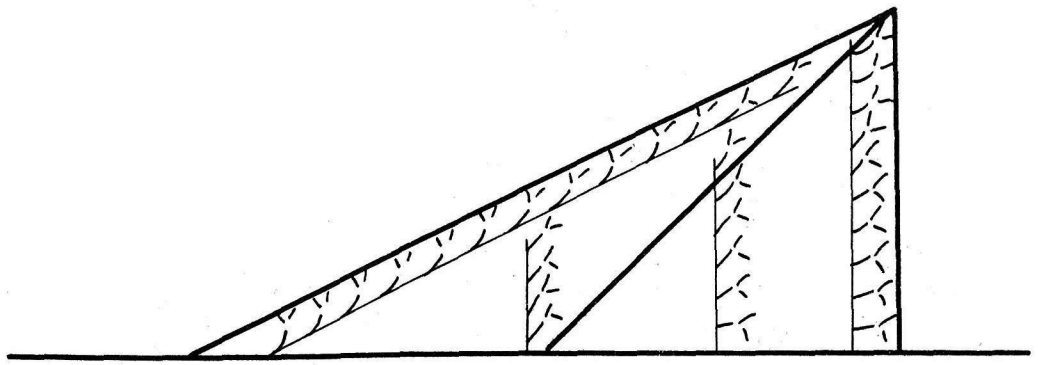

FUSELAGE $\mathcal{L}$

$\alpha = 30°$

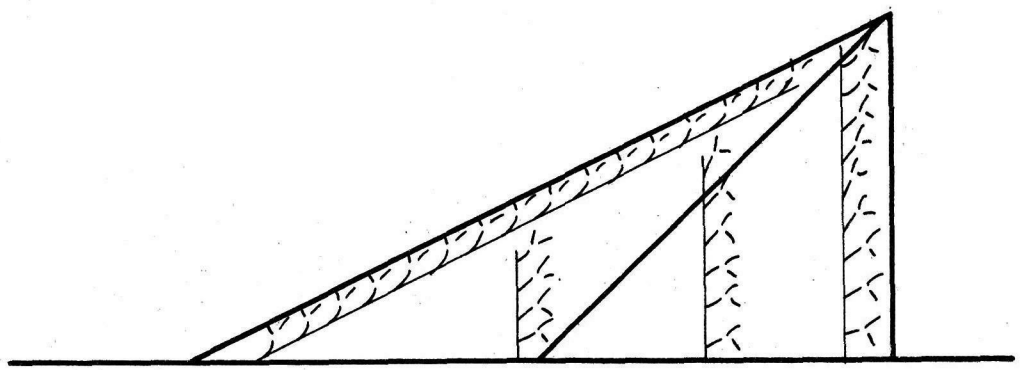

$\alpha = 35°$

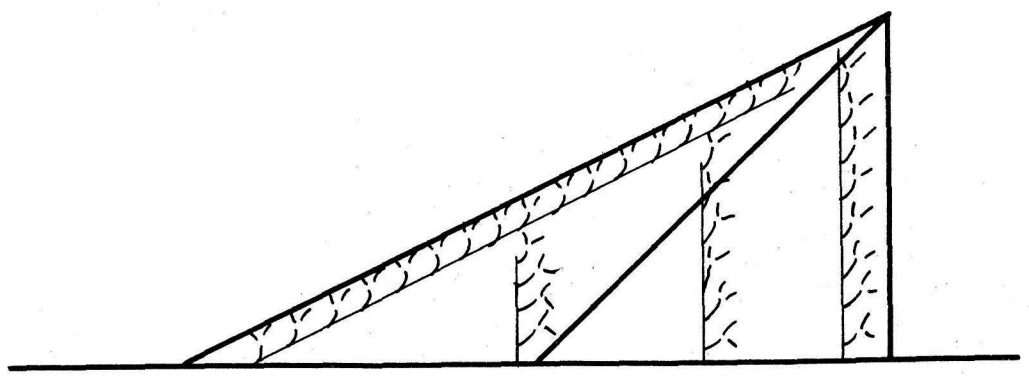

$\alpha = 40°$

WING VORTICES ON DELTA WING

TOP VIEWS

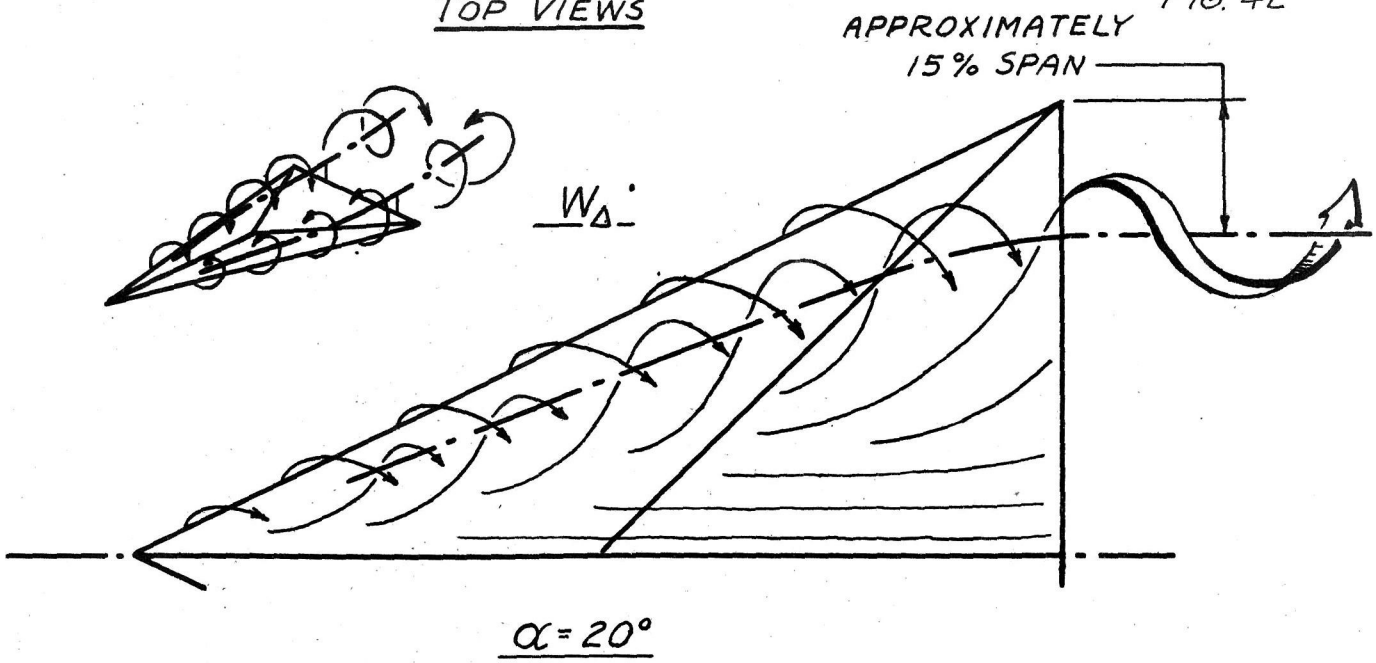

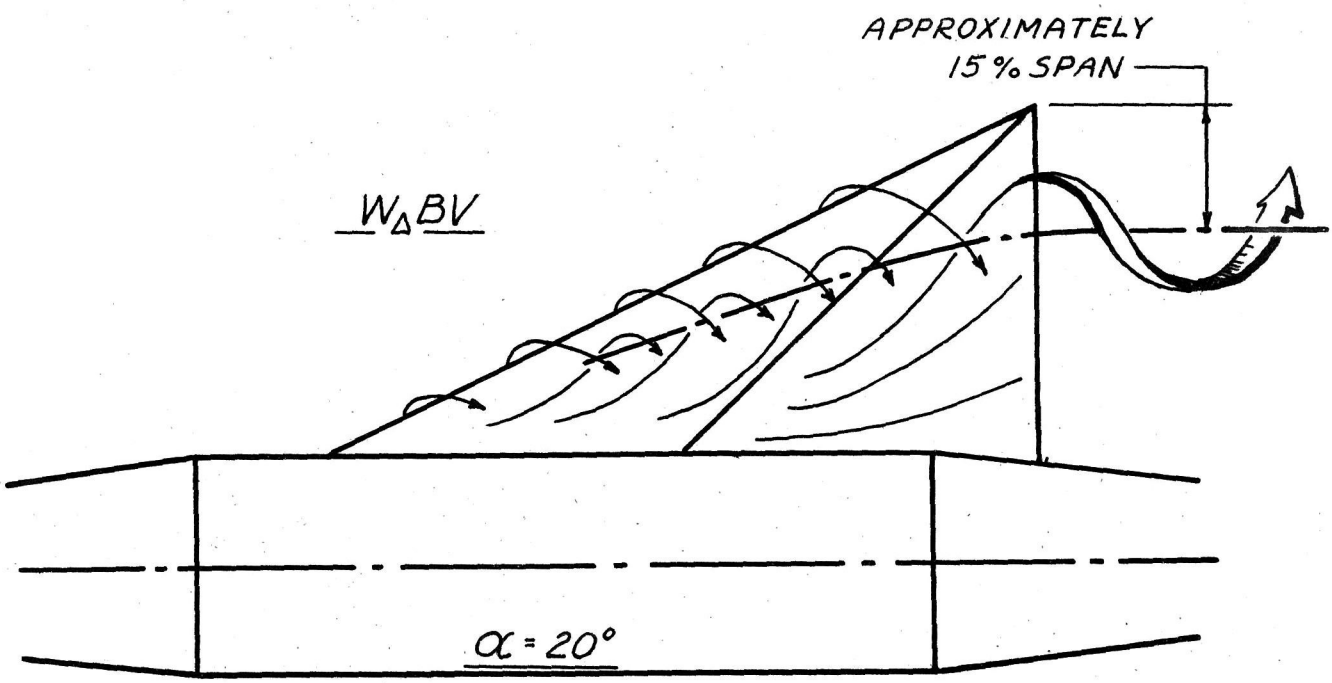

TYPICAL SIDE VIEWS OF VORTEX CORE:
AT $\alpha = 5°$; NO APPARENT VORTEX FORMATION.

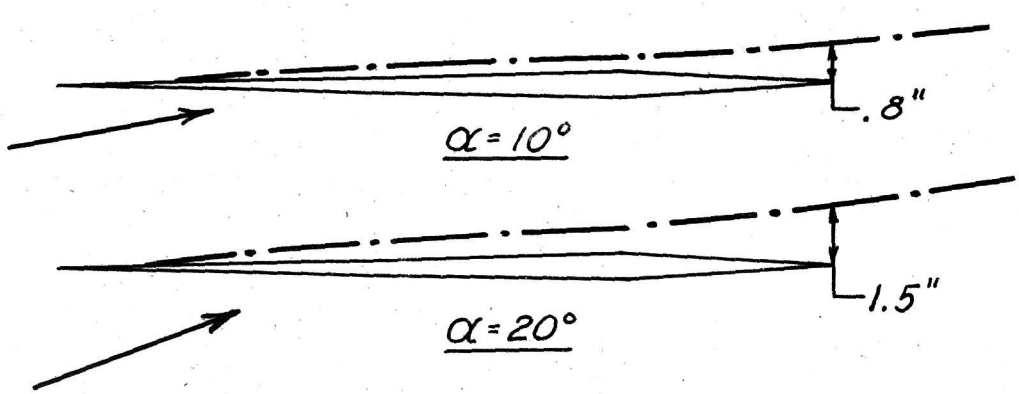

COMPARISON OF W AND W_Δ

PAGE 57
FIG. 43

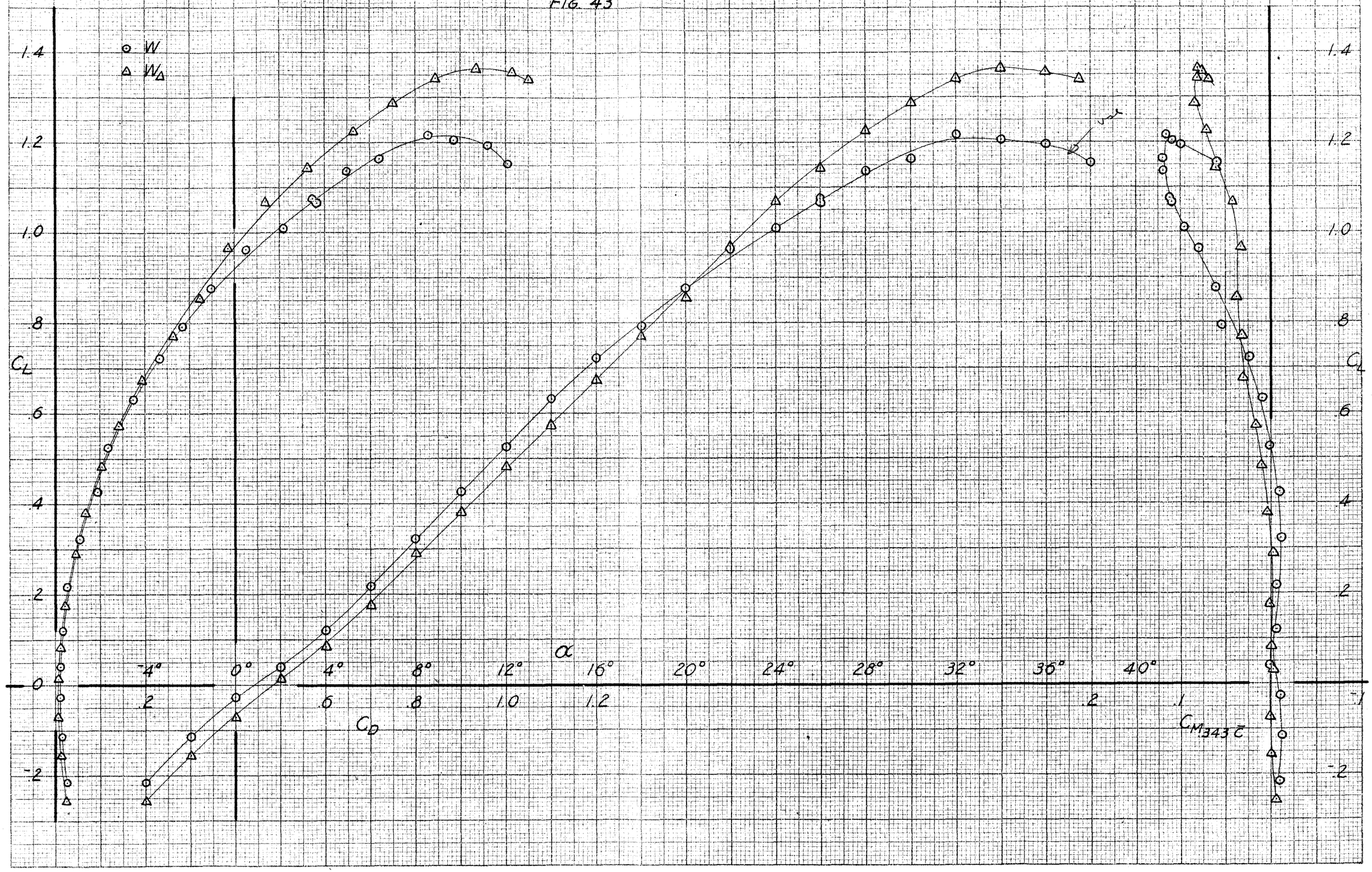

COMPARISON OF WBV AND $W_\Delta BV$

PAGE 58
FIG. 44

○ WBV
△ $W_\Delta BV$

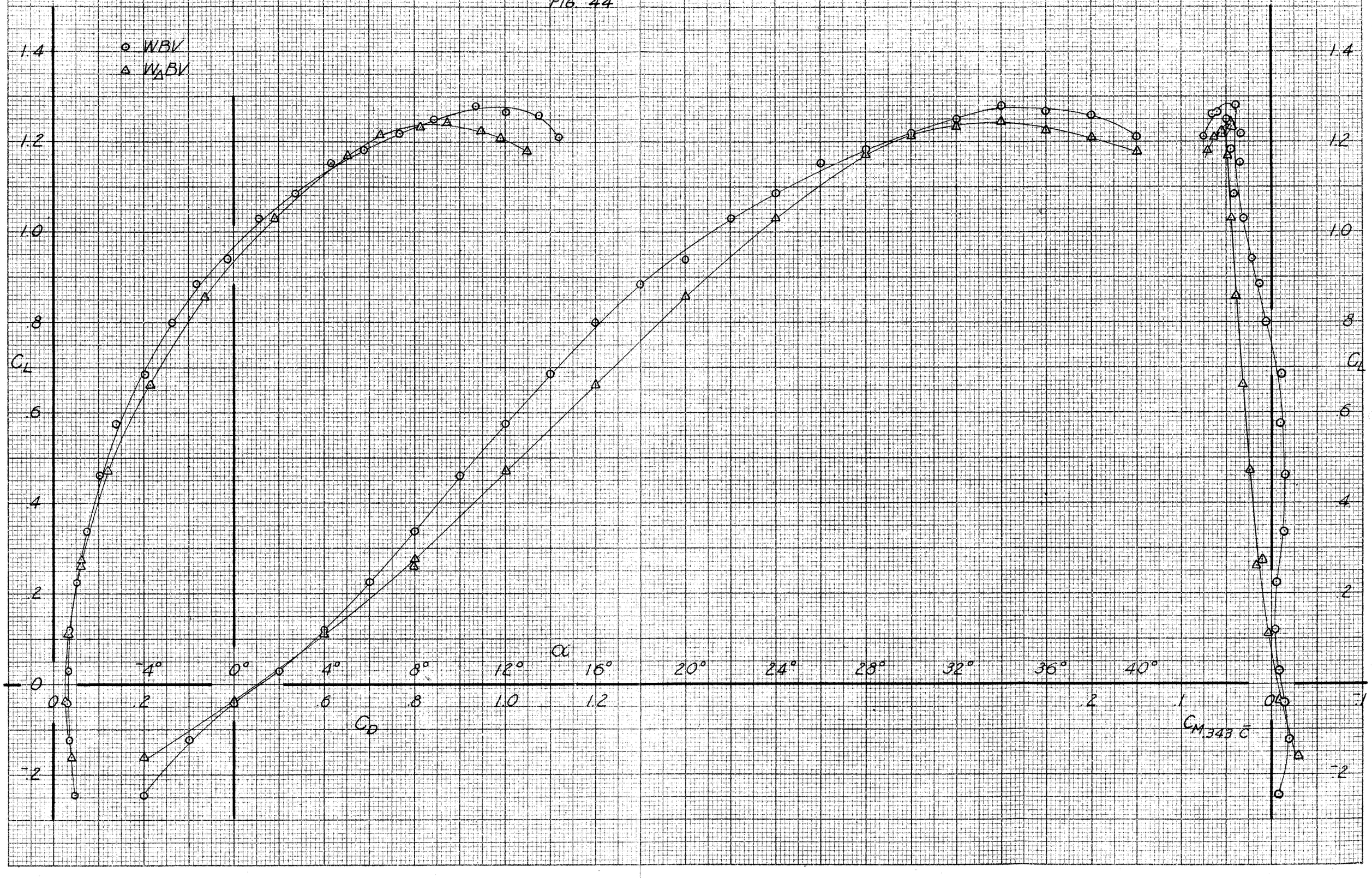

MODEL BUILD-UP WITH W

PAGE 59
FIG. 45.

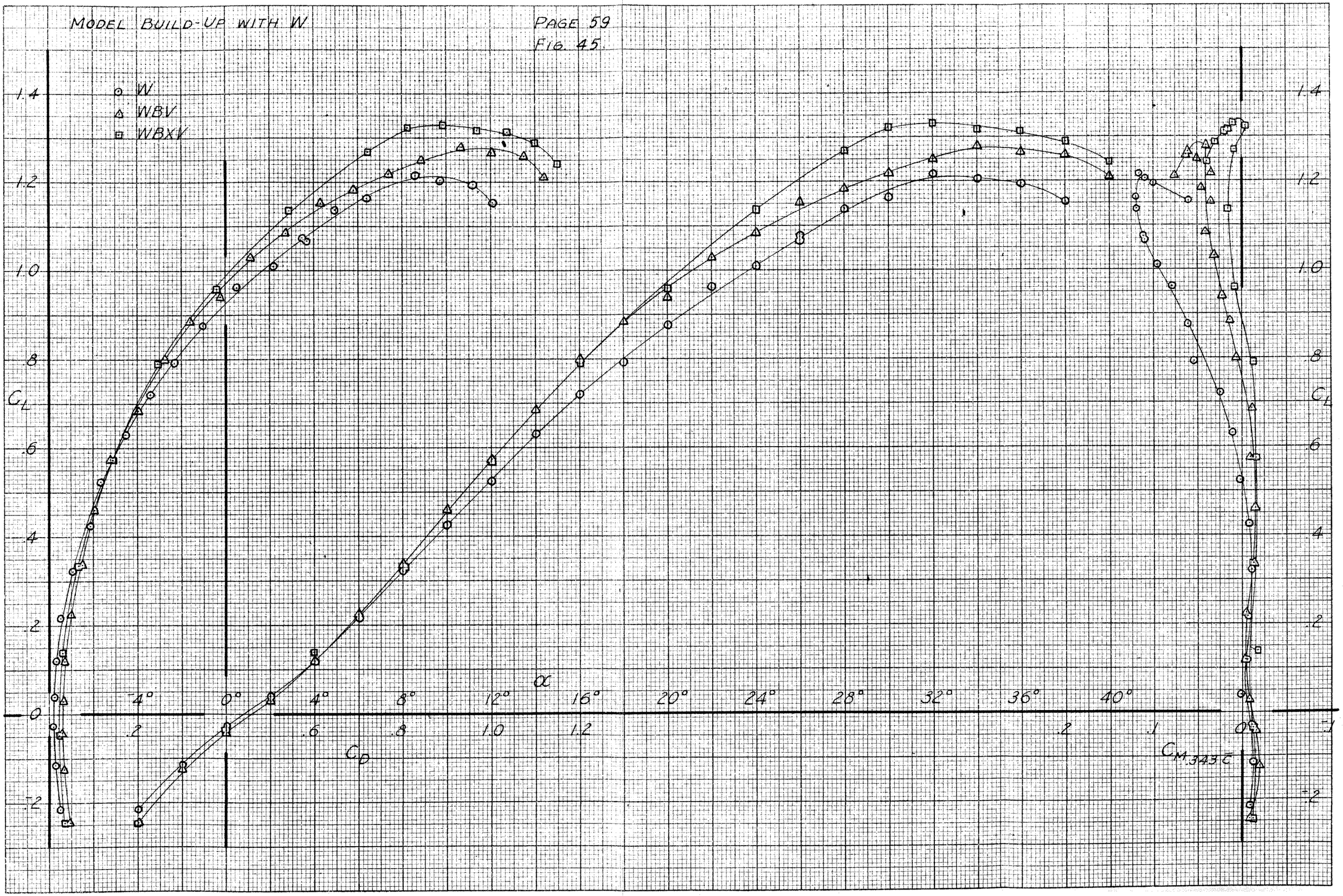

FULL SPAN SPLIT FLAP ON W

PAGE 60
FIG. 46.

W
WF 20
WF 40
WF 60
WF 75

C_L

$C_{L_{MAX.}}$ 1.1

δF - FLAP DEFLECTION

α

C_D

$C_{M_{.343\,\bar{c}}}$

PARTIAL SPAN (70%) SPLIT FLAP ON W

FIG. 47

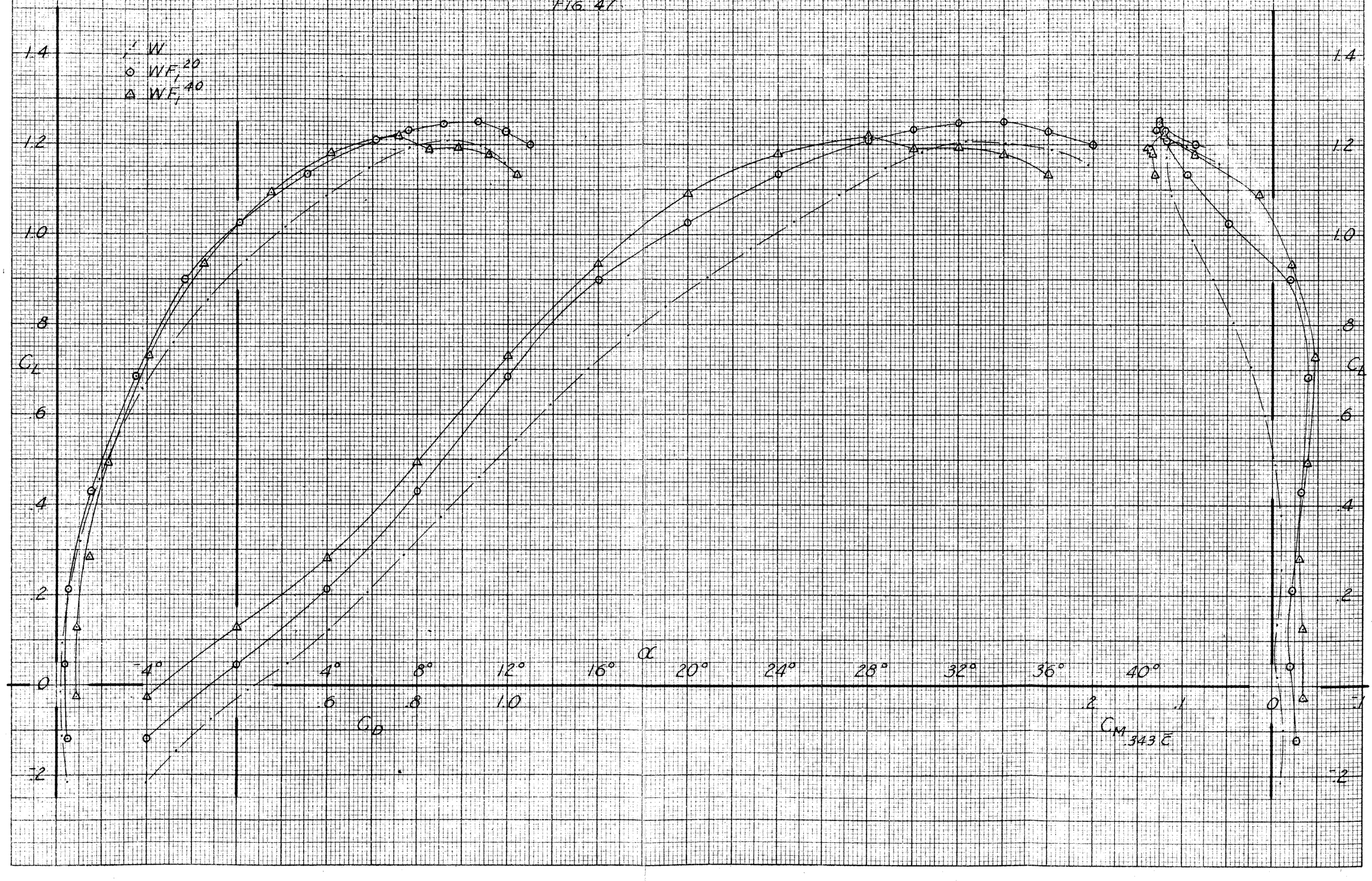

FULL SPAN NOSE FLAP ON W

PAGE 62
FIG. 48

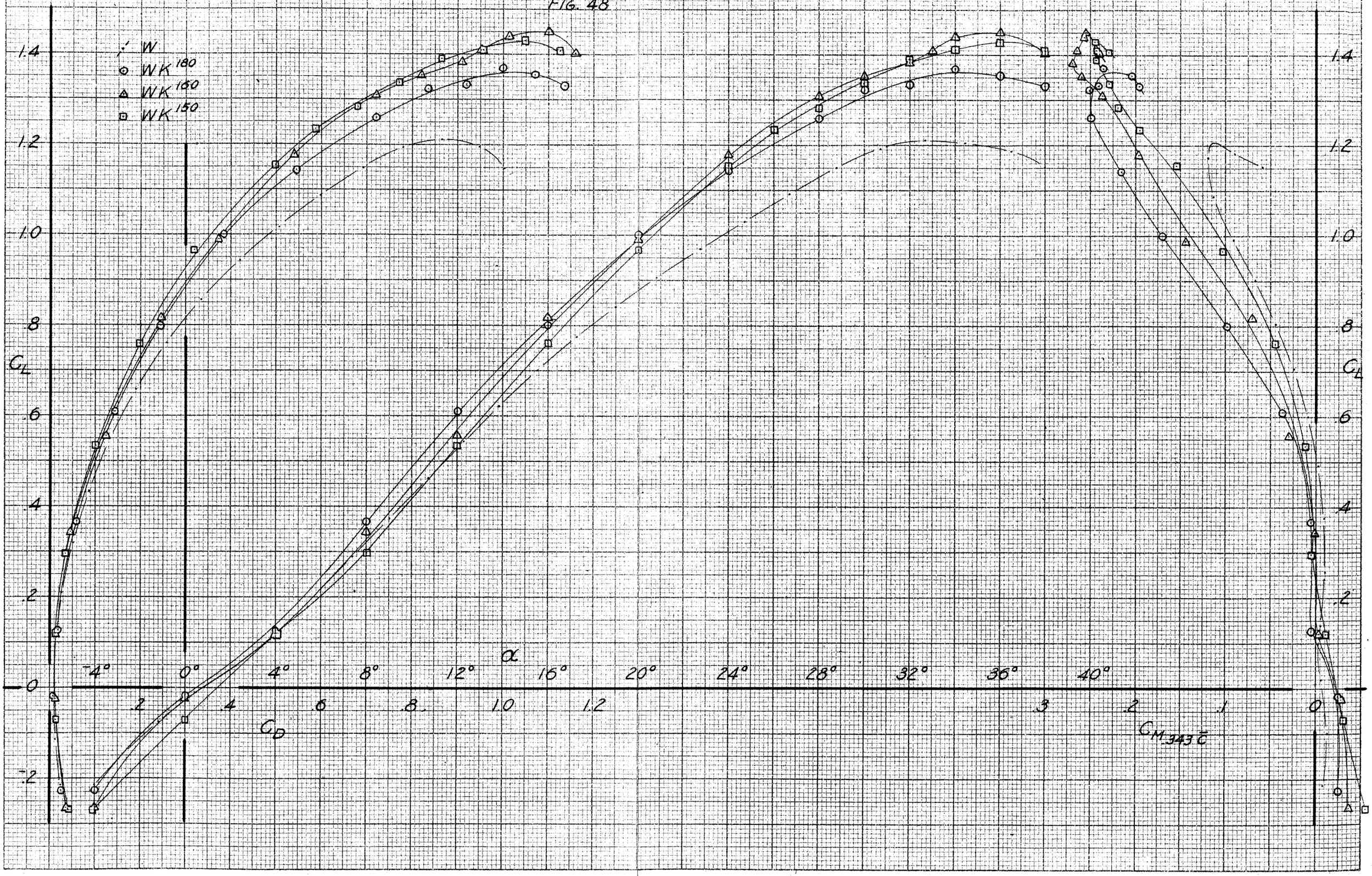

FULL SPAN NOSE FLAP ON W (CONT'D)

FIG. 49

W
WK 140
WK 130
WK 120

C_L

C_D

α

$C_{L_{MAX.}}$

δK - FLAP DEFLECTION

$C_{M.343\,\bar{c}}$

FULL SPAN NOSE FLAP AND FULL SPAN SPLIT FLAP COMBINATIONS ON W

PAGE 64
FIG. 50

W
WK 160 F 20
WK 160 F 40
WK 140 F 40
WK 120 F 40

1.4
1.2
1.0
.8
C_L
.6
.4
.2
0
-.2

-4° 0° 4° 8° 12° 16° 20° 24° 28° 32° 36° 40° α

.4 .6 .8 1.0 1.2 C_D

.3 .2 .1 0 $C_{M.343\,\bar{c}}$

FULL SPAN SPLIT FLAP ON WBV

PAGE 65
FIG. 51

WBV
$WBF_2^{20}V$
$WBF_2^{40}V$

C_L

1.4
1.2
1.0
.8
.6
.4
.2
0
-.2

α

-4° 0° 4° 8° 12° 16° 20° 24° 28° 32° 36° 40°

C_D

0 .2 .4 .6 .8 1.0 1.2

$C_{M_{.343\bar{c}}}$

0 .1 .2

1.4
1.2
1.0
.8
.6
.4
.2
0
-.2

FULL SPAN NOSE FLAP ON WBV

PAGE 66
FIG. 52

WBV
WBK$_V^{160}$V
WBK$_V^{140}$V

C_L

1.4
1.2
1.0
.8
.6
.4
.2
0
-.2

α

-4° 0° 4° 8° 12° 16° 20° 24° 28° 32° 36° 40°

C_D

0 .2 .6 .8 1.0 1.2

$C_{M_{.343\,\bar{c}}}$

.2 .1 0

FULL SPAN NOSE FLAP AND FULL SPAN SPLIT FLAP COMBINATIONS ON WBV

FIG 53

WBV
WBK$_1^{160}$F$_2^{40}$V
WBK$_1^{140}$F$_2^{40}$V

C_L

1.4
1.2
1.0
.8
.6
.4
.2
0
-.2

α

-4° 0° 4° 8° 12° 16° 20° 24° 28° 32° 36° 40°

C_D

0 .4 .6 .8 1.0 1.2 1.4

$C_{M_{.343\bar{c}}}$

.2 .1 0 -.1

1.4
1.2
1.0
.8
.6
.4
.2
0
-.2

PARTIAL SPAN (50%) SLAT AND INTERRUPTER PLATE ON WBV

PAGE 68
FIG. 54

WBV
WBS 30 V
WBIV

C_L

α

C_D

$C_{M_{34}\bar{3}\bar{c}}$

PARTIAL SPAN (40%) SPLIT FLAP AND
PARTIAL SPAN (25%) SLAT ON WBXV

FIG. 55

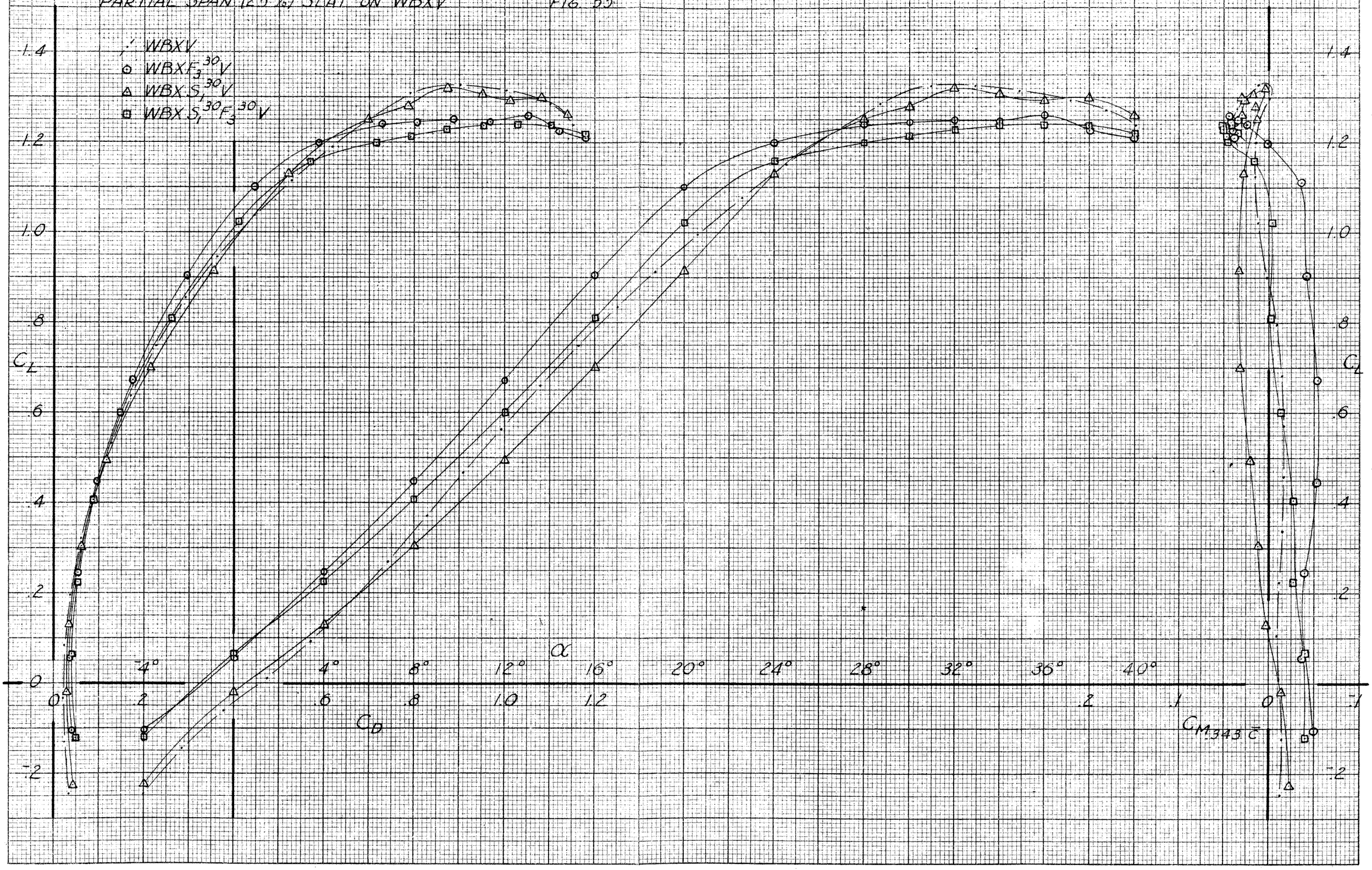

PARTIAL SPAN (50% AND 25%) NOSE FLAPS ON WBXV

PAGE 70
FIG. 56

WBXV
WBXK$_2^{160}$V
WBXK$_3^{160}$V

C_L

1.4
1.2
1.0
.8
.6
.4
.2
0
-.2

α

-4° 0° 4° 8° 12° 16° 20° 24° 28° 32° 36° 40°

C_D

0 .2 .4 .6 .8 1.0 1.2

$C_{M_{.343\bar{c}}}$

.2 .1 0 -.2

PARTIAL SPAN (40 %) TRAILING EDGE FLAP ON WBXV

FIG. 57

WBXV
WBXF$_4^{15}$V
WBXF$_4^{30}$V
WBXF$_4^{45}$V

C_L

1.6
1.4
1.2
1.0
.8
.6
.4
.2
0
-.2

α

0° 4° 8° 12° 16° 20° 24° 28° 32° 36° 40°

C_D

0 .2 .4 .6 .8 1.0 1.2 1.4

$C_{M_{343\bar{C}}}$

0 -.1

PARTIAL SPAN (25%) NOSE FLAP AND
PARTIAL SPAN (40%) TRAILING EDGE
FLAP ON WBXV

FIG. 58

- WBXV
- $WBXK_4^{160}V$
- $WBXK_4^{160}F_4^{30}V$

C_L 1.6, 1.4, 1.2, 1.0, .8, .6, .4, .2, 0, -.2

α -4°, 0°, 4°, 8°, 12°, 16°, 20°, 24°, 28°, 32°, 36°, 40°

C_D 0, .2, .4, .6, .8, 1.0, 1.2, 1.4

$C_{M.343\bar{c}}$ .2, .1, 0, -.2

TRAILING EDGE FILLET PLATE AND PARTIAL SPAN (25%) NOSE FLAP ON WBXV

FIG 59

△ WBXV
○ WBXTV
△ $WBXK_4^{/60}TV$

C_L

C_D

C_L

$C_{M_{.343\bar{c}}}$

α

HORIZONTAL TAIL AND PARTIAL SPAN (40%)
TRAILING EDGE FLAP ON WBXV

PAGE 74
FIG. 60

WBXV
WBXH$_1$V
WBXH$_2$V
WBXF$_4^{45}$H$_1$V

C_L 1.6 1.4 1.2 1.0 .8 .6 .4 .2 0 -.2

α -4° 0° 4° 8° 12° 16° 20° 24° 28° 32° 36° 40°

C_D 0 .2 .4 .6 .8 1.0 1.2 1.4 1.6 .1

$C_{M_{.343\bar{c}}}$ -.1 -.2

AILERON EFFECTIVENESS OF WBXV

PAGE 75
FIG. 61

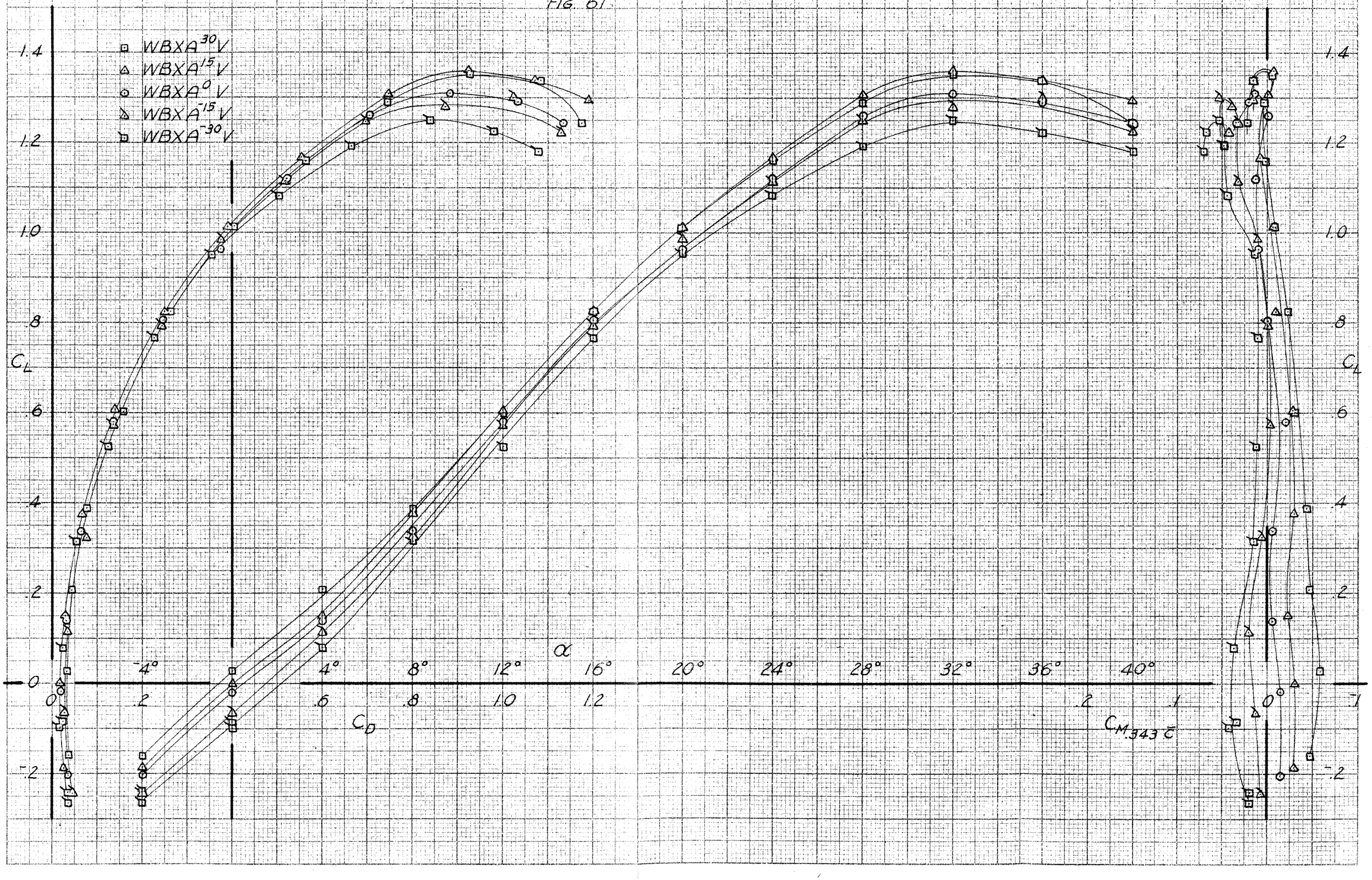

MODEL BUILD-UP WITH W_Δ

PAGE 76
FIG. 62

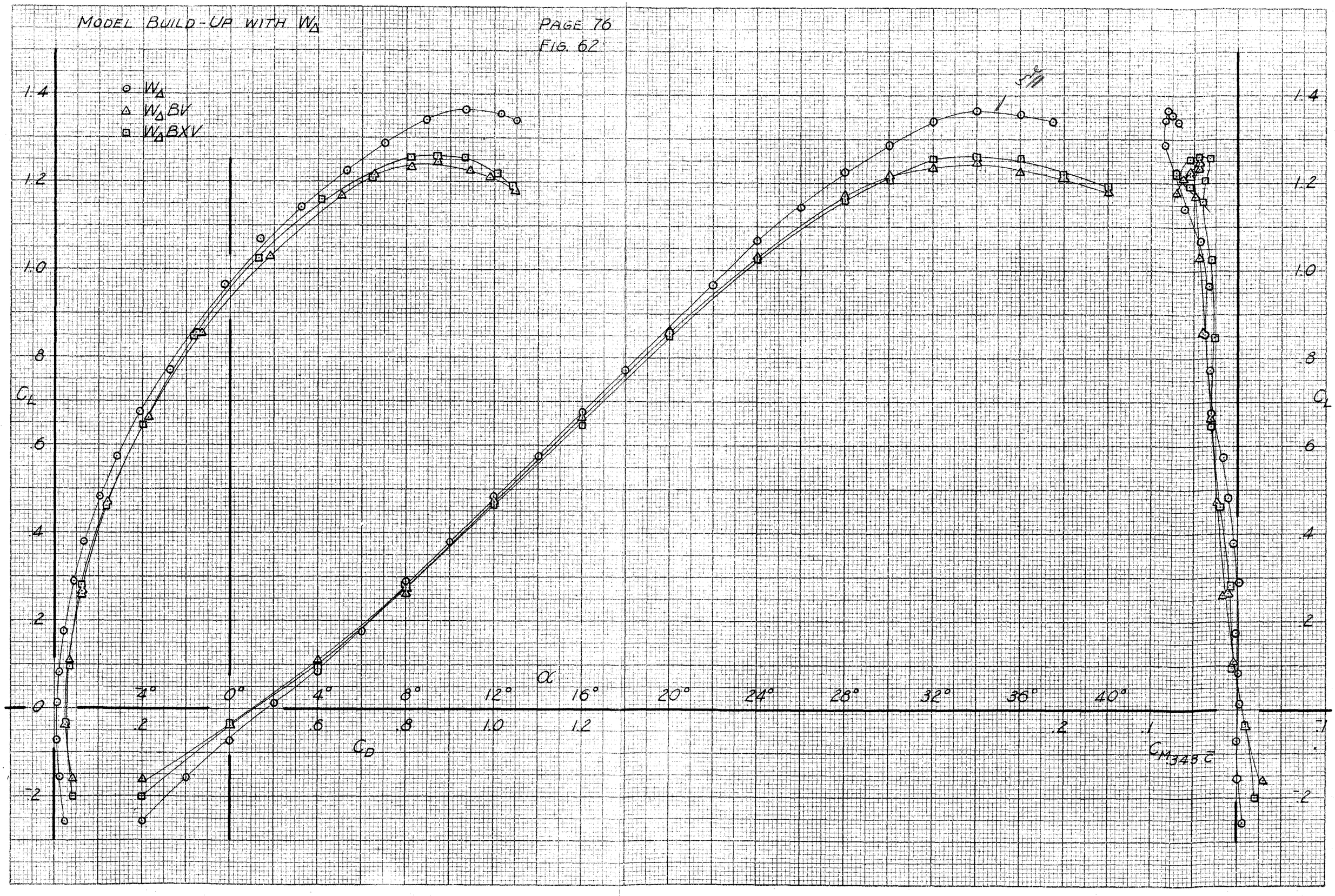

FULL SPAN PLAIN FLAP ON W_Δ

PAGE 77
FIG. 6.3

W_Δ
$W_\Delta F_5^{20}$
$W_\Delta F_5^{40}$

C_L

1.6
1.4
1.2
1.0
.8
.6
.4
.2
0
-.2

α

-4° 0° 4° 8° 12° 16° 20° 24° 28° 32° 36°

C_D

.2 .4 .6 .8 1.0 1.2

$C_{M_{.343\bar{c}}}$

.2 .1 -.1 -.2

FULL SPAN SPLIT FLAP ON W_Δ

PAGE 78
FIG. 64

W_Δ
$W_\Delta F_Z^{20}$

C_L 1.4 1.2 1.0 .8 .6 .4 .2 0 -.2

α -4° 0° 4° 8° 12° 16° 20° 24° 28° 32° 36° 40°

C_D .2 .4 .6 .8 1.0 1.2

C_L 1.4 1.2 1.0 .8 .6 .4 .2 -.2

$C_{M_{34}3\bar{c}}$ .2 .1 -.1

FULL SPAN PLAIN FLAP ON $W_\Delta BV$

PAGE 79
FIG. 65

$W_\Delta BV$
$W_\Delta BF_6^{20}V$
$W_\Delta BF_6^{40}V$

C_L 1.4, 1.2, 1.0, .8, .6, .4, .2, 0, -.2

α -4°, 0°, 4°, 8°, 12°, 16°, 20°, 24°, 28°, 32°, 36°, 40°

C_D 0, .2, .4, .6, .8, 1.0, 1.2

$C_{M_{34}\bar{C}}$ 0, -.1, -.2

FULL SPAN NOSE FLAP ON $W_\Delta BV$

PAGE 80
FIG. 66

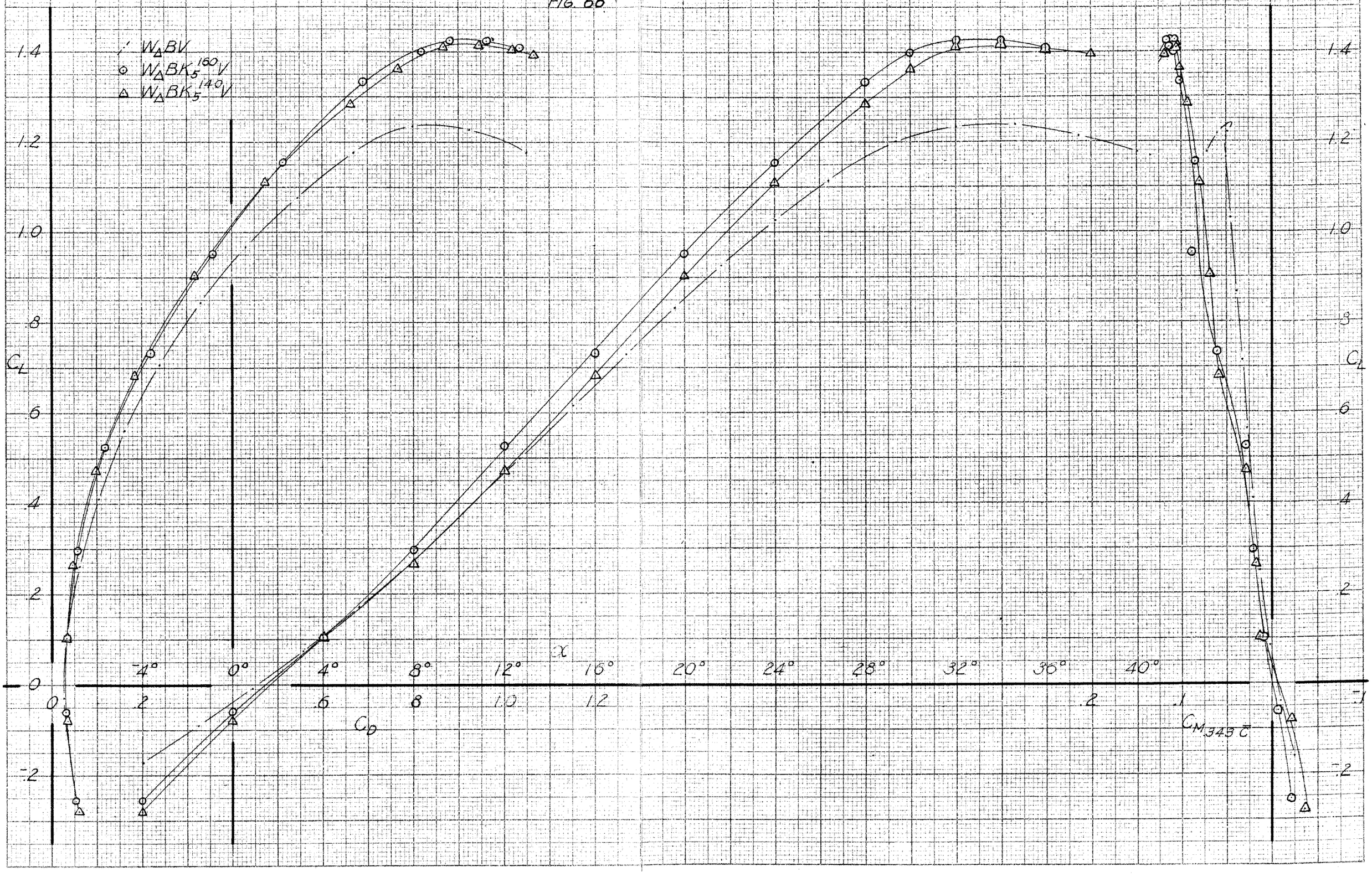

PARTIAL SPAN (25%) NOSE FLAP ON $W_\Delta BV$

PAGE 81
FIG. 67

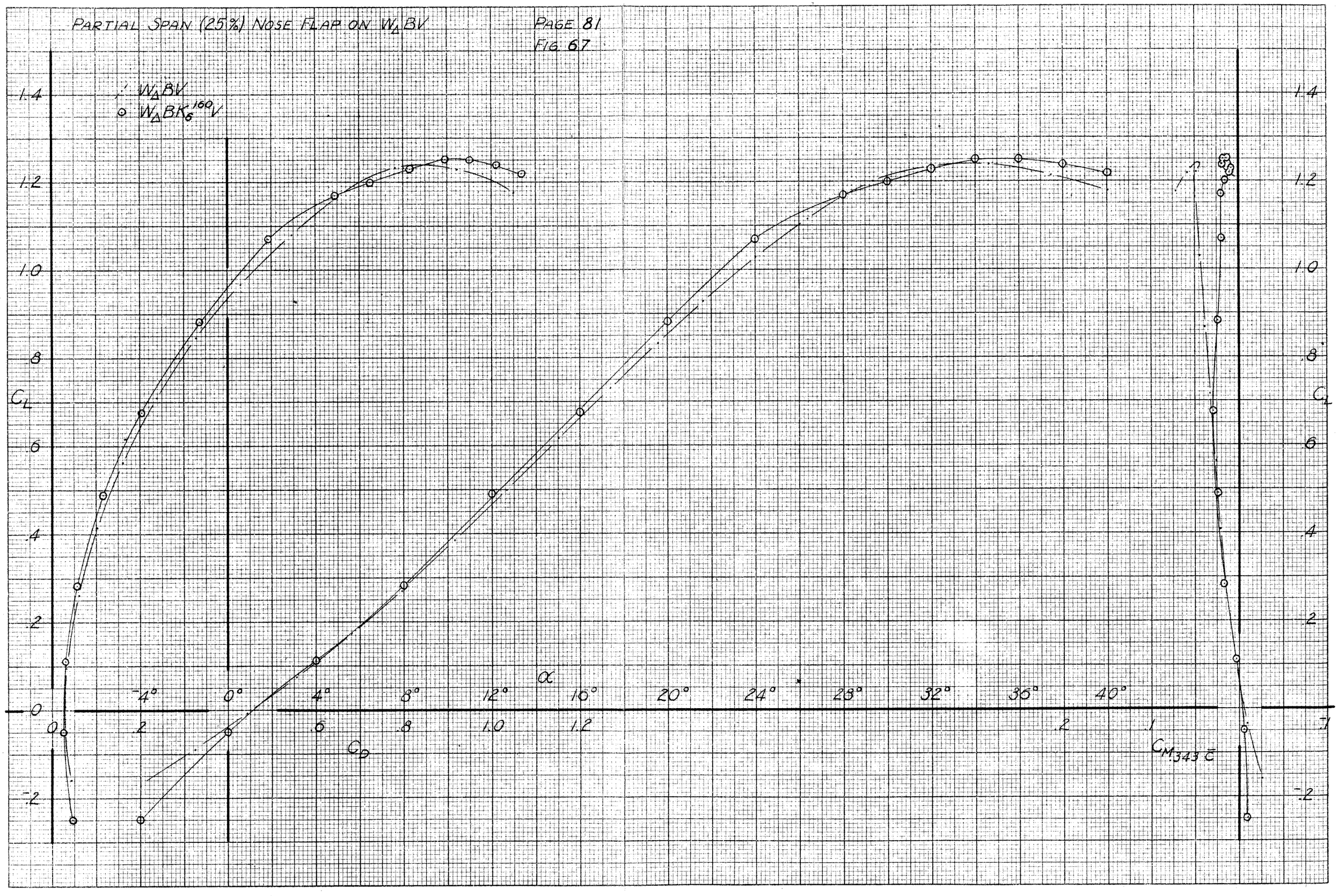

HORIZONTAL TAIL ON $W_\Delta BV$

PAGE 82
FIG 68

$W_\Delta BV$
$W_\Delta BH_1V$
$W_\Delta BH_2V$

C_L

1.4
1.2
1.0
.8
.6
.4
.2
0
-.2

α

-4° 0 4° 8° 12° 16° 20° 24° 28° 32° 36° 40°

C_D

0 .2 .4 .6 .8 1.0 1.2

$C_{M_{.343\,\bar{c}}}$

.2 .1 0 -.1

C_L

1.4
1.2
1.0
.8
.6
.4
.2
0
-.2